UNIVERSITY OF CALIFORNIA, SAN DIEGO

Dynamics of the Southern California Current System

A dissertation submitted in partial satisfaction of the

requirements for the degree Doctor of Philosophy in

Oceanography

by

Emanuele Di Lorenzo

2003

UNIVERSITY OF CALIFORNIA, SAN DIEGO

Dynamics of the Southern California Current System

A dissertation submitted in partial satisfaction of the

requirements for the degree Doctor of Philosophy in

Oceanography

by

Emanuele Di Lorenzo

Committee in charge:

Arthur Miller, Chair
Bruce Cornuelle
Peter Niiler
Peter Franks
Ivan Evans
Myrl Hendershott

2003

The dissertation of Emanuele Di Lorenzo is approved, and it is acceptable in quality and form for publication on microfilm:

_____

_____

_____

_____

_____

_____

Chair

University of California, San Diego

2003

To my future children
and my love Kim

TABLE OF CONTENTS

LIST OF FIGURES AND TABLES

AKNOWLEDGEMENTS

Financial support was provided by the Office of Naval Research (N00014-99-1-0045), the National Aeronautics and Space Administration (NAG5-6497, NAG5-9788), the National Oceanic and Atmospheric Administration (NA17RJ1231 through the Experimental Climate Prediction Center), the Department of Energy (DE-FG03-01ER63255), and the National Science Foundation (OCE-00-82543, OCE-01-21332).

Chapter 2 will appear in full as Di Lorenzo, E., Seasonal Dynamics of the surface circulation in the Southern California Current System. *Deep Sea Research II*, in press, 2003. I was the primary investigator and single author of this paper and conducted all of the analyses presented therein.

Chapter 3 has been submitted in full as Di Lorenzo, E., A.J. Miller, N. Schneider, J.C McWilliams, The warming of the California Current: Dynamics, thermodynamics and ecosystem implications, submitted to *Journal of Physical Oceanography*, 2003.

VITA

1997	Laurea in Marine Environmental Sciences University of Bologna, Italy
1997-2003	Graduate Research Assistant, University of California, San Diego
2003	Ph.D., Scripps Institution of Oceanography, University of California, San Diego

PUBLICATIONS

Miller A. J., E. Di Lorenzo, D. J. Neilson, B. D. Cornuelle and J. R. Moisan. (2000) Modeling CalCOFI observations during El Nino: fitting physics and Biology. CalCOFI Report 2000, Vol. 41.

Di Lorenzo, E., A.J. Miller, D.J. Neilson, B.D. Cornuelle, J.R. Moisan (2003) Modeling observed California Current mesoscale eddies and the ecosystem response. International Journal of Remote Sensing, in press.

Di Lorenzo, E. (2003) Seasonal Dynamics of the surface circulation in the Southern California Current System. *Deep Sea Research II*, in press.

Di Lorenzo, E., A.J. Miller, N. Schneider, J.C McWilliams (2003) The warming of the California Current: Dynamics, Thermodynamics and ecosystem implications. *Journal of Physical Oceanography*, submitted.

Di Lorenzo E. , M.G. G. Foreman, W.R. Crawford (2003) Modeling the Generation of Haida Eddies *Deep Sea Research II*, submitted.

Schneider, N., E. Di Lorenzo and P. Niiler (2003) Low frequency salinity changes in the California Current. *Journal of Physical Oceanography*, submitted.

Moore, A., H. Arango, B. Cornuelle, E. Di Lorenzo, A.J. Miller and D.J. Neilson.(2003) The ROMS Tangent Linear and Adjoint Models: A Comprehensive Ocean Prediction System. *Ocean Modeling*, submitted.

ABSTRACT OF THE DISSERTATION

Dynamics of the Southern California Current System

by

Emanuele Di Lorenzo
Doctor of Philosophy in Oceanography
University of California, San Diego, 2003

Dr. Arthur J. Miller, Chair

The dynamics of seasonal to long-term variability of the Southern California Current System (SCCS) is studied using a four dimensional space-time analysis of the 52 year (1949-2000) California Cooperative Oceanic Fisheries Investigations (CalCOFI) hydrography combined with a sensitivity analysis of an eddy permitting primitive equation ocean model under various forcing scenarios.

The dynamics of the seasonal cycle in the SCCS can be summarized as follows. In spring upwelling favorable winds force an upward tilt of the isopycnals along the coast (equatorward flow). Quasi-linear Rossby waves are excited by the ocean adjustment to the isopycnal displacement. In summer as these waves propagate offshore poleward flow develops at the coast and the Southern California Eddy (SCE) reaches its seasonal maxima. Positive wind stress curl in the Southern California Bight is important in maintaining poleward flow and locally reinforcing the SCE with an additional upward displacement of isopycnals through Ekman pumping. At the end of summer and

throughout the fall instability processes within the SCE are a generating mechanism for mesoscale eddies, which fully develop in the offshore waters during winter.

On decadal timescales a warming trend in temperature (1 C) and a deepening trend in the depth of the mean thermocline (20 m) between 1950 and 1998 are found to be primarily forced by large-scale decadal fluctuations in surface heat fluxes combined with horizontal advection by the mean currents. After 1998 the surface heat fluxes suggest the beginning of a period of cooling, which is consistent with colder observed ocean temperatures. The temporal and spatial distribution of the warming is coherent over the entire northeast Pacific Ocean. Salinity changes are decoupled from temperature and uncorrelated with indices of large-scale oceanic variability. Temporal modulation of southward horizontal advection by the California Current is the primary mechanism controlling local salinity changes in the SCCS.

Within 50 to 100 km of the coast, the ocean model simulations show strong evidence that the isopycnal deepening reduces the nutrient flux to the ocean surface. The long-term trend of the model proxy for surface nutrients is consistent with the observed decline in zooplankton concentration.

Chapter 1.

Introduction

1.1 The historical context and motivation

The southern component of the California Current System (SCCS, here defined as south of Point Conception) was first described in an early report by Sverdrup and Fleming [1941] (Figure 1.1) as a result of ship cruise measurements during March to July of 1937. Shortly thereafter in 1949, motivated by the collapse of the sardine populations off California, the California Cooperative Oceanic Fisheries Investigation (CalCOFI) began a routine sampling program of the physical and biological properties of the ocean off Central and Southern California. The CalCOFI historical sampling grid (Figure 1.2) extends from the tip of Baja to northern California. The program, still active today, provides us with a unique long-term (1949-present) hydrographic dataset that contains temperature, salinity and other measures of the ecosystem in the upper 500 meters of the California coastal ocean.

Timeseries of oceanic temperature, salinity and zooplankton derived from spatially averaging the CalCOFI hydrography over the sampling grid (Figure 1.3) reveal strong interannual to decadal variations of the coastal environment. In particular a warming trend in oceanic temperatures between 1950 and 1998 (Figure 1.3), first reported by Roemmich [1992], is thought to play an important role in the observed decline of zooplankton off the California coastal waters [*Roemmich and McGowan*, 1995] (Figure 1.4). Because the California Current System is one of the biggest upwelling systems of the world, the biological productivity is among the highest, as evident from modern satellite images of ocean surface chlorophyll-a (Figure 1.4). Therefore ecosystem variations, such

as these, have tremendous economic impacts on the California fisheries industry, one of the largest in the world.

Understanding the links between the physical and biological systems in the coastal environment is area of active research with broad implications that go beyond the California Current System and are relevant to the large-scale climate changes. For example it has become widely accepted that the planet is warming due to an increase in emission of greenhouse gases in the atmosphere [*Barnett et al.*, 2001; *IPCC*, 2001]. The oceanic ecosystem could potentially serve as a negative feedback of the climate system to future global warming. Increasing ocean temperatures could drive an increase in ocean biological productivity and enhance the flux of CO_2 from the atmosphere to the ocean through photosynthesis associated with marine phytoplankton. Consequently the carbon sequestered by the phytoplankton could sink into the deeper ocean in the form of detritus and be permanently removed from the carbon cycling. Therefore a spin up of the so called 'biological pump' could lead to a reduction in atmospheric CO_2.

Studies that use sophisticated numerical models of the climate system have become a common tool to improve our understanding of the spatial and temporal implications of global warming [*IPCC*, 2001]. Estimating the biological response to anthropogenic forcing and quantifying the contribution of the biological pump on the carbon budget is an important component in these models [*Pierce*, 2003]. However the resolution of these large-scale climate models is inadequate to resolve and predict the coastal ecosystem changes (Figure 1.5), which to this day remain a big uncertainties of the climate change problem.

One of the goals of this Ph.D. thesis is to provide a building block to further resolve the links between the physical changes in the oceanic circulation and the ecosystem in coastal upwelling system such as the California Current System. Specifically we provide a dynamical framework to interpret the long-term physical climate changes inferred from the CalCOFI hydrography. The strategy of the investigation presented in this thesis is to interpret the coastal observations with a numerical regional ocean circulation model for the coast of Southern California. This model takes into account the complex geometrical features of this region, such as realistic coastlines and bottom topography, which are critical elements in order to resolve the dynamics of the SCCS.

A substantial portion of this thesis work involves the development and testing of a regional ocean circulation model for the SCCS. The need for such a model as a tool to interpret the CalCOFI hydrography derives from the limitations of the dataset in resolving the spatial and temporal variability typical of the California Current System. This problem is illustrated in Figure 1.6, which shows an example of the spatial resolution associated with the CalCOFI sampling grid (the white dots) superimposed on a satellite image of sea surface temperature (SST). The SST image shows the entrainment by mesoscale eddies of cold waters from the coastal upwelling boundary (lighter color) giving rise to cold filaments that extend from the coast to the offshore waters. The cold filaments are generally rich in nutrients and therefore have important consequences for biological productivity. Such mesoscale structures are clearly aliased by the spatial CalCOFI sampling grid (Figure 1.6). Furthermore the seasonal sampling of the CalCOFI program is unable to properly resolve the temporal variability of these eddies, which have characteristic timescale of about a month. Interannual to long-term changes in eddy

variance can have tremendous implications on the ecosystem and the dynamics of the SCCS. Therefore the inadequate sampling of the eddy statistics in the CalCOFI hydrography is a major limitation to our understanding. Regional ocean circulation models, if properly understood, can provide a mean to reconstruct the dynamics and statistics of the ocean mesoscale structure. Figure 1.7 shows an image of SST from a simulation with the regional ocean modeling system [*Marchesiello et al.*, 2003] that will be used in this thesis work. The mesoscale structures in the model SST are qualitatively very similar to the one in the satellite SST (Figure 1.6). In the following chapters we will present evidence that the model variability is the result of dynamical processes that are also found in the available observations. We will then use the model and the CalCOFI observations to better resolve and interpret the climatic signals off the coast of Southern California.

1.2 An overview of the findings

Chapter 2 is devoted to the study of the seasonal dynamics of the SCCS and its sensitivity to different atmospheric mechanical forcing. We show that the model is capable of capturing basic statistics of the coastal oceanic system such as the observed mean circulation and seasonal cycle. The model solution critically depends on the spatial structure of the wind forcing. Different wind forcing can change not only the spatial response of the circulation but also the timing of the ocean seasonal cycle. Important dynamical processes isolated in this first chapter are the role of Ekman pumping, topography and coastlines in maintaining the mean circulation. We also show the role of

Rossby waves in controlling the timing of the seasonal cycle. These waves are forced both at the coast by the upwelling favorable winds and in the Southern California Bight by the wind stress curl [*Di Lorenzo*, 2003].

Chapter 3 builds on the knowledge gained in Chapter 2 and in other studies that are not included in this thesis [*Miller et al.*, 2000; *Di Lorenzo et al.*, 2003a]. The focus is on understanding the dynamics that control the long-term changes in the properties of the oceanic water masses in the SCCS. The study involves a reanalysis of the CalCOFI hydrography and several long-term targeted numerical model simulations that isolate the contribution of various ocean forcing functions.

The observed warming trend between 1950 and 1998 (Figure 1.3) and the decline in zooplankton raise some fundamental questions. What are the physics that control the long-term observed temperature changes? Are these temperature changes linked to global warming? Can we identify clear mechanisms by which these physical changes impact the ecosystem?

In summary we will find that the warming trend in ocean temperature between 1950 and 1998 is primarily forced by large-scale decadal fluctuations in surface heat fluxes. These heat flux variation are coherent and in phase over the entire north-east Pacific and exert a control on ocean temperatures both locally through ocean-atmosphere exchanges and remotely through horizontal advection by the mean currents [*Di Lorenzo et al.*, 2003c]. The temperature variance associated with the decadal variations in surface heat fluxes is much larger than the possible trend expected from global warming. Therefore the global warming signature on the coastal environment has yet to be clearly detected. In fact, after 1998 the surface heat fluxes suggest the beginning of a period of

cooling, which is consistent with colder observed ocean temperatures and an increase in zooplankton [*Lavaniegos and Ohman*, 2003; *Rau et al.*, 2003].

The ocean model simulations also show strong evidence that isopycnal deepening associated with the warming reduces the nutrient flux to the ocean surface, thus suggesting that the decline in zooplankton could be related to a decrease in nutrients availability. The changes in the atmospheric forcing over the last 50 years also contribute to an increase in mesoscale eddy variance in the model simulations. Further analyses of the ecosystem response to these physical changes are currently underway.

Chapter 3 also addresses the long-term variations of other ocean properties such as salinity, currents and eddy variance by comparing the dynamical effects of local forcing (wind forcing and heat fluxes) vs. remote forcing (e.g. large scale advection and ENSO) in the SCCS. For example an interesting observation is that the timeseries for salinity from CalCOFI (Figure 1.3) is weakly correlated with temperature on interannual timescales and uncorrelated on decadal timescales. Recently it has been shown that California coastal ocean temperatures changes are part of a large-scale Pacific Ocean decadal mode of variability [Mantua et al., 1997; Zhang et al., 1997; Lluch-Cota et al., 2001]. In this mode SST is coherent and in phase along the entire U.S. and Canadian west coasts. However salinity does not show strong correlations with indices of large-scale climate variability and its dynamics appear to be locally controlled by anomalous advection of the California Current [*Di Lorenzo et al.*, 2003c; *Schneider et al.*, 2003]. This finding is relevant to the understanding of the dynamics that control passive tracers in the SCCS.

References

Barnett, T. P., D. W. Pierce and R. Schnur, 2001, Detection of anthropogenic climate change in the world's oceans, *Science*, **292** (5515), 270-274.

Di Lorenzo, E., 2003, Seasonal dynamics of the surface circulation in the Southern California Current System, *Deep-Sea Research II*, (in press).

Di Lorenzo, E., A. J. Miller, D. J. Neilson, B. D. Cornuelle and J. R. Moisan, 2003a, Modeling observed California Current mesoscale eddies and the ecosystem response, *International Journal of Remote Sensing*, in press.

Di Lorenzo, E., A. J. Miller, N. Schnedier and J. C. McWilliams, 2003c, The warming of the California Current: Dynamics, thermodynamics and ecosystem implications, *Journal of Physical Oceanography*, submitted.

Lavaniegos, B. and M. D. Ohman, 2003, Long-term changes in pelagic tunicates of the California Current, *Deep Sea Research II*, in press.

Lluch-Cota, D. B., W. S. Wooster and S. R. Hare, 2001, Sea surface temperature variability in coastal areas of the Northeastern Pacific related to the El Nino-Southern Oscillation and the Pacific Decadal Oscillation, *Geophysical Research Letters*, **28** (10), 2029-2032.

Mantua, N. J., S. R. Hare, Y. Zhang, J. M. Wallace and R. C. Francis, 1997, A Pacific interdecadal climate oscillation with impacts on salmon production, *Bulletin of the American Meteorological Society*, **78** (6), 1069-1079.

Marchesiello, P., J. C. McWilliams and A. Shchepetkin, 2003, Equilibrium Structure and dynamics of the California Current System., *Journal of Physical Oceanography*, **33** 753-783.

Miller, A. J., E. Di Lorenzo, D. J. Neilson, B. D. Cornuelle and J. R. Moisan, 2000, Modeling CalCOFI observations during El Nino: Fitting physics and biology, *California Cooperative Oceanic Fisheries Investigations Reports*, **41** 87-97.

Pierce, D. W., 2003, The effects of anthropogenic forcing on biological activity, *Climate Change*, submitted.

Rau, G. H., M. D. Ohman and A. Pierrot-Bults, 2003, Linking nitrogen dynamics to the climate variability off Central California: A 51 year record based 15N/14N in CalCOFI Zooplankton, *Deep Sea Research II*, in press.

Roemmich, D., 1992, Ocean Warming and Sea-Level Rise Along the Southwest United-States Coast, *Science*, **257** (5068), 373-375.

Roemmich, D. and J. McGowan, 1995, Climatic Warming and the Decline of Zooplankton in the California Current, *Science*, **267** (5202), 1324-1326.

Schneider, N., E. Di Lorenzo and P. Niiler, 2003, Decadal salinity changes in the California Current, *Journal of Physical Oceanography*, submitted.

Sverdrup, H. U. and R. H. Fleming, 1941, The waters off the coast of Southern California, *Scripps Inst. Oceanography Bulletin*, (4), 261-387.

Zhang, Y., J. M. Wallace and D. S. Battisti, 1997, ENSO-like interdecadal variability: 1900-93, *Journal of Climate*, **10** (5), 1004-1020.

Figure 1.1. Harald Sverdrup 1931.

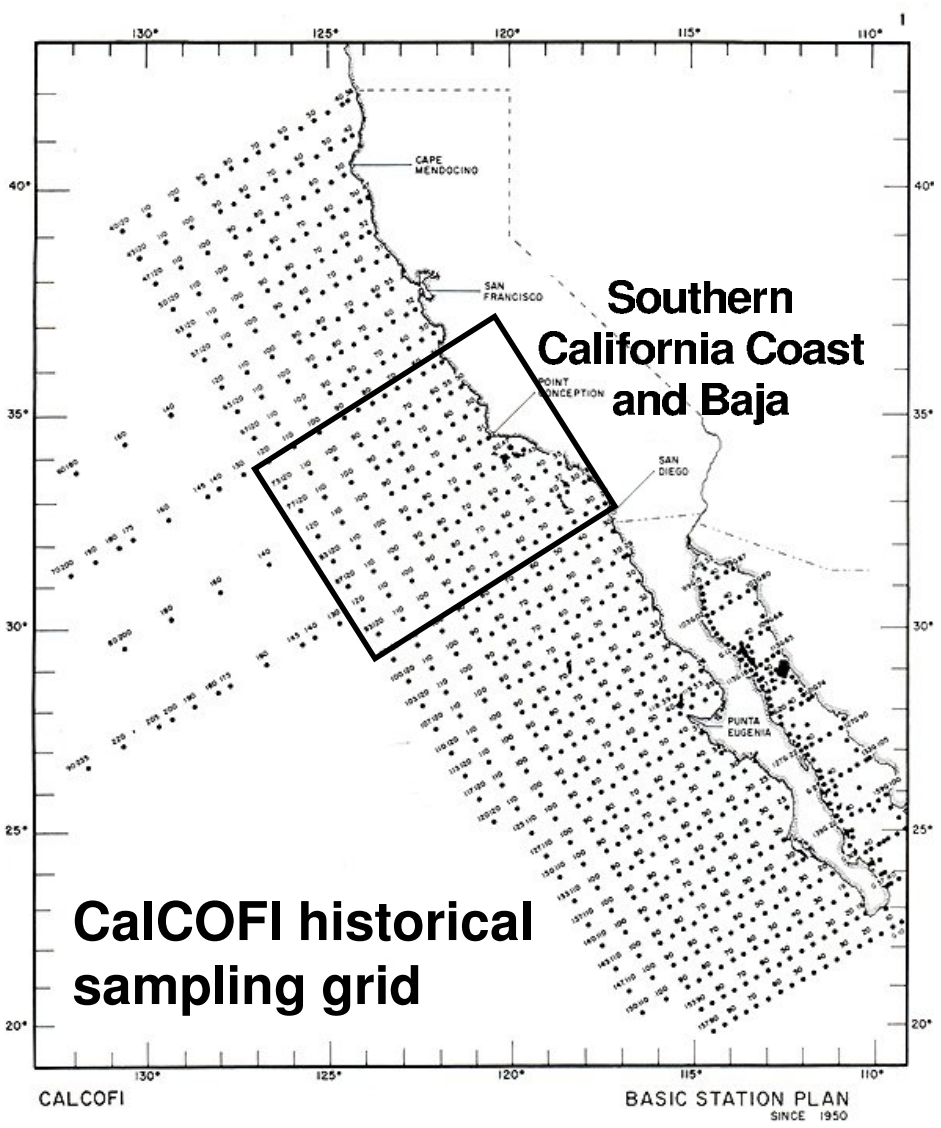

Figure 1.2. CalCOFI historical sampling grid.

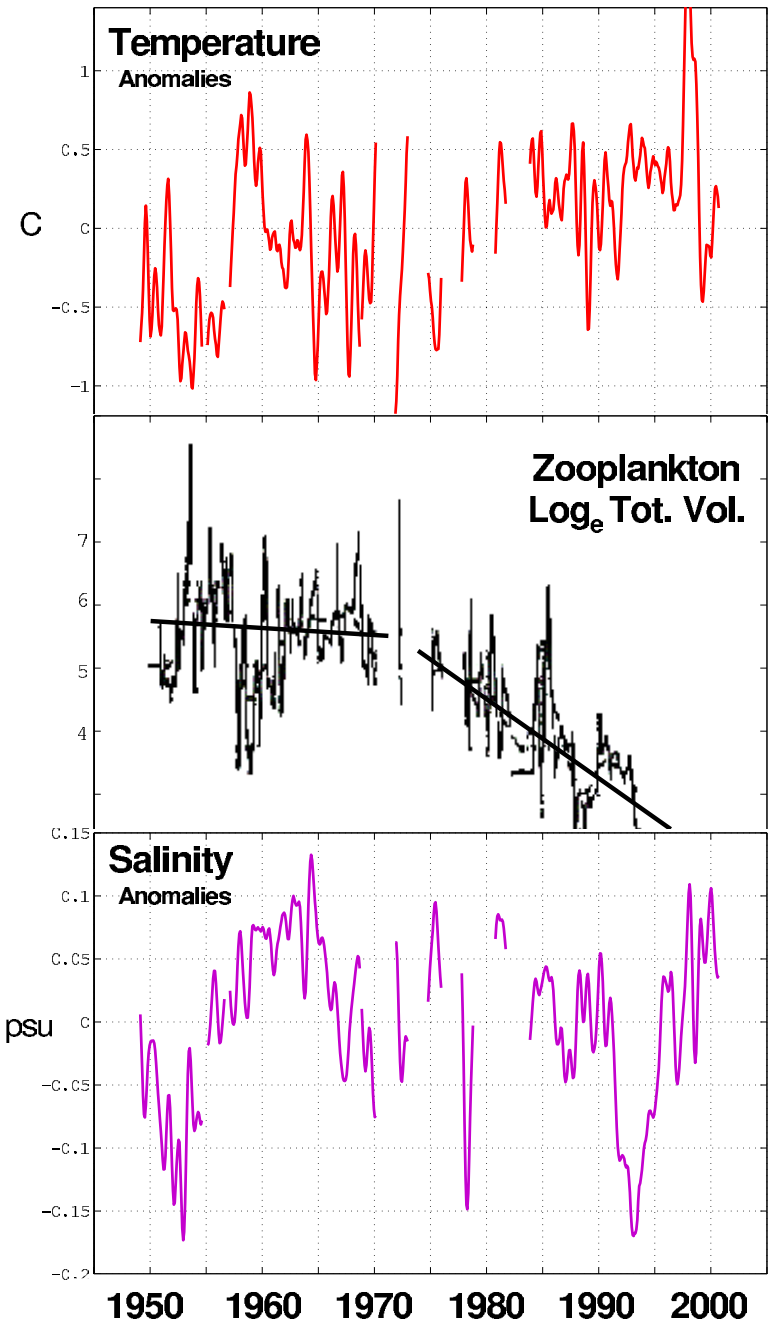

Figure 1.3. Timeseries of ocean temperature and salinity anomalies, and total volume zooplankton averaged over the Southern California domain. The source of the zooplankton plot is Roemmich and McGowan [1995].

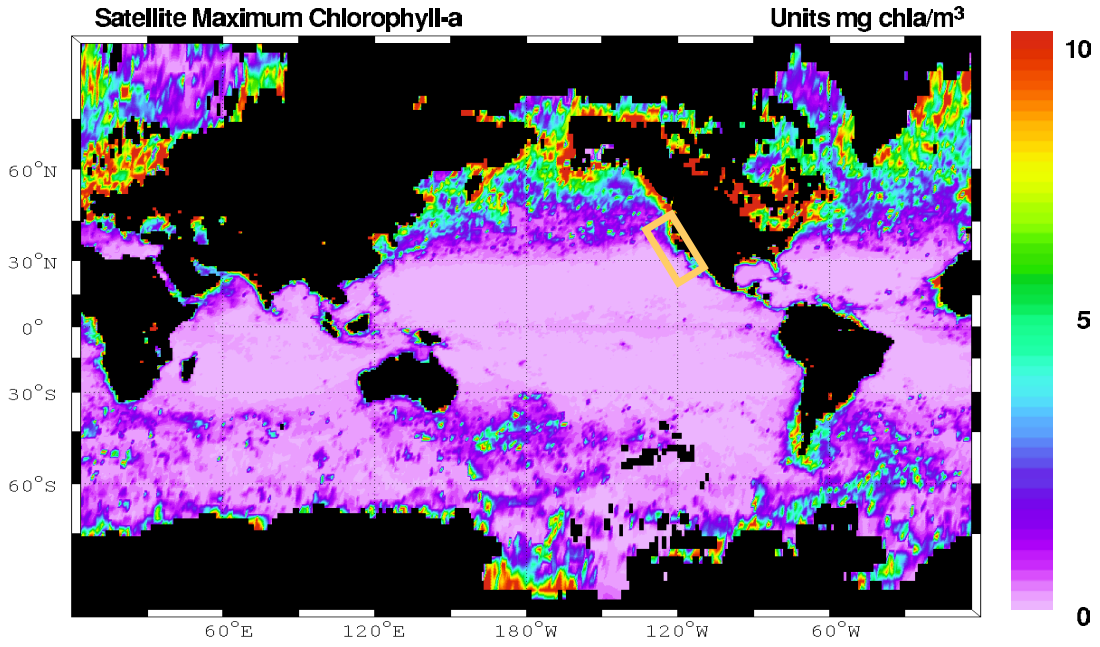

Figure 1.4. Map of maximum surface chlorophyll-a from the Coastal Zone Color Scanner.

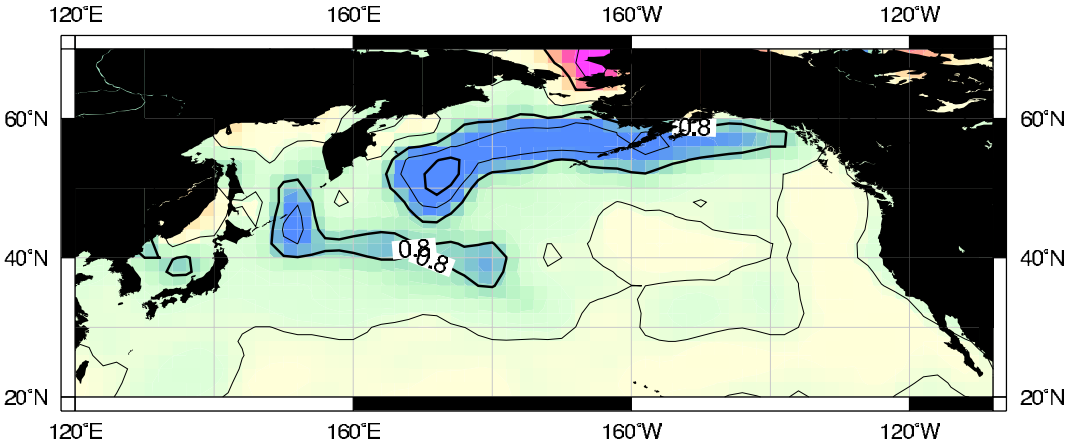

Figure 1.5. Map of spatial distribution of biological activity changes in a greenhouse gas model simulations. Plotted is the ratio between year 2090/2000 from Pierce [2003].

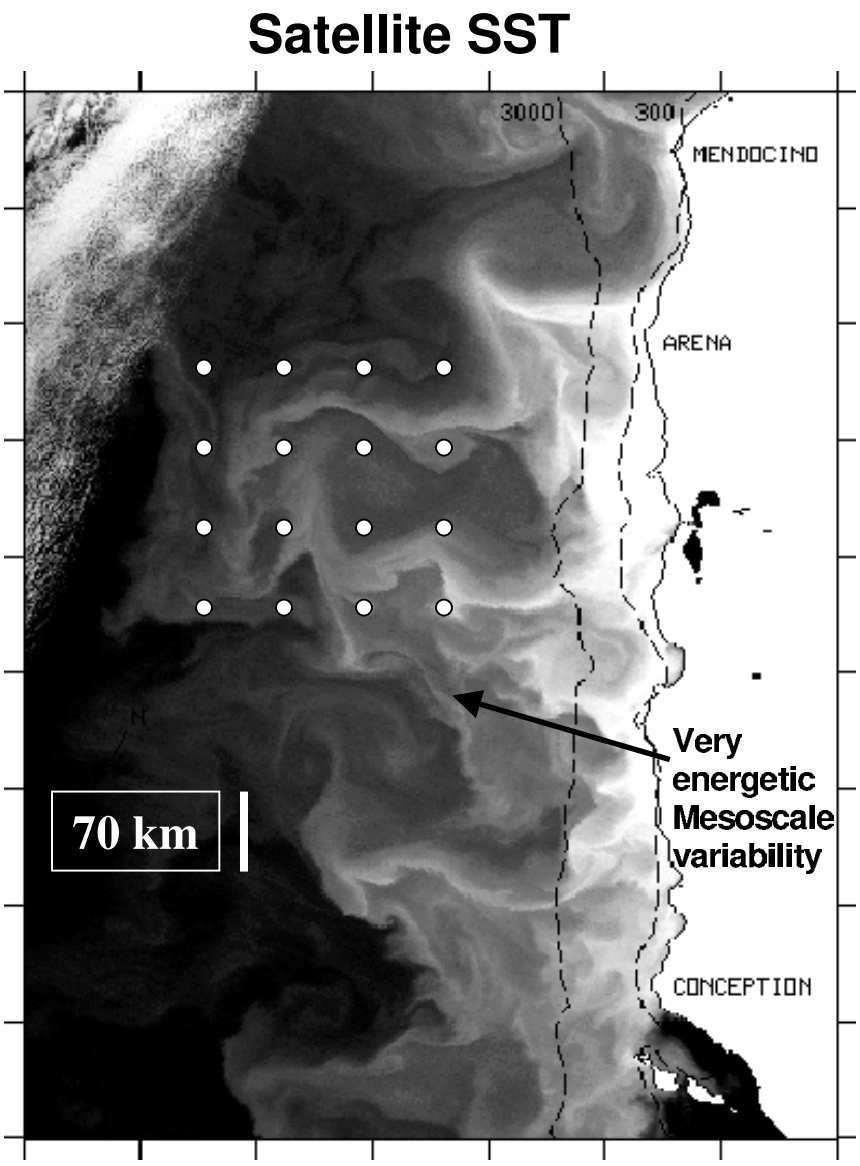

Figure 1.6. Snapshot of satellite sea surface temperature. No units or time available. Cold water are in light color and warm waters are in dark color. White dots represent an example of a 70 km sampling grid.

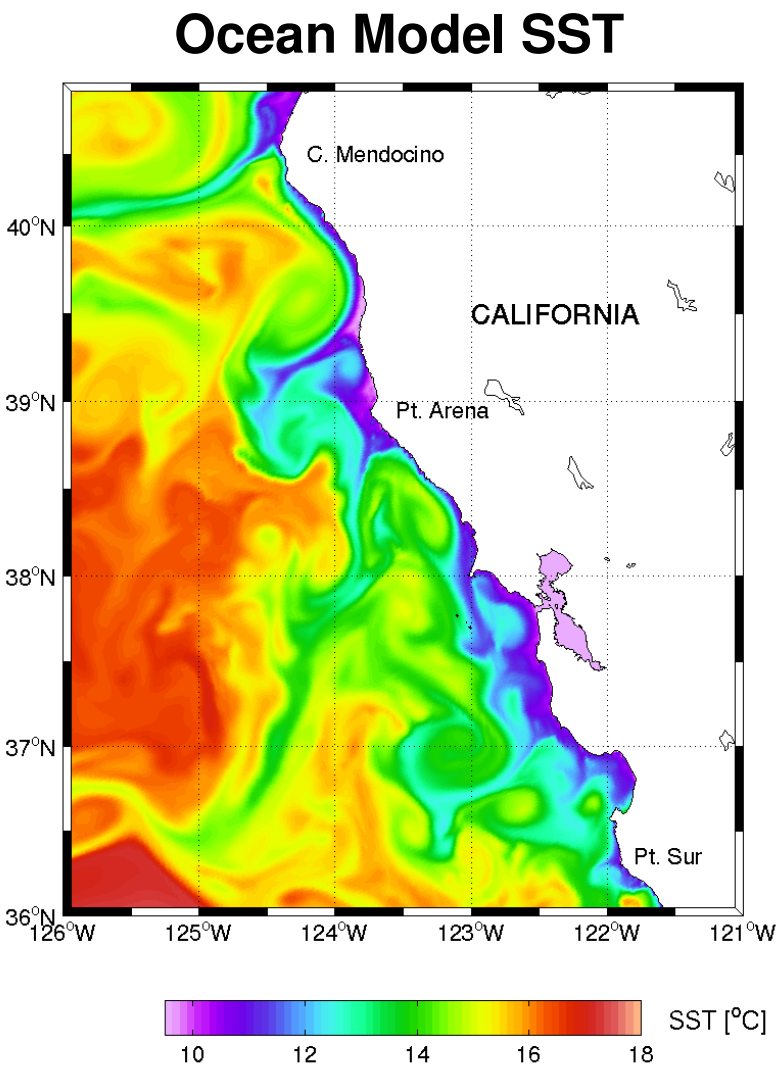

Figure 1.7. Snapshot of model sea surface temperature from Marchesiello et al. [2003].

Chapter 2.

Seasonal dynamics of the surface circulation in the Southern California Current System

Abstract

The seasonal dynamics of the Southern California Current System (SCCS) are investigated using a primitive equation ocean model with real coastlines and topography. The model is tested with different wind forcing and the resulting flow fields are compared to the mean and seasonal circulation inferred from long-term in situ observations (California Cooperative Fisheries Investigation (CalCOFI)). The model integration forced with the output winds of a regional atmospheric model (RSM) best captures the statistics of the observed circulation with a 0.9 correlation coefficient for the streamlines and 0.5 for the velocity fields. The model integrations reveal a pronounced linear response of the flow field to changes in winds on the shelf region.

A dynamical feature inferred from CalCOFI hydrography, also suggested in TOPEX/ERS maps, is an annually recurrent westward propagation of SSH anomalies originated in the Southern California Bight (SCB) during the upwelling season. The RSM integration is the only one to capture the correct timing and spatial evolution of this process. We therefore use this model integration for guidance in constructing a dynamical framework to interpret the observed circulation and its variability.

In summary: along the coast during the upwelling season in spring, there is an upward tilt of the isopycnals toward the coast directly forced by the winds in the Bight. As the spring transitions to the summer the upwelling winds relax in the Bight but are still strong in the region offshore, corresponding approximately to the continental slope (positive winds stress curl situation). Anomalous denser waters in the location of the Southern California Eddy are maintained and reinforced by the combined interaction of

the coastal/islands geometry and the wind stress curl (through Ekman dynamics). The process of adjustment to the appearance of denser water initiates a westward propagation of ocean density anomaly through Rossby waves, and reinforces the cyclonic gyre-like circulation of the SCE (increasing positive vorticity). Surface poleward flow, maintained by the positive wind stress curl, is also reinforced in proximity of Point Conception as a consequence of the adjustment. During the summer the cyclonic gyre becomes increasingly unstable as the core of the ocean anomalies crosses the continental slope. Instability processes within the cyclonic region, characterized by a sharp increase in eddy kinetic energy, shed eddies which leave the region either drifting to the west or interacting with existing eddies in the region offshore. The eddy kinetic energy reaches a seasonal maxima at the end of summer in the cyclonic region and late fall and winter further offshore where the eddies are fully developed.

The shedding of eddies cannot be directly seen in the CalCOFI observations because of the sampling aliasing. For this point we rely on the strong suggestion of the model, which we assume is able to capture the leading order dynamics. Additional integrations with a linearized version of the model are also presented to reinforce our interpretation of the westward propagation of the isopycnal anomalous displacement associated with Rossby wave dynamics.

2.1 Introduction

The southern component of the California Current System (SCCS, here defined as being South of Point Conception) was first described in an early report by Sverdrup

and Fleming [1941]. In their study based on ship cruise measurements, they isolate three circulation features: an offshore equatorward alongshore current (California Current, CC), a surface Inshore Countercurrent (IC) directed poleward along the coast, and a northward undercurrent (California Undercurrent, CU) over the continental slope at a depth of 200 meters. Because the IC does not always flow continuously around Point Conception, the recirculation feature that includes the inshore poleward current in the Southern California Bight and the offshore equatorward current has been referred to as the Southern California Eddy (SCE: [Schwartzlose, 1963]).

In 1949, following the effort of Sverdrup, the California Cooperative Fisheries Investigation (CalCOFI) began a routine sampling program of the physical and biological properties of the ocean off Central and Southern California at seasonal resolution. The program is still active today and observational studies make use of these hydrographic measurements to describe the seasonal and interannual variations of the circulation patterns in the SCCS [Lynn and Simpson, 1987; Hayward et al., 1994; Bograd et al., 2000].

Although CalCOFI provides an unprecedented timeseries of oceanographic data, the coarse spatial (80 km) and temporal (3 month) resolution of the sampling array leaves us with an incomplete understanding of the rich mesoscale oceanic structure that is more evident in satellite and drifter observations [Simpson and Lynn, 1990; Swenson and Niiler, 1996; Miller et al., 1999; Strub and James, 2000]. The effect of these mesoscale features on the variability of the mean and seasonal circulation is yet to be fully determined. Simplified numerical ocean models of the California Current System (CCS) isolate several physical processes as potential candidates in generating the observed variability [Paressierra and Obrien, 1989; Auad et al., 1991; Haidvogel et al., 1991;

Paressierra et al., 1993; Batteen, 1997], but the nature of these experiments does not allow for a quantitative assessment of the dominant physical processes of the real system. More sophisticated numerical models that incorporate realistic representation of the intricate California coastline and the outstanding topographic features [Marchesiello et al., 2003] can allow a more quantitative analysis of the CCS dynamics. These simulations generate realistic levels of variability along most of the US West Coast (USWC) north of Point Conception but poorly capture the statistics of the flow in the SCCS.

In the Southern California Bight (SCB) both the geometry and the circulation patterns differ dramatically from the ones north of Point Conception [Hickey, 1992]. Very close to the coast, the spatial and temporal characteristic of the currents depend on the local surface winds [Allen, 1980]. Regional winds which retain the effects of smaller scale coastal orography have not yet been included as forcing functions in numerical simulations of the circulation in the SCCS.

The objective of this study is to quantify the dominant physical processes that characterize the seasonal dynamics in the SCCS by using an ocean primitive equation model. Different available wind products, both from regional and large scale analysis, are used to force the model and the results are compared with the 50 year CalCOFI in situ observations. It is shown that the use of regional winds is critical to resolve the spatial and temporal patterns of the circulation. On the shelf the dominant signal of oceanic seasonal variability is associated with a quasi-linear response of the currents to changes in the winds. Off the continental shelf the variability is associated with ocean intrinsic variability characterized by a strong eddy field with energy spread over a broad frequency range.

A dynamical framework of the seasonal dynamics in the SCCS based on the model experiments validated with observations is provided. Important elements of the dynamics isolated in this study are: (a) the role of Ekman Pumping in intensifying the Southern California Eddy, (b) the timing of the seasonal cycle of the currents associated with westward propagation of ocean anomalies from the Southern California Bight and (c) the generation of eddies over the continental slope through barotropic and baroclinic instability.

We proceed now to introduce the model and data (2), comparisons of the mean and seasonal circulation of the model runs with observations (3), a linearized version of the ocean model to investigate the role of quasi-linear Rossby waves in the westward propagation of ocean anomalies from the SCB (4), the relationship between the winds and the current (5) and a dynamical framework of the SCCS to summarize the results (6).

2.2 Model, data and experiment setup

We use an eddy-resolving primitive equation ocean model called the Regional Ocean Modeling System (ROMS), a descendent of SCRUM [Song and Haidvogel, 1994]. The model uses a generalized sigma-coordinate system in the vertical and a curvilinear horizontal grid (9 km resolution) that extends about 1200 km along the U.S. West Coast from northern Baja to north of San Francisco Bay with roughly 1000 km offshore extent normal to the coast (Figure 2.1). The vertical grid has 20 levels with enhanced resolution in the surface and bottom boundary layer. The model bathymetry is obtained by a smooth interpolation of the ETOPO5 analysis [NGDC, 1998] and is characterized by an

extended (about 150-200 km) continental shelf in the Southern California Bight followed by a steep continental slope offshore.

A modified radiation condition [Marchesiello et al., 2001], which allows for stable, long-term integration of the model, is used at the three open boundaries together with a nudging term for relaxation to observed climatologies. The nudging is strong (timescale of 1 day) if the direction of the flow is inward and weak (timescale of 1 year) for the outflow. Marchesiello et al. [2003] have successfully used the model in this configuration to study the long-term equilibrium structures of the California Current over the entire U.S. West Coast. A more complete report of the model numerics, open boundary conditions and mixed layer parameterizations can be found in Shchepetkin and McWilliams [1998; 2003] and Large et al. [1994].

For the model initial condition and open boundary we use the Levitus et al. [1994] temperature (T) and salinity (S) monthly climatologies. At the surface, the model is forced with monthly climatologies for heat and freshwater flux derived from COADS [da Silva et al., 1994]. Different monthly wind-stress climatologies are used to test the model as follows:

RSM Case: The wind stress is obtained by averaging the daily output of a regional atmospheric model of Southern California to form monthly climatologies. The atmospheric regional model is part of the Experimental Climate Prediction Center (ECPC) forecasting system ([Roads et al., 2001], http://ecpc.ucsd.edu) and is used to downscale daily global NCEP analyses. The data available from ECPC runs from 1997 to current conditions. Building a monthly climatology with this shorter time series is questionable, since we only have 5 realizations for each month. Nevertheless, during this

time frame the system experienced both normal years and El Niño/La Niña events so that we can fairly assume that the mean monthly conditions will not be biased towards any of these states.

COADS Case: Monthly climatologies of wind stress at 2x2 degree resolution have been downloaded from the Climate Diagnostics Center (CDC) website (http://www.cdc.noaa.gov) and interpolated to the model grid. These winds are the same winds used by Mareschiello et al. [2003]. The COADS at 1x1 degree resolution did not show a well defined seasonal cycle in the SCB so the model results from this integration will not be presented.

NCEP Pacific Ocean Analysis Case: Monthly means (1980-present) of wind stress at 1x1.5 degree resolution were interpolated to the model grid. The NCEP Pacific Ocean Analysis data are provided by CDC (http://www.cdc.noaa.gov).

The observations we are trying to interpret are 50 years (1949 – present) of T and S CTD data collected from cruises by the California Cooperative Oceanic Fisheries Investigations (CalCOFI; http://www-mlrg.ucsd.edu/calcofi.html). The data has monthly resolution for the first 15 years and then varies from monthly to seasonal (four cruises per year). To compare the dataset with model runs we binned the cruises by month and objectively analyzed the data at standard depth from the surface to 500 m depth.

2.3 The Southern California Current System: Observation and model experiment results

In order to assess which model integration yields a better understanding of the physical processes that characterize the mean and seasonal variation of the SCCS, a comparison with observations is required. Our goal is to show that the model captures the leading order dynamics of the observed system when driven by adequately realistic atmospheric forcing. A rigorous quantitative measure of the model's skill in capturing the dynamics of the system based on individual synoptic observations is addressed in a different study by Di Lorenzo et al. [2003].

2.3.1 The mean

The CCS in Southern California between 29 N and 36 N, inferred from the CalCOFI hydrography, is described in the literature in terms of four distinct features: an offshore equatorward flow (California Current) located approximately 300 km from the coast, an inshore surface (Inshore Countercurrent) and sub-surface (California Undercurrent) poleward flow, and a region of cyclonic circulation (Southern California Eddy) that connects the inshore and the offshore circulation [Lynn and Simpson, 1987; Chereskin and Trunnell, 1996]. The mean circulation from CalCOFI hydrography is represented in Figure 2.2a as the depth h of the density surface ϱ = 26.5 which approximately corresponds to the interfacial depth of the first baroclinic mode. The main circulation patterns in this map are now compared to those obtained by integrating the model with different wind forcing.

California Current (CC): Offshore equatorward flow in CalCOFI observations is found in all seasons (Figure 2.3) and thus appears as a strong signal in the annual mean circulation (Figure 2.2a). The model experiments all capture this equatorward flow (Figure 2.2). The pattern correlation coefficient (Corr.) with CalCOFI (Figure 2.2a) is 0.9 in RSM (Figure 2.2b), 0.79 in NCEP (Figure 2.2d) and 0.85 in COADS (Figure 2.2c). A more stringent test of verisimilitude is to compare the gradient of the interfacial height ($\approx dh/dx$) which is a proxy for the geostrophic flow at that level. By this index the modeled alongshore geostrophic flow associated with the core of the CC does not correlate well with that observed. In Cases COADS and NCEP, the flow is much weaker than in CalCOFI and the spatial structure is broader (correlations near zero). The strength of the flow in Case RSM is more similar to CalCOFI than either other case, and the pattern correlation is relatively high (Corr. =0.48).

Inshore Countercurrent (IC): Poleward inshore coastal flow in the observations is characterized by pronounced seasonal variability in the Southern California Bight, stronger in the summer and almost zero in spring (Figure 2.3). In the mean it appears as the inshore components of the Southern California Eddy (Figure 2.2a). In Cases COADS (Figure 2.2c) and NCEP (Figure 2.2d), a clear expression of inshore poleward flow in the Bight cannot be found. On the contrary, Case RSM shows a strong poleward flow that extends from the Bight to north of Point Conception. A qualitative explanation for the differences in the model experiments is associated with the different patterns of the mean wind stress curl in the Bight. Studies by Oey [1999] and McCreary et al. [1987] suggest that the forcing mechanisms of the poleward flow rely on positive wind stress curl and its

alongshore gradient. NCEP (Figure 2.4d) and COADS (Figure 2.4c) wind stresses have a weak or almost zero curl along the coast in the Bight, therefore missing these forcing mechanisms. In RSM winds, the region of positive wind stress curl is well defined and strong in the coastal shelf region, supporting the idea of a relationship between curl of the winds and poleward flow in the Southern California Bight. A more detailed discussion of the dynamics of this poleward flow and its vertical structure, as inferred by the ocean model experiments of this study will be addressed in a later paper by Di Lorenzo et al..

Southern California Eddy (SCE): The cyclonic gyre-like circulation south of Point Conception is a prominent feature in mean dynamic height maps from CalCOFI hydrography. On seasonal timescales the SCE is better described as a region of recirculation with offshore equatorward flow and inshore poleward flow rather than a closed eddy. Indeed, a closed gyre, with structure resembling this mean flow, cannot be identified in any of the individual CalCOFI synoptic maps or in the more recent ADCP current analyses [Bray et al., 1999]. The strength of this recirculation has a clear seasonal cycle being strongest in the summer when the IC has its seasonal maximum [Lynn and Simpson, 1987] and almost zero during the upwelling season in springtime.

Case COADS (Figure 2.2c) is clearly unable to capture the spatial pattern of this recirculation region. Case NCEP has a weak and offshore signature of the recirculation. Only Case RSM (Figure 2.2b) has a strong and nearshore recirculation as observed in CalCOFI.

Mean wind stress curl maps of the different forcing (Figure 2.4) show a strong local correlation between the positive wind curl and the location of the model SCE

recirculation. In Case RSM, the positive wind stress curl is very strong and close to shore as is the recirculation. In Case NCEP, the recirculation (Figure 2.2d) pattern is farther offshore and tracks the offshore region of positive wind stress curl (Figure 2.4d). In Case COADS, there occurs no region of positive wind stress curl at the coast (Figure 2.4c) and no clear recirculation.

We note that the region of maximum positive wind stress curl in Case RSM is not as far inshore as that of the product derived by Winant and Dorman [1997] from buoy winds in the SCB which show a strong peak in the Santa Barbara Channel. The SCE, and its dynamics, can be further understood in the context of the seasonal cycle, which we address in the next section.

2.3.2 The seasonal cycle

Although characterizing the mean circulation in a schematic way is useful and has been adopted by most authors when describing the Southern component of the California Current System (SCC) [Lynn and Simpson, 1987; Chereskin and Trunnell, 1996; Hickey, 1998], it is also important to recognize that any given synoptic map will hardly resemble this schematic picture. Satellite observations of SST and SSH have revealed a variety of mesoscale features such as cold filaments [Strub et al., 1991] and mushroom shaped SST patterns [Mied et al., 1991] associated with the strong eddy field.

Strub and James [2000] suggested that the primary source of energy for these eddies is the potential energy of a density front in proximity of the coast generated by the upwelling winds in spring. They characterized the seasonal cycle of eddy kinetic energy

(EKE) in the context of the seasonal wind variations along the coast of California as follows. (a) An equatorward coastal jet develops along the coast in spring with the strong upwelling winds. (b) The jet undergoes westward displacement away from the coast, during spring and summer, likely associated with Rossby wave dynamics. (c) During this offshore propagation, dynamical instabilities associated with the jet and with baroclinic energy conversion from the density front are the generating mechanism of the eddies and meanders of the CC. (d) Along the coast a surface poleward flow develops and intensifies during summer and fall. (e) In winter and early spring the jet has dissipated its energy and a weaker equatorward flow is typically found in the offshore waters. The cycle starts again with the new upwelling winds in the following spring.

A prominent and important component of the seasonal cycle, as depicted by Strub, is the westward propagation. Kelly et al. [1998] documented a region of maximum EKE migrating westward on seasonal timescales associated with instabilities in the core of the CC.

The CalCOFI hydrography (Figure 2.6) and the 10-day average TOPEX/ERS maps (Figure 2.5) also suggest an annually recurrent westward propagation of SSH anomalies that originated in the Southern California Bight (SCB) during the upwelling season. The kinematics differ from that described by Strub and James [2000] because of the complex geometry and forcing in the Southern California Bight, but the general character is similar. We therefore seek the signature of this dynamical feature in the model integrations as a qualitative measure of the ability of the different winds to generate the seasonal cycle with the correct time and space signature.

For the model-data comparison we choose the east-west transect W1 (Figure 2.1) of the anomalous depth *h* of the density layer 26.5, plotted as a function of the month of the year (Figure 2.6). The first element common to all of the model integrations and the observations is the signature of the upwelling winds in April. This can be seen as the shoaling of the density layer at the coast (dark negative values to the right in all panels of Figure 2.6). As we progress towards the summer, Cases COADS (Figure 2.6c) and NCEP (Figure 2.6d) show a clear westward propagation of the disturbances that originated at the coast. In CalCOFI (Figure 2.6a) the disturbance develops throughout the spring and early summer over the entire shelf region in contrast to Cases NCEP and COADS in which the disturbances develop only in a very narrow coastal band. Furthermore the westward propagation in CalCOFI (Figure 2.6a), only occurs offshore of the shelf region with a maximum at the end of the summer (from arrow a to arrow b in 6a). Although the phase speed of the disturbances in Cases COADS and NCEP is comparable with the observations (arrow b in Figure 2.6 a, c, d), the spatial development of these anomalies and their path is not captured. We therefore conclude that these two wind forcing datasets are inadequate to investigate the seasonal dynamics of the Southern California Current System.

We now focus our attention on the RSM (Figure 2.6b) experiment. We first note that the pattern correlation coefficient with CalCOFI (0.73) is significantly higher than in Cases COADS (Figure 2.6c) and NCEP (Figure 2.6d). The development of the seasonal anomaly occurs over the entire shelf region as observed in CalCOFI and the propagation path (arrow a and b in Figure 2.6) is comparable with the observed as well.

The timing and spatial distribution of the anomaly in Case RSM seems to be associated with the seasonal development of stronger positive wind stress curl over the entire shelf region during the upwelling season (April, Figure 2.7a). This positive wind stress curl pattern persists and intensifies during the summer over the shelf in the RSM wind product and is consistent with observational studies [Bakun and Nelson, 1991; Winant and Dorman, 1997], although the exact spatial pattern and amplitude are still a matter of discussion. The mean wind stress curl spatial pattern in the RSM product (Figure 2.4b) has maximum curl further offshore than the observed (from Winant and Dormant, 1991) and has amplitude that is 25% smaller.

Before ending this section it is useful to investigate the relationship between wind forcing and the oceanic depth anomaly in Cases NCEP and COADS as a measure of the sensitivity of the circulation to changes in the winds. In Case NCEP the positive wind stress curl is located offshore (Figure 2.7c) and it forces a westward propagating depth anomaly in the deeper ocean (Figure 2.6d). This offshore pulse is independent of the one generated in the near coastal region (Figure 2.6d) from the upwelling winds. The Rossby wave response to Ekman pumping in the California offshore waters has been previously suggested by Kelly et al. [1993]. In Case COADS the upwelling favorable winds generate a depth anomaly only along the coast (Figure 2.6d). The wind stress curl in COADS is so weak that we only plot a transect of the alongshore component of the wind stress in Figure 2.7c.

In summary we suggest that the seasonal development of the ocean anomaly in the bight is strongly controlled by both the alongshore winds (coastal upwelling) and the positive wind stress curl acting over the entire shelf region (Ekman pumping) between

spring and summer. The westward propagation of the ocean anomaly from the continental shelf cannot be explained in terms of wind forcing alone, but requires an understanding of the dynamical response of the ocean. A more careful analysis of the dynamics is provided in the following sections under the assumption that the ocean model forced with the RSM winds captures the leading order seasonal dynamics of the system and therefore can be used as a guide.

2.4 Linearized dynamics and westward propagation

We now attempt to evaluate the extent to which the dynamics of westward propagating disturbances that originate on the shelf region in the Southern California Bight can be explained in the framework of quasi-linear long waves forced by the wind. In order to do so we linearize the primitive equation model around a state of rest and force it with the RSM winds. In the linearization we also drop the advection term $u' \cdot \nabla \overline{\rho}$. This is motivated by our interest in retaining only the long wave response of the system and the linearization around a state of rest. Under this assumption, advection appears as a second order term in the expansion, so that the equation for the perturbation density in the interior to first order becomes:

$$\frac{\partial \rho'}{\partial t} + w' \cdot \frac{\partial \overline{\rho}}{\partial z} \approx 0$$

We integrate the linearized model for 12 years. No eddies are found in the model results. Each model year shows the same seasonal cycle in which the dominant variability is associated with the development of SSH anomalies on the shelf region and their

westward propagation towards the deep ocean (Figure 2.8a). A comparison of this signal with the one in the non-linear RSM integration along the westward transect W1 (Figure 2.1), reveals that the linearized model is able to explain up to 80% of the temporal variance of the density surface (26.5) depth anomaly in the region of strongest positive wind stress curl (Figure 2.7a). In this shelf region the Ekman pumping (through w' in the perturbation density equation) is the generating mechanism of the density surface depth anomaly. (Note: because we are only resolving the long wave response of the system, the linearized model is unable to resolve the contribution of upwelling due to the alongshore component of the wind at the coast (Figure 2.8c 0)). As we proceed westward along the transect W1, the explained variance drops to 62 % over the continental slope (hereinafter referred to as the *transition zone* in Figure 2.8c 2), and 40% further offshore (hereinafter referred to as the *eddy field zone* in Figure 2.8c 3). In the *transition* and *eddy field zone* the positive wind stress curl is now negligible (Figure 2.7a) and the explained variance is associated with westward propagating disturbances excited on the shelf.

In order to assess the relative contribution of Rossby wave dynamics controlled by the beta effect versus other types of dynamics, we make an additional integration of the linearized model on the *f*-plane. The result of this integration (Figure 2.8b) shows the same seasonal development of SSH anomaly in the region of strong positive wind stress curl but not the westward propagation beyond the continental slope. We therefore are confident that the assumption of quasi-linear Rossby waves to explain the westward propagation is valid. Notice that in the *f*-plane case the depth anomaly perturbation on the shelf persists longer throughout the fall.

It is also interesting to note that far from the coast on transect W1 the explained variance associated with the quasi-linear Rossby waves that have successfully propagated to the deeper ocean increases to 85% (Figure 2.8c 4). This suggests that other processes are important in the *eddy field zone* (Figure 2.8c 2 and 3). An energetic analysis of the non-linear RSM integration case suggests that instability processes on the continental slope (Figure 2.8c 2) contribute to increasing the energy of the offshore mesoscale *eddy field zone*, defined as the region of maximum variance of SSH anomalies. The non-linear component of these eddies cannot be captured by the linearized model.

In summary, the linearized model analysis suggests the existence of a shelf region and *transition zone*, in which the dominant dynamical signal is controlled by a quasi-linear response to the changes in the forcing, an *eddy field zone*, in which the dominant dynamics are non-linear, and a further offshore region (Figure 2.8c 4) where the linear dynamics are recovered. This distinction is also evident in a spectral analysis of the SSH anomalies in the inshore region (Figure 2.9a), defined as the shelf and continental slope, and in the offshore region (Figure 2.9b). The linearized model average spectra (blue line) in the inshore and offshore region are essentially the same showing a strong peak at the frequency of the seasonal cycle and its harmonics. The same spectral analysis on the non-linear model (red line) shows similar peaks in the inshore region but noticeable differences in the offshore spectra. In particular in the offshore region the seasonal peak and its harmonics are no longer separable. The offshore spectral energy in the non-linear case is much higher and spreads uniformly across the seasonal to intra-seasonal frequency band, indicating the presence of the eddy field. It is noteworthy that the energy of the

non-linear model is also higher in the inshore region, but not nearly as much as in the offshore.

Based on this analysis, which suggests that the inshore seasonal circulation can be largely explained by a linear dynamical response of the circulation to the forcing. In the next section we attempt to linearly decompose the forcing and circulation patterns.

2.5 Relationship between the winds and circulation patterns

We have identified that the dominant component of the seasonal variability of the oceanic thermocline is the upward titling of the isopycnals at the coast and over the shelf region. This is forced by the intensification of the alongshore winds and the positive wind stress curl during spring and part of the summer. In the previous section we also verified that the ocean response also involves westward propagation that can be explained through quasi-linear Rossby wave dynamics in the region of the continental slope and deeper ocean.

To succinctly describe the spatial and temporal evolution of the seasonal circulation and wind forcing over the shelf region we linearly decompose the density surface (26.5) depth anomaly ($\perp h$) and the wind stress curl anomaly using empirical orthogonal functions (EOFs). Figure 2.10 shows the spatial pattern and the temporal amplitudes for the first two modes which together account for more than 95% of the seasonal variance (80-85% for first mode and 10-14% for the second).

The first mode of $\perp h$ shows a region of strong negative anomaly (low) over the northern part of the shelf region (Figure 2.10a, color bars are not the same in each panel).

Negative anomalies indicate an upward tilting of the density surface, so that the low is interpreted as an intensification of cyclonic circulation. This intensification is clearly associated with the input of relative vorticity by the anomalous positive wind stress curl (Figure 2.10b) through Ekman Pumping, as previously verified in the linearized model. The intensification of one cyclonic gyre as it appears in the 1st mode is rarely observed in synoptic maps of the ocean model circulation. The increase in relative vorticity of the currents does not spatially match the smooth pattern of the positive wind stress curl used to force the model because of the geometrical constraints of islands and sudden changes in the topography that affect the flow field. In the real ocean non-seasonal winds introduce even more ambiguity in identifying a clear closed cyclonic gyre intensification in the observations. This explains why the Southern California Eddy is a feature that is strongly evident in the mean but is hardly ever observed in a synoptic map.

Observations shows that the Southern California Eddy has a seasonal peak toward early summer [Lynn and Simpson, 1987]. The temporal evolution of the first modes of $\nabla^{-1}b$ (Figure 2.10c) and the anomalous wind stress curl (Figure 2.10f) also show a peak towards early summer and are strongly correlated.

In the second mode we find an inshore/offshore dipole in the ocean $\nabla^{-1}b$ anomalies (Figure 2.10b). The sign of the mode is negative inshore and positive offshore during late winter and spring as seen in the temporal evolution of the amplitude (Figure 2.10c). Towards summer the amplitude of the mode switches sign sharply to positive. The maximum of the positive phase is reached in the summer and then decays towards negative values during the end of fall. A physical interpretation is as follows: during early spring the upwelling winds (associated with positive wind curl at the coast) force

equatorward flow along the coast (associated with negative $\nabla\perp h$ at the coast). Toward summer the anomalous wind stress curl at the coast becomes negative and intensifies poleward flow in the bight (positive $\nabla\perp h$ at the coast). It is important to notice that the mode 2 principal component of wind (Figure 2.10f) leads that of the ocean during winter and spring but lags during late summer. This is the signature of the offshore propagation of the $\nabla\perp h$ anomaly associated with Rossby dynamics which acts on a time scale faster than the wind stress curl anomaly reversal.

2.6 Conclusions

A numerical ocean simulation that uses downscaled winds from a regional atmospheric model (Case RSM) as surface forcing is successful in capturing the mean and seasonal circulation in the SCCS as observed in the CalCOFI in situ long-term hydrographic data. The seasonal cycle in the model is characterized by an annually recurrent westward propagation of a negative isopycnal depth anomaly that develops over the entire continental shelf during upwelling favorable winds in spring and summer. Sensitivity analysis of the ocean model to different wind forcing, including large-scale analyses and downscaled products, reveals that the spatial and temporal signature of these anomalies depends strongly on the details of wind stress and its curl. A linearized version of the model, which only includes the long-wave response of the oceanic system, shows that quasi-linear Rossby wave dynamics explains a significant fraction of the variance (up to 80 %) associated with the westward propagation in the non-linear model. The explained variance is higher in the near shore regions where the circulation responds

more linearly to changes in the forcing, as confirmed by a distinct seasonal peak in the energy spectra of SSH anomalies. Farther offshore this peak is not as clear and the spectral energy spreads over a broader range of frequencies. In this region, referred as the mesoscale *eddy field zone*, the linearized model explains a smaller fraction of the variance (about 40 %) and other processes such as baroclinic and barotropic instabilities become important dynamical elements.

A conceptual dynamical framework that summarizes the relationship between the winds and the seasonal circulation in the Southern California Current System as deduced from the observational and ocean model analysis is as follows:

1) In spring, strong upwelling winds along the coast generate an upward tilt of the isopycnals in the Bight, thereby developing a negative anomaly (Δh) of the density surface (Figure 2.11a) and southward flow along the coast in the Bight.

2) As the spring transitions to the summer (Figure 2.11b) the upwelling winds relax in the Bight but are still strong further offshore over the continental slope (positive winds stress curl in the SCB). Adjustment of the anomalously dense waters in the coastal upwelling region initiates a westward displacement of the ocean density anomaly. Coastal poleward flow develops as the density anomaly progresses westward over the shelf region.

3) The shoaling of isopycnals over the northern part of the shelf is reinforced by Ekman pumping (Figure 2.11b). The combined action of the wind stress curl and the coastal deflection of the poleward flow generate positive relative vorticity (reinforcing cyclonic recirculation) in early summer. This is historically referred to in the literature as the Southern California Eddy in the northern part of the shelf. Because of the geometry of the domain (coastline, topography, and islands in particular), the relative vorticity of the

flow is not spatially uniform as the density anomaly and a closed cyclonic eddy is hardly ever observed in individual synoptic maps of the ocean.

3) As summer progresses, the westward propagation of the $\nabla^4 h$ anomaly over the entire Southern California Bight region continues further offshore while along the coast poleward flow intensifies. The intensification and dynamics of the poleward flow has not been addressed explicitly in this study. However, our results corroborate previous work which suggests that poleward flow along the coast requires positive wind stress curl [Oey, 1999].

4) Towards the end of summer the recirculation region is broader and becomes increasingly unstable as the core of the ocean $\nabla^4 h$ anomaly crosses the continental slope (Figure 2.11c). Instability processes, characterized by barotropic and baroclinic energy conversion terms of comparable amplitude (not shown), are a generating mechanism for eddies at this point of the seasonal cycle. These eddies are commonly found in observations and are a robust feature in the numerical model. Their signature is also found in the model EKE (Figure 2.12), which reaches a seasonal maximum at the end the summer in the cyclonic recirculation region (over the continental slope where the instabilities develop) and in late fall further offshore where the eddies are fully developed. A careful look at an animation of the model SSH anomaly (http://horizon.ucsd.edu/movies/rsm-dssh.gif) confirms this view of the seasonal cycle in the surface EKE and shows the complicated evolution of the generated eddies.

References

Allen, J. S., Models of Wind-Driven Currents on the Continental-Shelf, *Annual Review of Fluid Mechanics*, 12 389-433, 1980.

Auad, G., A. Paressierra and G. K. Vallis, Circulation and Energetics of a Model of the California Current System, *Journal of Physical Oceanography*, 21 (10), 1534-1552, 1991.

Bakun, A. and C. S. Nelson, The seasonal cycle of wind-stress curl in subtropical eastern boundary current regions, *Journal of Physical Oceanography*, 21 1815-1834, 1991.

Batteen, M. L., Wind-forced modeling studies of currents, meanders, and eddies in the California Current system, *Journal of Geophysical Research-Oceans*, 102 (C1), 985-1010, 1997.

Bograd, S. J., P. M. Digiacomo, R. Durazo, T. L. Hayward, K. D. Hyrenbach, R. J. Lynn, A. W. Mantyla, F. B. Schwing, W. J. Sydeman, T. Baumgartner, B. Lavaniegos and C. S. Moore, The state of the California Current, 1999-2000: Forward to a new regime?, *California Cooperative Oceanic Fisheries Investigations Reports*, 41 26-52, 2000.

Bray, N. A., A. Keyes and W. M. L. Morawitz, The California Current system in the Southern California Bight and the Santa Barbara channel, *Journal of Geophysical Research-Oceans*, 104 (C4), 7695-7714, 1999.

Chereskin, T. K. and M. Trunnell, Correlation scales, objective mapping, and absolute geostrophic flow in the California Current, *Journal of Geophysical Research-Oceans*, 101 (C10), 22619-22629, 1996.

da Silva, A., C. Young and S. Levitus, Atlas if Surface Marine Data 1994, *NOAA Atlas NESDIS 6-10. U.S. Gov. Printing Office, Wash., D.C.*, 1-5, 1994.

Di Lorenzo, E., A. J. Miller, D. J. Neilson, B. D. Cornuelle and J. R. Moisan, Modeling observed California Current mesoscale eddies and the ecosystem response, *International Journal of Remote Sensing*, (in press), 2003.

Haidvogel, D. B., A. Beckmann and K. S. Hedstrom, Dynamic Simulations of Filament Formation and Evolution in the Coastal Transition Zone, *Journal of Geophysical Research-Oceans*, 96 (C8), 15017-15040, 1991.

Hayward, T. L., A. W. Mantyla, R. J. Lynn, P. E. Smith and T. K. Chereskin, The State of the California Current in 1993-1994, *California Cooperative Oceanic Fisheries Investigations Reports*, 35 19-35, 1994.

Hickey, B. M., Circulation over the Santa-Monica San-Pedro Basin and Shelf, *Progress in Oceanography*, 30 (1-4), 37-115, 1992.

Hickey, B. M., Coastal oceanography of western North America from the tip of Baja California to Vancouver Island. Coastal segment., *The Sea*, 11 (eds. A.R. Robinson and K.H. Brink, New York, John Wiley and Sons), 345-391, 1998.

Kelly, K. A., R. C. Beardsley, R. Limeburner, K. H. Brink, J. D. Paduan and T. K. Chereskin, Variability of the near-surface eddy kinetic energy in the California Current based on altimetric, drifter, and moored current data, *Journal of Geophysical Research-Oceans*, 103 (C6), 13067-13083, 1998.

Kelly, K. A., M. J. Caruso and J. A. Austin, Wind-Forced Variations in Sea-Surface Height in the Northeast Pacific-Ocean, *Journal of Physical Oceanography*, 23 (11), 2392-2411, 1993.

Large, W. G., J. C. McWilliams and S. C. Doney, Oceanic Vertical Mixing - a Review and a Model with a Nonlocal Boundary-Layer Parameterization, *Reviews of Geophysics*, 32 (4), 363-403, 1994.

Levitus, S., R. Burgett and T. P. Boyer, World Ocean Atlas 1994, *NOAA Atlas NESDIS 4, U.S. Gov. Printing Office, Wash., D.C.*, 3-4 1994.

Lynn, R. J. and J. J. Simpson, The California Current System - the Seasonal Variability of Its Physical Characteristics, *Journal of Geophysical Research-Oceans*, 92 (C12), 12947-&, 1987.

Marchesiello, P., J. C. McWilliams and A. Shchepetkin, Open boundary conditions for long-term integration of regional oceanic models, *Ocean Modelling*, 3 1-20, 2001.

Marchesiello, P., J. C. McWilliams and A. Shchepetkin, Equilibrium Structure and dynamics of the California Current System., *Journal of Physical Oceanography*, in press 2003.

McCreary, J. P., P. K. Kundu and S. Y. Chao, On the Dynamics of the California Current System, *Journal of Marine Research*, 45 (1), 1-32, 1987.

Mied, R. P., J. C. McWilliams and G. J. Lindemann, The Generation and Evolution of Mushroom-Like Vortices, *Journal of Physical Oceanography*, 21 (4), 489-510, 1991.

Miller, A. J., J. C. McWilliams, N. Schneider, J. S. Allen, J. A. Barth, R. C. Beardsley, F. P. Chavez, T. K. Chereskin, C. A. Edwards, R. L. Haney, K. A. Kelly, J. C. Kindle, L. N. Ly, J. R. Moisan, M. A. Noble, P. P. Niiler, L. Y. Oey, F. B. Schwing, R. K. Shearman and M. S. Swenson, Observing and modeling the California Current System, *Eos, Transactions, American Geophysical Union*, (80), 533-539, 1999.

NGDC, Digital relieve of the surface of the Earth, *NOAA, National Geophysics Data Center, Boulder, Colorado*, (Data announcement 88-MG-02), 1998.

Oey, L. Y., A forcing mechanism for the poleward flow off the southern California coast, *Journal of Geophysical Research-Oceans*, 104 (C6), 13529-13539, 1999.

Paresierra, A. and J. J. O'brien, The Seasonal and Interannual Variability of the California Current System - a Numerical-Model, *Journal of Geophysical Research-Oceans*, 94 (C3), 3159-3180, 1989.

Paresierra, A., W. B. White and C. K. Tai, Wind-Driven Coastal Generation of Annual Mesoscale Eddy Activity in the California Current, *Journal of Physical Oceanography*, 23 (6), 1110-1121, 1993.

Roads, J., S. C. Chen, J. Ritchie, F. Fujioka, H. Juang and M. Kanamitsu, ECPC's Global to Regional Fire Weather Forecast System, *Early warning systems for natural disaster reduction*, 2001.

Schwartzlose, R. A., Nearshore currents of the Western United States and Baja California as measured by drift bottles., *California Cooperative Oceanic Fisheries Investigation Progress Report, 7-1-60 to 6-3-62, Marine Research Committee, California Department of Fish and Game, Sacramento, California*, 15-22, 1963.

Shchepetkin, A. and J. C. McWilliams, Quasi-monotone advection schemes based on explicit locally adaptive dissipation, *Monthly Weather Review*, (126), 1541-1580, 1998.

Shchepetkin, A. and J. C. McWilliams, A method for computing horizontal pressure-gradient force in an oceanic model with a non-aligned vertical coordinate, *Journal of Computational Fluid Dynamics*, in press 2003.

Simpson, J. J. and R. J. Lynn, A Mesoscale Eddy Dipole in the Offshore California Current, *Journal of Geophysical Research-Oceans*, 95 (C8), 13009-13022, 1990.

Song, Y. H. and D. Haidvogel, A Semiimplicit Ocean Circulation Model Using a Generalized Topography-Following Coordinate System, *Journal of Computational Physics*, 115 (1), 228-244, 1994.

Strub, P. T. and C. James, Altimeter-derived variability of surface velocities in the California Current System: 2. Seasonal circulation and eddy statistics, *Deep-Sea Research Part Ii-Topical Studies in Oceanography*, 47 (5-6), 831-870, 2000.

Strub, P. T., P. M. Kosro and A. Huyer, The Nature of the Cold Filaments in the California Current System, *Journal of Geophysical Research-Oceans*, 96 (C8), 14743-14768, 1991.

Sverdrup, H. U. and R. H. Fleming, The waters off the coast of Southern California, *Scripps Inst. Oceanography Bulletin*, (4), 261-387, 1941.

Swenson, M. S. and P. P. Niiler, Statistical analysis of the surface circulation of the California Current, *Journal of Geophysical Research-Oceans*, 101 (C10), 22631-22645, 1996.

Winant, C. D. and C. E. Dorman, Seasonal patterns of surface wind stress and heat flux over the Southern California Bight, *Journal of Geophysical Research-Oceans*, 102 (C3), 5641-5653, 1997.

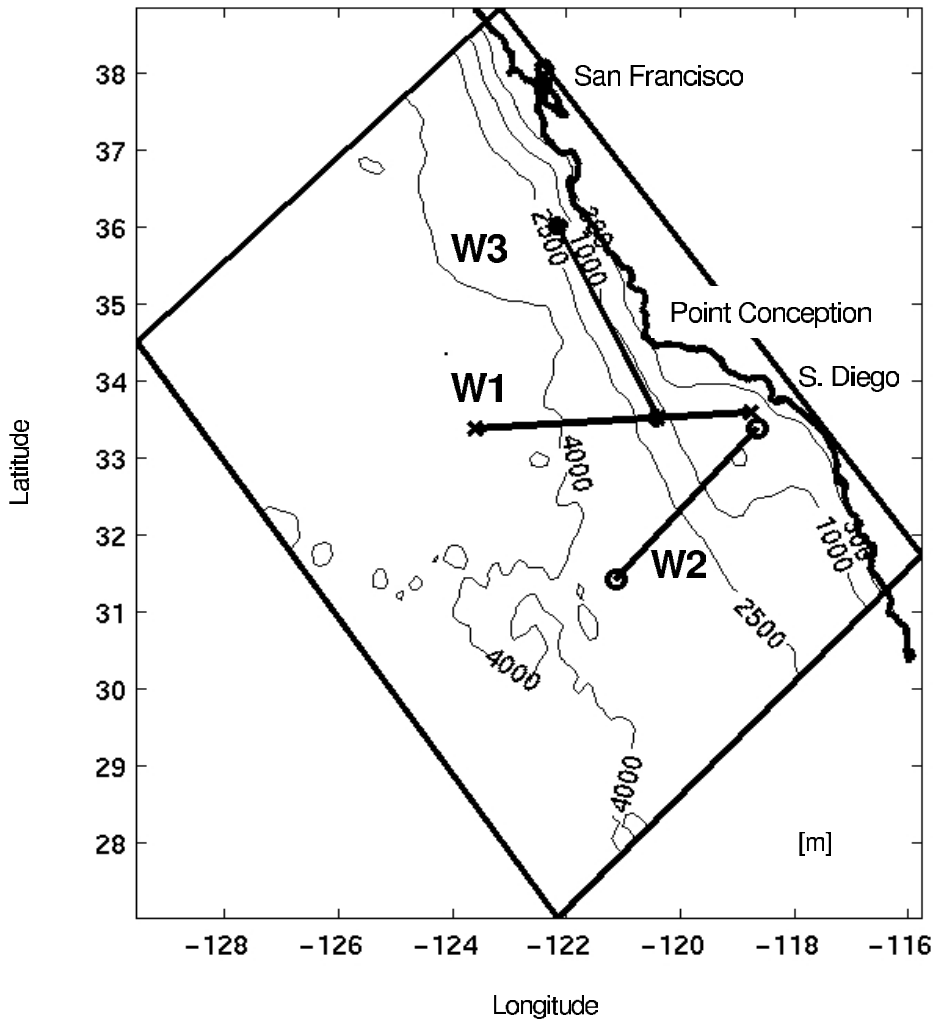

Figure 2.1. Model domain, coast line and bathymetry [m] . Superimposed W1 westward transect, W2 cross-shore transect and W3 northward transect following topographic slope.

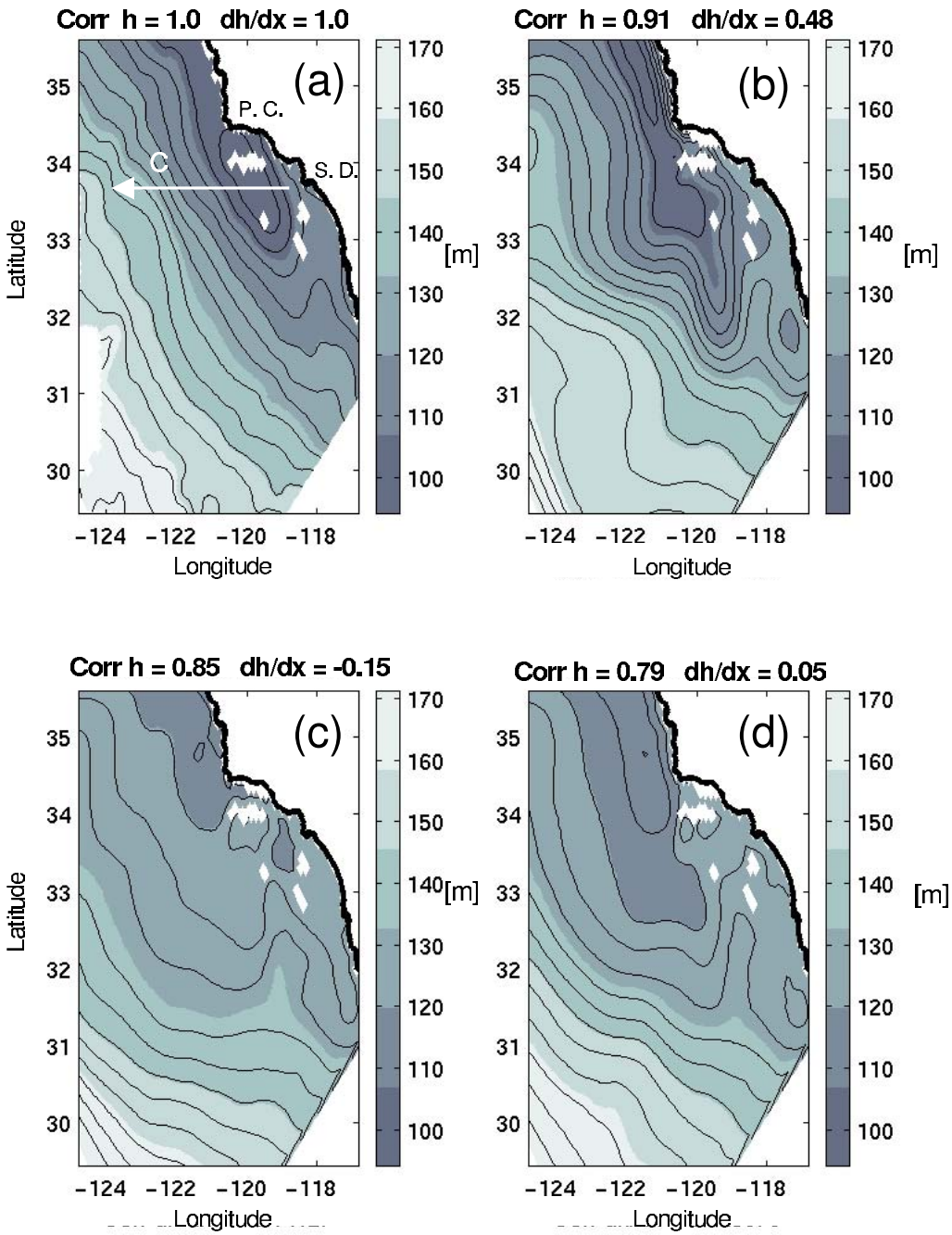

Figure 2.2. Mean depth h of the 26.5 isopycnal (a) from CalCOFI observations compared to the one obtained by integrating the model with the (b) RSM winds, (c) COADS 2x2 and (d) NCEP Pacific Ocean Analysis. The correlation pattern coefficient of the model field with observations are indicated in the top label for each panel.

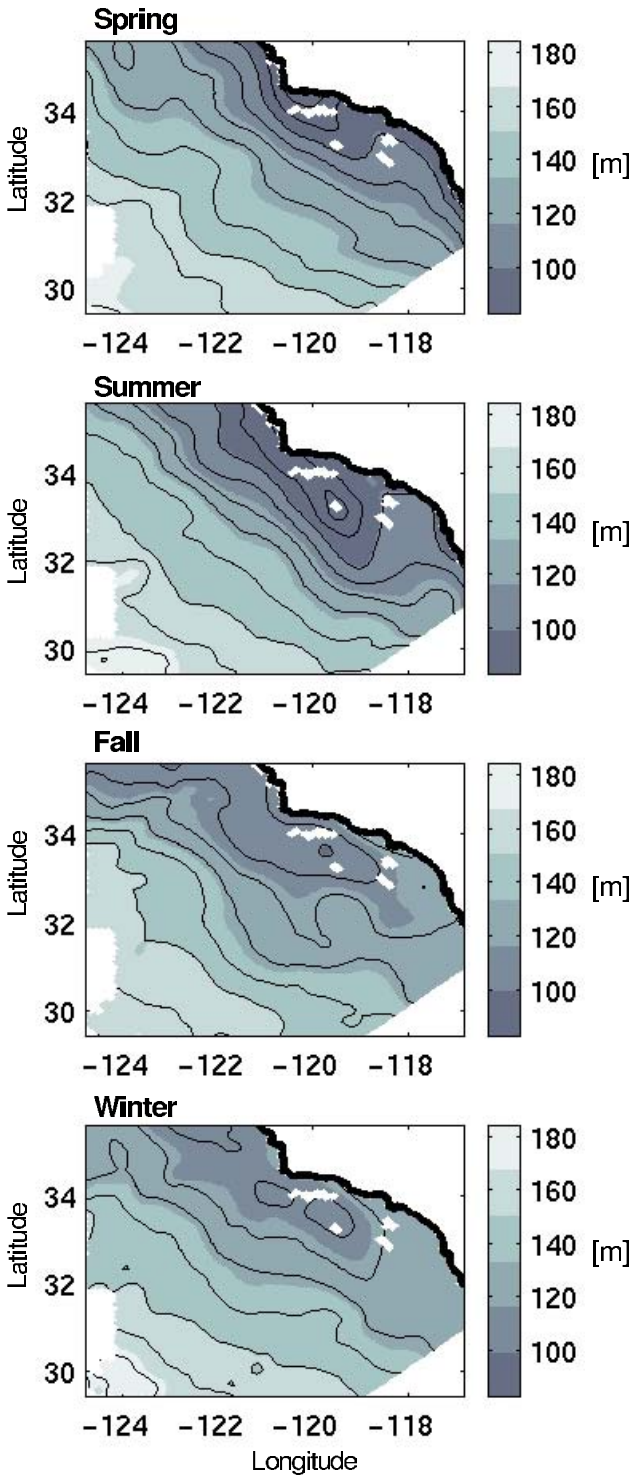

Figure 2.3. Mean depth h of the 26.5 isopycnal from CalCOFI observations for the seasons of spring, summer, fall and winter. Contour interval is 10 meters.

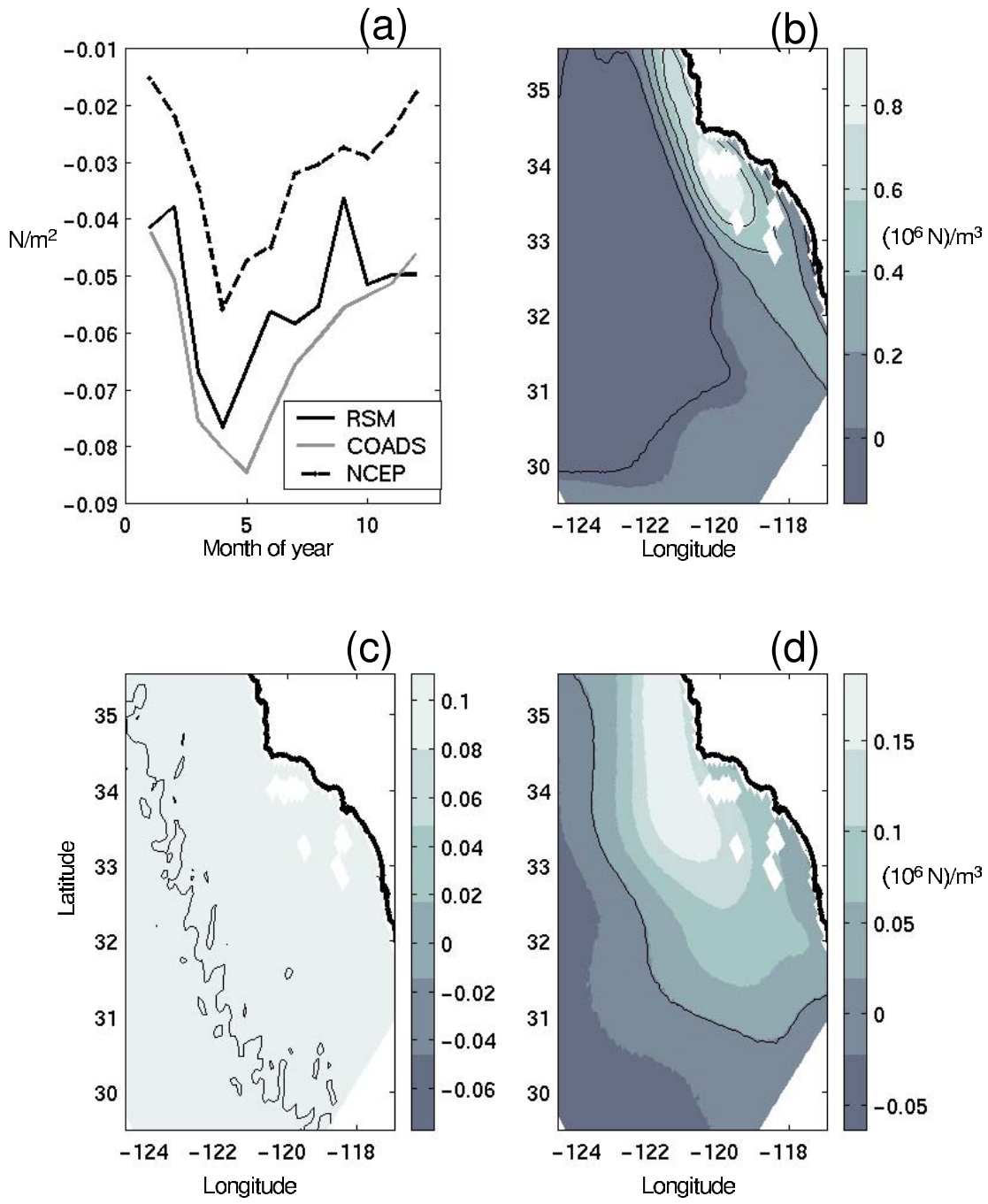

Figure 2.4. (a) Seasonal cycle of alongshore winds averaged over model domain (negative is towards the south) for the three different cases. Mean wind stress curl of (b) RSM winds, (c) COADS 2x2 and (d) NCEP Pacific Ocean Analysis. The color bars are different on each panel in order to better show the contours.

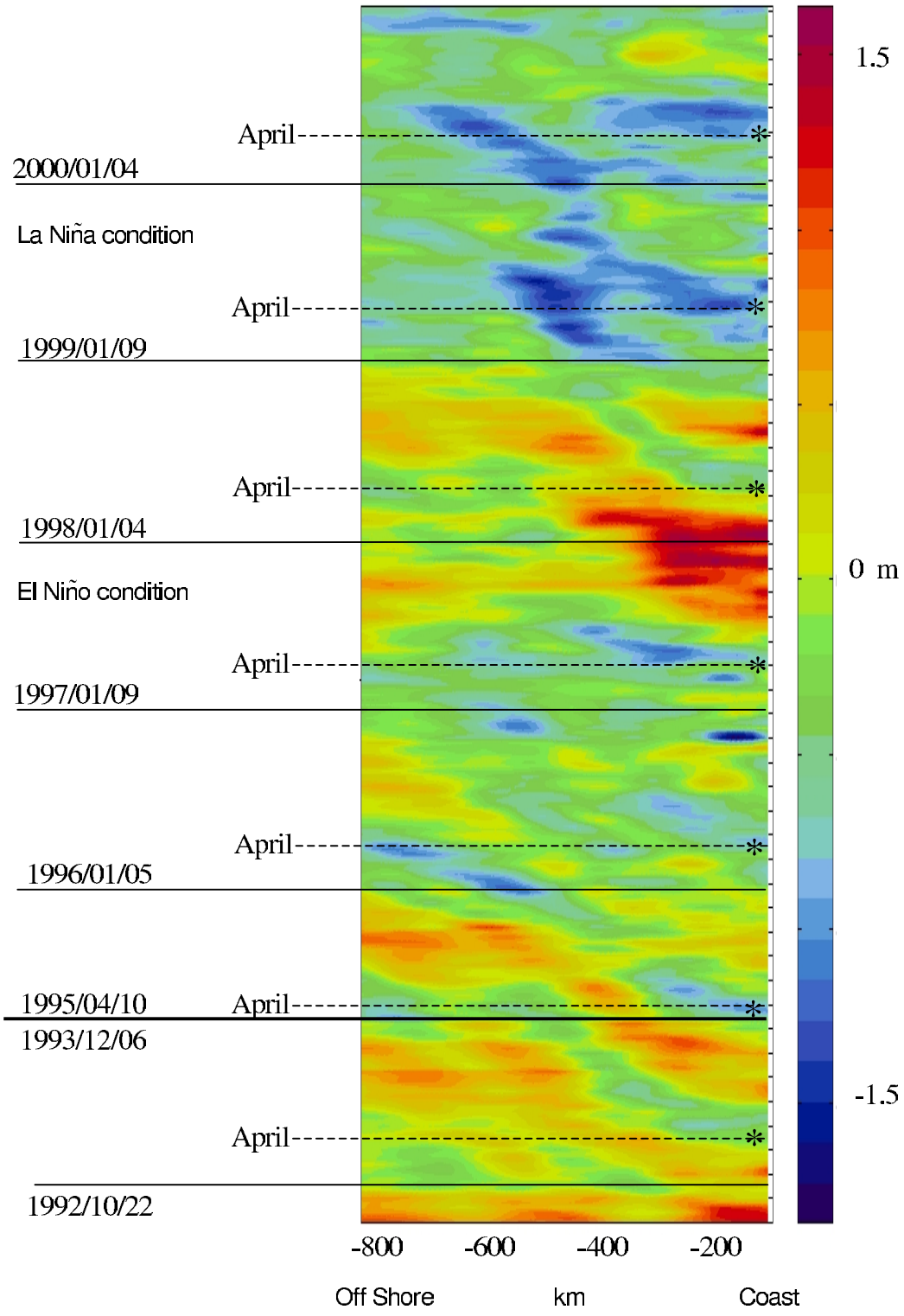

Figure 2.5. Hofmuller plots of SSH anomalies from TOPEX/ERS 10 days maps averaged alongshore.

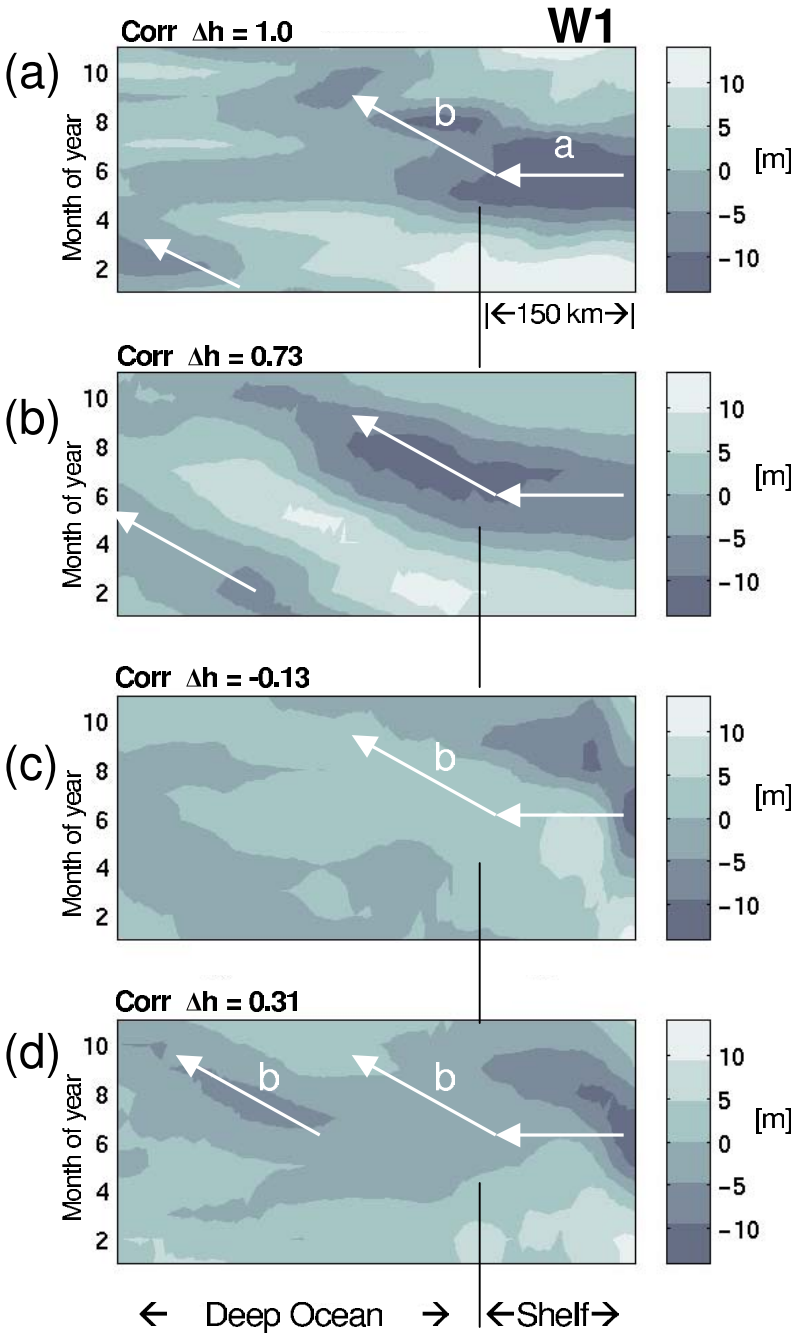

Figure 2.6. Westward transect W1 (x axis) of the mean 26.5 isopycnal depth anomaly ($\perp h$) as a function of month of the year (y axis). (a) CalCOFI observations, (b) Case RSM winds, (c) Case COADS 2x2 and (d) Case NCEP Pacific Ocean Analysis. Correlation coefficients with (a) are plotted in the top left corner of each panel.

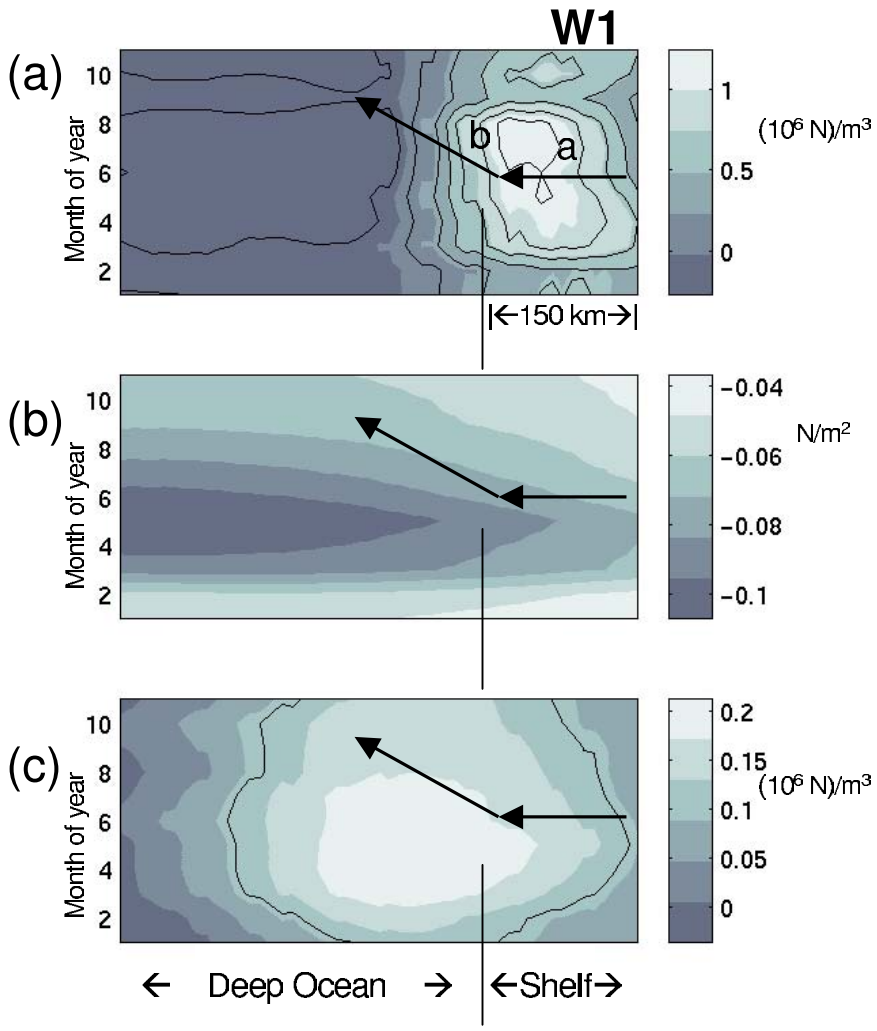

Figure 2.7. Same transect as Figure 2.6, but now plotted are the (b) RSM wind stress curl, (c) COADS 2x2 alongshore component of the winds and (d) NCEP Pacific Ocean Analysis wind stress curl. Note that (c) is wind stress and not wind stress curl.

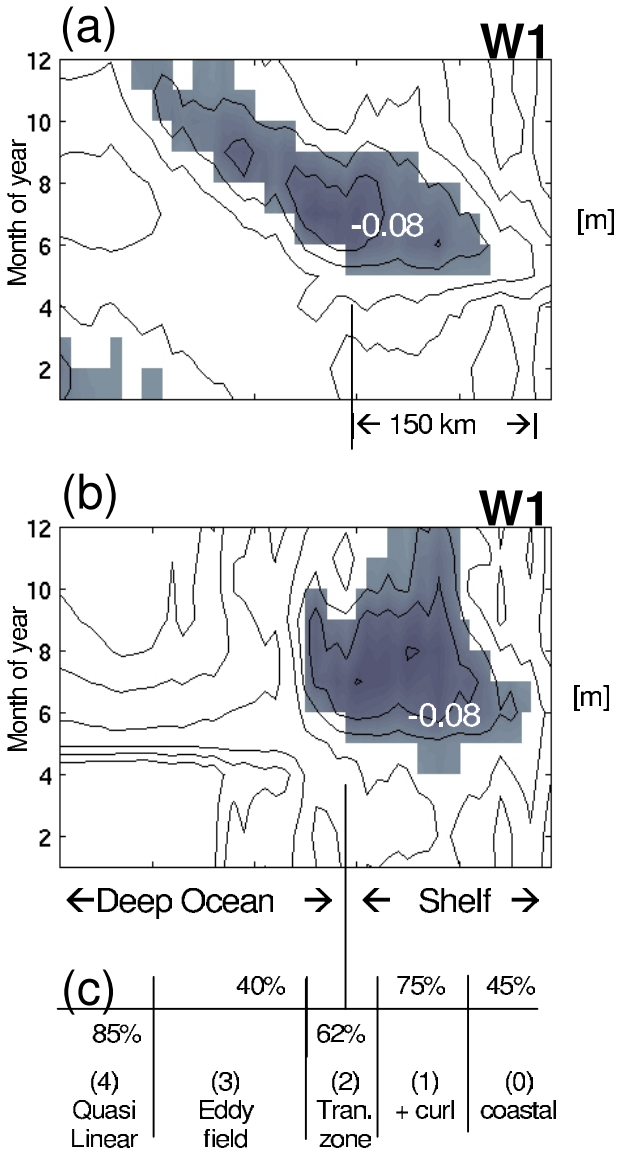

Figure 2.8. Westward transect W1 (x axis) of SSH anomalies [m] from the linearized model. Dark area is negative and increases towards the white CI=0.03). Integrations with $\beta \neq 0$ (a) and with $\beta = 0$ (b). (c) Fraction of variance explained by the linearized model when compared to the non-linear as a function of cross-shore location. The variable used for the comparison is the depth anomaly of the density surface 26.5.

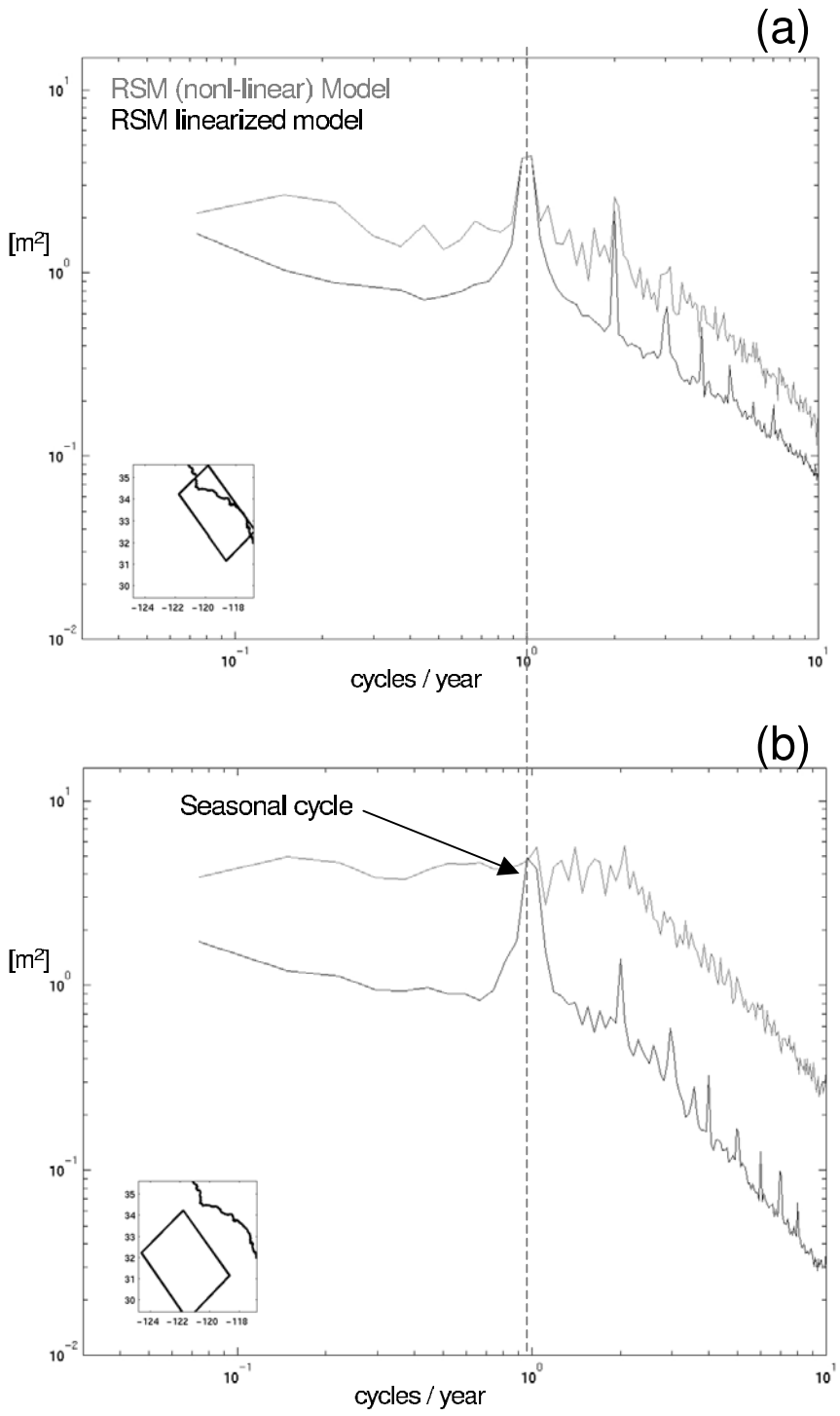

Figure 2.9. Average spectra of SSH anomaly [m] for the non-linear and linearized version of the model in the Bight (a) and offshore region (b). The averaging region is shown in the bottom left corner of each panel.

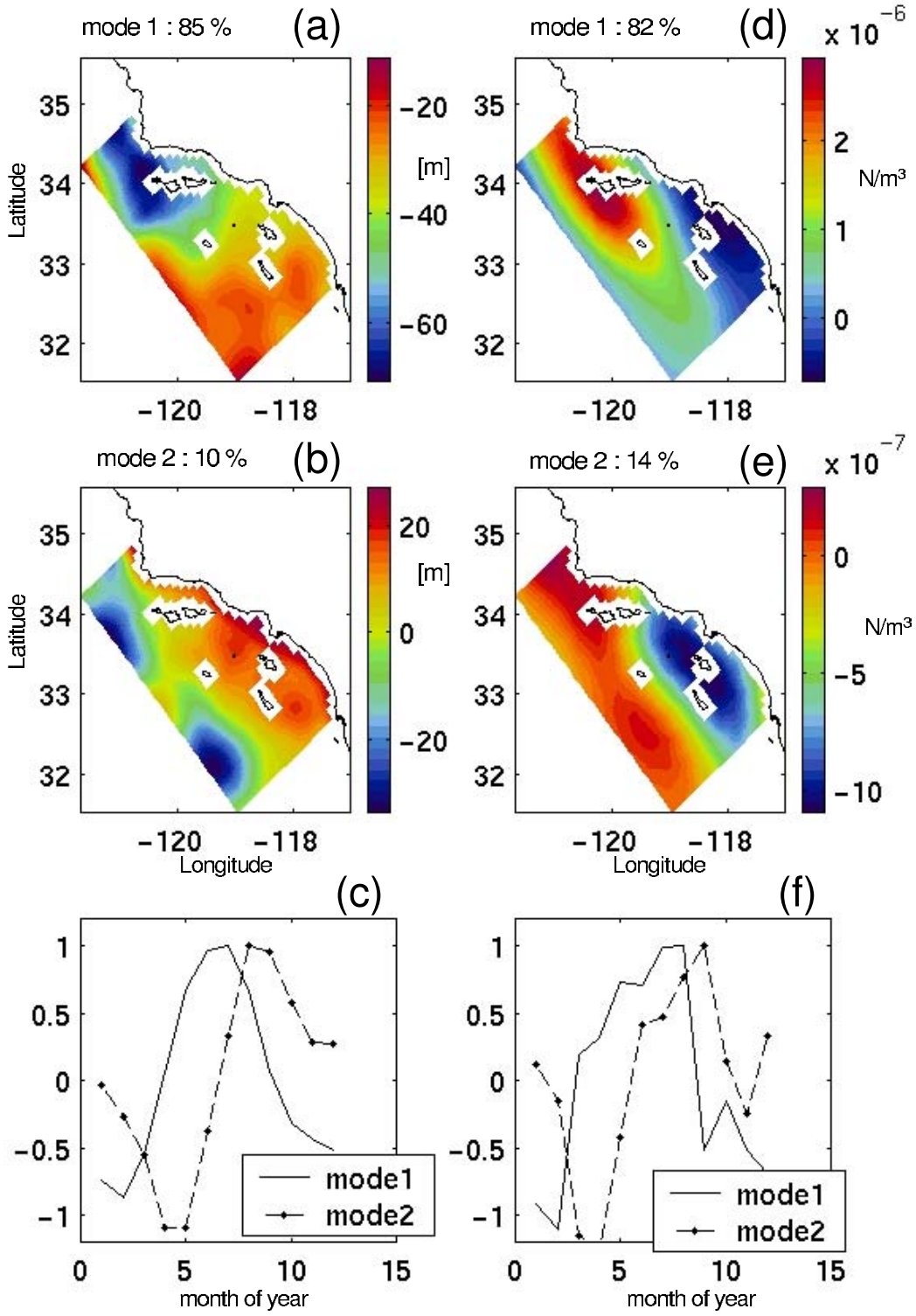

Figure 2.10. Empirical orthogonal functions. Mode 1 (a) and Mode 2 (b) for the 26.5 isopycnal depth and their temporal amplitudes (c). Mode 1 (d) and Mode 2 (e) for the RSM wind stress curl and their temporal amplitudes (f).

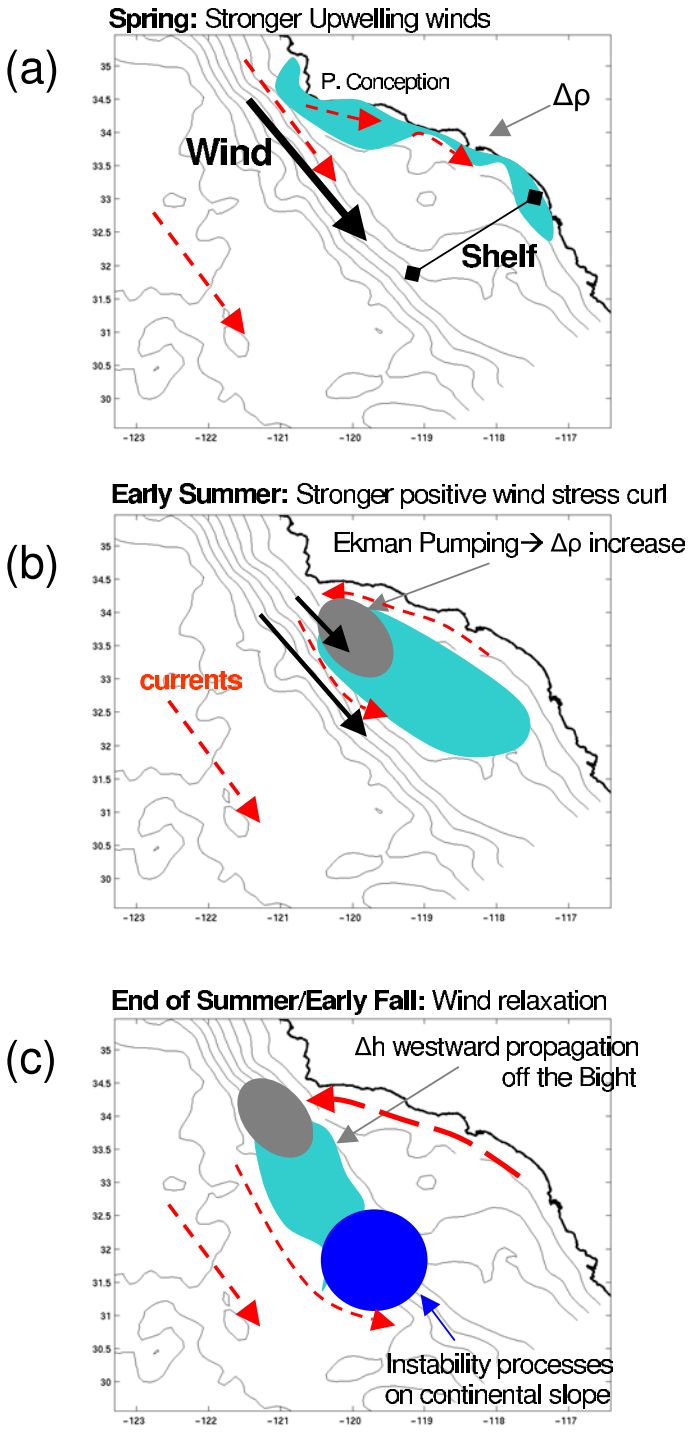

Figure 2.11. Schematic of the seasonal dynamics in the Southern California Current System for spring (a) , early summer (b) and fall (c). Black arrows are wind stress, red arrows are current and shaded areas denote areas of shoaling of isopycnal depths (positive density anomaly).

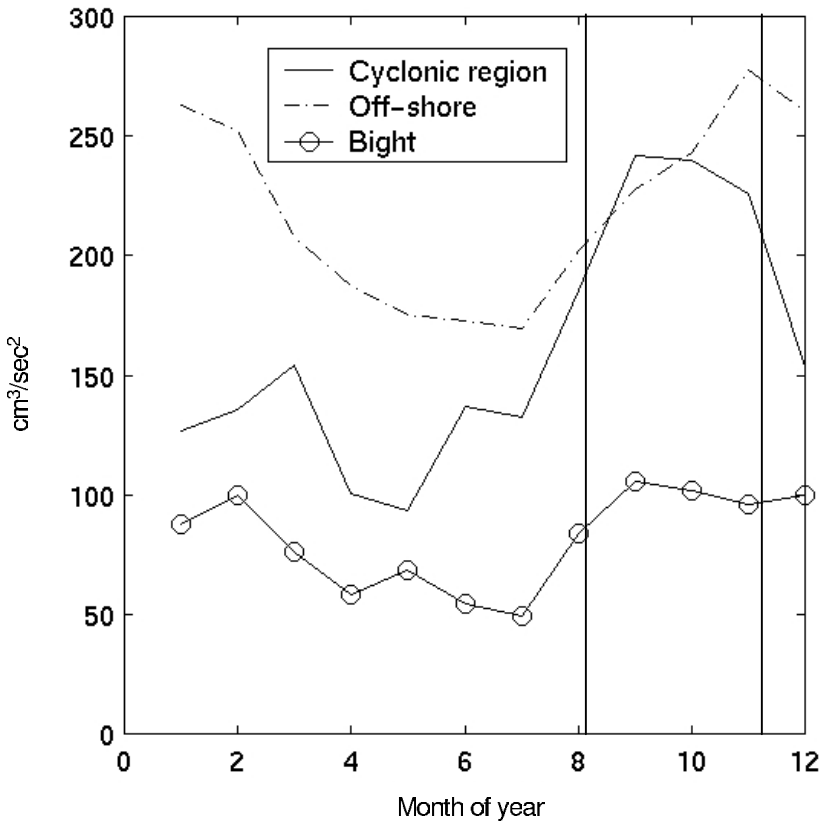

Figure 2.12. Model EKE integrated over different domains: the Bight region (solid line with circles), the cyclonic recirculation region (solid line), and the deep ocean off the continental slope (dashed line).

Chapter 3.

The warming of the California Current: Dynamics, thermodynamics and ecosystem implications

Abstract

The long-term changes in the observed temperature and salinity along the Southern California coast are studied using a four dimensional space-time analysis of the 52 year (1949-2000) California Cooperative Oceanic Fisheries Investigations (CalCOFI) hydrography combined with a sensitivity analysis of an eddy permitting primitive equation ocean model under various forcing scenarios. A warming trend in temperature and a deepening trend in the depth of the mean thermocline between 1950 and 1998 are found to be primarily forced by large-scale decadal fluctuations in surface heat fluxes combined with horizontal advection by the mean currents. After 1998 the surface heat fluxes suggest the beginning of a period of cooling, which is consistent with colder observed ocean temperatures. Salinity changes are decoupled from temperature and are primarily controlled by horizontal advection by anomalous currents.

A cooling trend in SST is driven in the ocean model by the 50 year NCEP wind reanalysis, which contains a positive trend in upwelling favorable winds along the Southern California Coast. The magnitude of this cooling (0.2 degrees Celsius), however, is small compared to the observed warming trend (1 degree Celsius) and is not detectable in the CalCOFI hydrography. The signature of the increased winds also is evident in both model and observations as an intensification of the mean currents of the Southern California Current System (SCCS). Model mesoscale eddy variance significantly increases in recent decades in response to both the stronger upwelling winds and the deepened isopycnals, suggesting that the stability properties of the SCCS have also changed.

Within 50 to 100 km of the coast, the ocean model simulations show strong evidence that the isopycnal deepening reduces the nutrient flux to the ocean surface, counteracting any effects of the increased upwelling winds. The long-term trend of the model proxy for surface nutrients is consistent with the observed decline in zooplankton concentration.

3.1 Introduction

A warming trend of about 1 degrees Celsius in sea surface temperature (SST) over the last 50 years has been observed along the Southern California coast [Roemmich, 1992]. Deepening of the mean thermocline and declining zooplankton has been linked with this warming trend [Roemmich and McGowan, 1995]. The cause of the warming and its links with coastal ocean dynamics still remain to be fully understood [McGowan et al., 2003]. More recently it has been suggested that these SST changes are part of a large scale Pacific Ocean decadal mode of variability [Mantua et al., 1997; Zhang et al., 1997; Lluch-Cota et al., 2001]. This mode has SST that is coherent and in phase along the entire U.S. and Canadian west coasts.

An open question is how the long-term ocean temperature variations are driven in the Southern California Current System (SCCS). Are they a local dynamical response to changes in winds? Are they a simple thermal response to changes in local surface heat fluxes? Are remote forcings important in driving these variations? Another open question is how these long-term changes alter the nutrient flux to the surface layer. How does the thermocline deepening affect the dynamics of the upwelling system?

Previous analyses of observed surface heat fluxes [Cayan, 1992] and ocean model hindcasts of the surface layer heat budget over the entire North Pacific Ocean [Miller et al., 1994] suggest that along the California coast the long-term SST signal is dominated by changes in surface heat fluxes. However, it is still unclear whether these findings are consistent with observations in the SCCS. The coastal portion of the warming trend could also be a result of a decrease in the strength of upwelling winds. Although appealing, this hypothesis is not consistent with the evidence that coastal alongshore winds have increased in recent decades, which would be expected to cool, not warm, SST [Schwing and Mendelssohn, 1997]. This finding is consistent with the ideas of Bakun [1990] who suggested that alongshore winds should intensify as a response to global greenhouse warming. Nevertheless the magnitude of the cooling trend suggested by Schwing and Mendelssohn (1997; hereinafter SM97) is of order 0.1 degree Celsius, which is small compared to the general warming trend (1 degree Celsius).

Long-term changes in salinity are also important because they represent an independent signature of ocean dynamical response. Are decadal temperature and salinity variations correlated in the SCCS? Can they be explained by similar dynamical mechanisms? The 52 year-long California Cooperative Oceanic Fisheries Investigations (CalCOFI) timeseries of salinity and temperature provides a unique data set to address these questions.

The goal of this paper is to address the preceding questions by studying the available observations together with targeted ocean model experiments. We quantify the contributions of the various processes controlling these long-term changes in temperature and salinity by computing a four dimensional space-time analysis of the 1949-2000

CalCOFI hydrography and executing a sensitivity analysis of a primitive equation ocean model of the California coast driven by various forcings. We show that the observed temperature (T) and salinity (S) variability have very different low frequency variability. We find evidence that anomalous horizontal advection, which appears to be controlling the salinity variability, is unimportant in modulating the decadal changes in temperature. We demonstrate that the temperature changes are likely forced by large-scale surface heat fluxes combined with horizontal advection by the mean currents. We find that increased alongshore winds are associated with intensification of mean and eddy horizontal currents. Finally, we present evidence that thermocline deepening reduces the flux of nutrients to the surface, which likely explains the long-term decline in zooplankton.

In section 2 we introduce the observational data and the analysis process. We then give a brief description of the primitive equation ocean model and the experiments setup in section 3 and the forcing functions in section 4. In section 5 we present the observed temperature (T) and salinity (S) variability. In section 6 we explain the intensification of the mean currents. In section 7 we discuss the low-frequency salinity variations. In section 8 we explain the warming trend using simple and full-physics models. In section 9 we identify the effects of warming on changes in coastal upwelling and their impact on nutrient flux to the surface layer. In section 10 we present evidence for an increase in mesoscale eddy variance in recent decades.

3.2 CalCOFI hydrography analysis

From 1949 to the present CalCOFI (http://www.calcofi.org) has sampled the upper 500 meters of the California coastal ocean. The data consists of in-situ measurements of temperature and salinity and also of biological quantities such as chlorophyll-a, nitrate and zooplankton. The sampling grid in the early cruises extends northward from Baja California up to the coast of Oregon with almost monthly resolution. Starting in 1965 the grid size was reduced to cover only the Southern California coast and the temporal resolution became seasonal, although each season is not always sampled during the same month of the year. This introduces temporal aliasing of the seasonal circulation patterns. The data also has gaps during the 1970s and 1980s where few cruises occurred.

Because of the spatial and temporal inhomogeneity of the CalCOFI hydrography we regrouped the data from all cruises following their temporal and spatial location rather than there cruise number. The resulting data was then re-binned into time snapshots and the date of the snapshot was assigned to be the average time of all data that occur in that bin. This procedure was not done automatically because it is difficult to identify a unique criterion that will insure a correct binning. After the binning we retained the bins that have both temperature and salinity data within the range of values acceptable for this oceanic region. We then gridded each set of binned data with an objective map [Bretherton et al., 1976] for each depth. The along-shore (cross-shore) decorrelation length scale used in the mapping is 110 km (100 km) as determined by Chereskin and Trunnell [1996]. Of the gridded data we retained only the portion for which the value of the normalized error was below 0.4. In order to simplify the analysis and the plotting of

the data we also interpolated in time (monthly) the various spatial maps with a temporal objective analysis using a decorrelation timescale of 4 months. This timescale was chosen because on average there are always two maps within any four months period, except during the 1970's and 1980's, which therefore result in gaps. After taking into account the errors from the spatial and temporal mapping, the resulting data used for the analysis in the next sections covers the region between 30 and 34 N with a cross-shore extent of 550 km from the coast (Figure 3.1). This analysis of the CalCOFI hydrography is now freely available on the web (http://horizon.ucsd.edu/calcofi).

3.3 Model experiment setup

3.3.1 The primitive equation (PE) model

The ocean model is a regional eddy-resolving primitive equation ocean model called the Regional Ocean Modeling System (ROMS), a descendent of SCRUM [Song and Haidvogel, 1994]. This model uses a generalized sigma-coordinate system in the vertical and a curvilinear grid in the horizontal (9 km resolution). The grid extends roughly 1200 km along the U.S. West Coast from northern Baja to north of San Francisco Bay with approximately 1000 km offshore extent normal to the coast (Figure 3.1). The vertical grid has 20 levels with enhanced resolution in the surface and bottom boundary layer. The model bathymetry is obtained by a smooth interpolation of the ETOPO5 analysis [NGDC, 1998] and is characterized by an extended (about 150-200 km) continental shelf in the Southern California Bight (typical depth of 400 m) followed by a steep continental slope offshore (typical depth of 4000 m).

A modified radiation condition [Marchesiello et al., 2001], which allows for stable, long-term integration of the model, is used at the three open boundaries together with a nudging term for relaxation to prescribed boundary values. The nudging is strong (timescale of 1 day) if the direction of the flow is inward and it is weak (timescale of 1 year) if the flow is outward. Using this model configuration, Di Lorenzo [2003] was able to model the dynamics of the seasonal cycle as inferred from CalCOFI observations and assess the sensitivity of the circulation to different wind stress forcing. Marchesiello et al. [2003] have also successfully used this same model to study the long-term equilibrium structure of the California Current over the entire U.S. West Coast. A more complete report of the model numerics, open boundary conditions, and mixed layer parameterizations can be found in Shchepetkin and McWilliams [1998; 2003] and Large et al.[1994].

Table 3.1: Primitive equation model experiments. Column 2 to 5 list the type of forcing data used in the experiments.

Exp. name	Wind Stress	Heat Flux	OBC Temperature	OBC Salinity
LF_MEAN	Clima	Clima	Clima	Clima
LF_TAU	NCEP	Clima	Clima	Clima
LF_Q	NCEP	COADS	Clima	Clima
LF_REMOTE	NCEP	COADS	CALCOFI	Clima
LF_REMOTE2	Clima	NCEP	CALCOFI	Clima

3.3.2 Experiment configurations

The sensitivity experiments for the various forcing functions are summarized in Table 1. Each row represents a separate 51-year integration starting in January 1950 and ending in December 2000. The label name of the experiment is in column 1. The types of forcing functions used for the sensitivity analysis are: mechanical surface forcing by the wind stress, buoyancy forcing associated with surface heat fluxes, and open boundary nudging of temperature and salinity (indicated in the remaining columns in Table 1). The labels of the forcing functions are:

CLIMA: A 12-month climatology is used to force repetitively each year of a model simulation from 1950 to 2000. The climatologies for the different forcings are derived by taking averages of the time-dependent forcing functions described next.

NCEP: The 51-year monthly averaged winds from the National Center for Environmental Prediction (NCEP) from 1950 to 2000 are used as mechanical forcing.

CALCOFI: Temperature is specified for each month at the model boundaries as a function of space and time. The spatial patterns are determined by a monthly mean climatology defined over the first 15 years of CalCOFI when nearly complete coverage prevailed. The long-term temporal changes are represented by adding a spatially constant value each month defined as the difference between the observed and climatological mean values in the present CalCOFI box. A different constant is computed at each depth. This removes the effects of mesoscale eddies from the boundary conditions and allows for long-term changes in boundary values consistent with CalCOFI observations. Because CalCOFI extends only to 500 m depth, deeper values are specified from the Levitus et al. [1994] monthly climatologies.

COADS: Net surface heat fluxes at monthly temporal resolution and 1 degree spatial resolution from 1950 to 2000 from the Cayan [1992] analysis of the Comprehensive Ocean-Atmosphere Data Set (COADS) are used.

3.3.3 Experiment descriptions

A brief description of the various experiments is listed below as a reference for the sections ahead where they will be discussed. In general these experiments are designed to investigate what fraction of the variability in T and S is generated locally in the SCCS by the time dependent surface forcing function and what fraction is remotely driven.

LF_MEAN: The control run. It uses climatology for all the forcing functions.

LF_Q: Sensitivity to the time dependent wind stress forcing and surface heat fluxes. All other forcing functions are set to climatology. The integration is used to verify to what extent the observed salinity and temperature variability can be explained locally over the SCCS by time dependent winds and surface heat flux forcings. The attribute "locally" is used here to mean that the signals in T and S are generated locally in the SCCS. Signals from outside the model domain are not allowed to propagate into the SCCS.

LF_TAU: Sensitivity to the time dependent wind stress forcing only. All other forcing functions are set to climatology. The integration is used to isolate the variability of temperature and salinity forced locally in the SCCS by the time dependent winds, and to assess the contribution of upwelling.

LF_REMOTE: Sensitivity of upwelling to changes in thermocline depth. This experiment has the same setup of LF_Q with the addition of the time dependent variations of the

thermocline depth. These variations are introduced at the open boundaries by nudging the temperatures to the CalCOFI observations. Salinity at the open boundaries is set to climatology. This experiment is complementary to LF_TAU and is used to assess changes in the upwelling system under the effects of changes in the depth of isopycnals. Because this experiment nudges the temperature of the open boundaries to the observed, it is also discussed in the next sections to show that the bulk of the temperature variability appears to be remotely forced and cannot therefore be explained just by local changes in the winds and surface heat.

LF_REMOTE2: Same as LF_REMOTE except that climatological winds are used.

3.4 Model surface forcings

Net surface heat flux observations and wind stress analyses over the last 50 years are used to investigate the sensitivity of the ocean PE model. A description of the forcing functions and their spatial and temporal characteristic is provided.

3.4.1 Net surface heat fluxes

An estimate of the net surface heat flux $Q(x,y,t)$ used to force the PE model is provided by an updated version of the Cayan [1992] analysis of the COADS [D. Cayan, private communication, 2002]. A spatial characterization of the net surface heat flux over the eastern North Pacific is given by the first Empirical Orthogonal function (EOF) that explains 58% of the variance (Figure 3.2a). This mode is coherent and in phase over a much larger area than the CalCOFI data domain. The time evolution of this first EOF is strongly correlated (r=0.9) to the timeseries of heat flux anomaly averaged over the

smaller CalCOFI data domain (Figure 3.2b). This time series shows a period of positive fluxes into the ocean during the late 1960s and 1970s followed by a negative period in the 1980's and 1990's. A decomposition of the various term in the heat flux budget reveals that this periods are dominated by the latent heat flux term. The bulk formula used for the calculation of the latent heat flux is:

$$Q_l = \rho L C_E w \Delta q$$

where Q_l is the latent flux, ρ is the density of air, L is the latent heat of evaporation of water, w is the wind speed, Δq is the sea surface saturation minus air specific humidity, and C_E is a transfer coefficient (see Cayan et al. [1992] for details). A closer analysis of this term reveals that the coherent spatial pattern of the flux is controlled by Δq [D. Cayan, private communication, 2002]

3.4.2 NCEP wind stress

A spatial and temporal characterization of the 51-year NCEP wind stress reanalysis within the PE model domain is given by the first EOF of alongshore winds and wind stress curl anomalies for the upwelling seasons from 1950–2000 (Figure 3.3). The first mode for the alongshore wind stress anomaly (explaining 72% of the variance) is uniformly negative (upwelling favorable) with a region of stronger amplitude near the coast north of the Southern California Bight (SCB). The corresponding temporal evolution of this mode (Figure 3.4a) reveals strong interannual variability and a clear positive trend in upwelling favorable winds. The first mode for wind stress curl anomaly shows a pattern that is similar to the mean wind stress curl in this region, with positive curl in the SCB and negative offshore [Bakun and Nelson, 1991; Winant and Dorman,

1997]. The temporal evolution of this mode (not shown) is well correlated with that of the alongshore wind stress anomalies (Figure 3.4a). The spatial patterns of variability identified in NCEP, which alone capture a very high percentage of the variance, are similar to their respective mean patterns indicating that the temporal changes in the signal are modulations in amplitude of the mean patterns.

A trend in upwelling favorable winds along the California Coast has also been identified by Bakun [1990] and recently by SM97 through an analysis of raw COADS and coastal station observations, which are available at the Pacific Fisheries Environmental Laboratory (PFEL; www.pfeg.noaa.gov). A comparison between the NCEP and SM97 equatorward winds in the SCCS shows remarkable correspondence after 1962 (Figure 3.4b), suggesting that the NCEP winds are suitable for the numerical experiments. The trend in the winds is roughly 0.015 Nm^{-2} over the last forty years, which amounts to a 10% increase relative to the mean.

We further verify the quality and representativeness of the NCEP winds over the SCCS by comparing the interannual signal in NCEP with the PFEL upwelling indices (Figure 3.4c). Visual inspection of the two timeseries reveals very good agreement for the period after 1962, although the upwelling indices do not show any clear trend.

During the interpolation process to the model grid, the NCEP winds have been shifted of 0.5 degrees in the north-east direction to better match the NCEP land mask with the model coastline. This is justified by taking into account the coarse resolution of the NCEP winds data product that we used over this region (1.5 degree). Such a shift is also important because it shifts the region of maximum positive wind stress curl over the

Southern California Bight, a critical condition to properly resolve the seasonal dynamics of the SCCS [Di Lorenzo, 2003].

3.5 Observed temperature, salinity and velocity changes

In order to provide a dynamical framework to understand the long-term changes in the oceanic conditions of the Southern California Current System (SCCS), we will first describe the mean circulation patterns averaged from 1949 to 2000. We will then proceed to characterize the spatial and temporal variability of T, S, and alongshore geostrophic currents.

3.5.1 The mean circulation from 1949 to 2000

At the surface the circulation (Figure 3.5a) is characterized by broad equatorward flow (California Current; CC) in the offshore region, poleward flow close to the coast (Inshore Countercurrent; IC) and a region of cyclonic circulation (Southern California Eddy; SCE) that connects the inshore and the offshore circulation [Lynn and Simpson, 1987; Chereskin and Trunnell, 1996; Di Lorenzo, 2003]. At depth, below the mixed layer, the core of the CC is still well defined and the signature of the SCE is stronger (Figure 3.5b). The coastal poleward flow that closes the recirculation region of the SCE is termed in literature the California Undercurrent (CU). This current brings salt and warm water from the south into the Southern California Bight (SCB). Because of the high salt and heat content, these water masses are traceable on isopycnal layers as a tongue of high spiciness (defined as the coordinate orthogonal to density on a TS diagram) originating from the coastal region. In contrast the offshore water masses of northern origin are cold and fresh and therefore have low spiciness.

3.5.2 Observed temperature and salinity variability

Time series of SST and surface salinity averaged over the Southern California domain (Figure 3.6a,b) are strongly correlated (correlation exceeding 0.9) with domain averages of T and S integrated from the surface to the time-dependent 26.4 isopycnal (hereinafter the depth-integrated signal). The depth of the 26.4 isopycnal ($Z_{26.4}$) ranges between 180 to 220 meters and is always located below the surface mixed layer.

Visual inspection of the 52-year time series (Figure 3.6a,b,c) reveals that T, S, and $Z_{26.4}$ display prominent low frequency variability. Temperature is dominated by interannual variability and is well correlated with indices of large-scale climate variability such as ENSO and PDO. On the other hand, salinity is dominated by interdecadal variability and is not coherent with large-scale climate indices [Schneider et al., 2003]. The T and S signals appear to be uncorrelated on timescales longer than a few years. The temperature signal exhibits a warming trend of roughly 1 degrees Celsius over the last 50 years, as found in previous studies [Roemmich, 1992]. A deepening of $Z_{26.4}$ of roughly 20 m is correlated with this warming. The salinity signal exhibits no evidence of such a trend. The spatial structure of depth integrated T and S variability, as inferred from an EOF analysis, shows that the low frequency variations seen in the timeseries are associated with like-signed structures spanning the entire data domain (Figure 3.7). The first salinity EOF is characterized by a core of higher variance located around the offshore branch of the SCE. The first temperature EOF has an inshore-offshore gradient but smaller spatial scales than the salinity EOF mode.

It is also interesting to notice that low frequency salinity modulation in EOF 1 is well correlated ($r > 0.6$) with the salinity signal in the deeper ocean away from surface

exchange processes (Figure 3.8a). In the temperature such a correlation does not exist ($r < 0.1$) and the upper ocean signal is decoupled from the deep one (Figure 3.8b).

To characterize the vertical structure of these low frequency changes we compute vertical EOFs along an averaged transect, W1 in Figure 3.5. The warming trend is captured by EOF 1. It extends to 200 meters (Figure 3.9a) and varies weakly in the cross-shore direction. The temporal dependence of this mode is very well correlated with the temperature timeseries in Figure 3.6a. The first transect EOF of salinity (Figure 3.9c) shows that the offshore core of maximum variance (400 km from the coast), previously identified in the horizontal EOFs, is found to extend below 200 m. At the coast the signal is shallower and weaker.

Vertical sections for the difference in means for T and S (Figure 3.10) over the period E1 (1950 to 1970) and E2 (1980 to 2000) show a warming (Figure 3.10f) of roughly 1 degree Celsius and an isopycnal deepening of roughly 20 m. The core of the warming is located offshore in correspondence with a core of low salinity (roughly -0.05 psu), which also extends inshore in the surface layers (Figure 3.10e). A core of saltier water (roughly 0.05 psu) is also evident closer to shore at depth.

3.5.3 Alongshore geostrophic currents variability

The vertical transect W1 intersects the center of the mean location of the SCE (Figure 3.5b). At this location the signature of the SCE is very strong and less affected by the noise in the data that comes from the aliasing of mesoscale eddies, which are poorly resolved by CalCOFI. To characterize the variability in intensity of the SCE we perform a vertical EOF of the alongshore total geostrophic flow (including the mean) computed

from the CalCOFI temperature and salinity (Figure 3.9e) relative to 500 m. The first mode vertical structure shows alongshore velocity with equatorward flow offshore and poleward flow inshore. The temporal evolution of this pattern (Figure 3.9f) contains a strong mean component (the SCE) along with a positive trend from the late 1950s to the present, suggesting an intensification of the recirculation region of the SCE. The explained variance associated with the trend component alone is 30%. The higher modes contain no evidence of a trend and capture the displacement of the CC core on interannual timescales.

3.6 Intensification of ocean currents

In the previous section we found evidence of an intensification of the recirculation region of the SCE over the last 50 years. Model studies of the SCCS show that the SCE linearly responds to changes in amplitude of the mean wind stress curl pattern similar to the one showed in Figure 3.3b [Di Lorenzo, 2003]. A Hofmuller plot of the 51 year NCEP wind stress curl anomalies in the CalCOFI domain (Figure 3.11a) shows a period of more negative curl in the coastal region during the 1950s and 1960s (defined as the period E1), and then a transition to stronger positive curl in the 1980s and 1990s (defined as the period E2). The PE model experiment LF_TAU, which is used to isolate the ocean response to changes in wind forcing alone (see section 3 for details), responds with anomalously high free surface elevation during the period E1 and low during period E2. During period E2 the cross-shore gradient in free surface height becomes stronger and the recirculation region intensifies. The spatial structure of this

response is also evident in the 1st EOF mode of the model free-surface elevation (Figure 3.12a). This implies that on average during period E2, the alongshore velocity is more southward in the offshore branch of the recirculation region and more northward inshore. These model results compare well with the observations (Figure 3.13), which show somewhat stronger changes. The magnitude of the observed change between period E2 and E1 is 2-3 cm s^{-1}, roughly a 25% increase of the mean flow.

In the model, the offshore equatorward flow intensifies as a response to the trend in the winds but does not show much variability in the cross-shore location of its core. The location of the core is generally modulated by cross-shore variations of the zero wind stress curl line, which are not well resolved in the NCEP data. We therefore note the possibility that some of the changes in CalCOFI are also associated with these cross-shore modulations in wind stress curl that the model cannot resolve. Nevertheless the similarity between the model and observations suggests that a significant strengthening of the observed currents has occurred in the SCCS as a consequence of the trend in the winds. These results also give more evidence that the wind stress trend in the NCEP reanalysis is not an artifact of the wind product so that its use as a forcing function for PE model integrations is acceptable for this study.

3.7 Low frequency salinity variations

The salinity signal (Figure 3.6b) does not show any strong evidence of a trend and is characterized by low frequency fluctuations. These low frequency variations do not correlate with any index of large-scale climate variability, such as the PDO, so the

interpretation of the signal may be difficult. In a separate study, Schneider et al. [2003] show, using the CalCOFI hydrography along a particularly data rich cross-shore transect, that these oscillations can be partly explained with a conceptual model of anomalous advection:

$$\frac{\partial S'}{\partial t} = -v' \frac{\partial \overline{S}}{\partial y}$$

where v' is the alongshore velocity and the prime indicates anomaly from the time mean. Although they find that this model reasonably fits the observed variations of salinity, some portions of the fluctuations remain unexplained (see Schneider et al., 2003 for details). A better model should also include anomalous advection from the cross-shore velocity u' associated with changes in the cross-shore location of the CC core. This contribution cannot be estimated in the cross-shore transect and is difficult to reconstruct using the CalCOFI analysis. However, support for this idea can be provided by using our 4D CalCOFI analysis combined with PE model experiments.

3.7.1 Salinity variations in the deeper ocean

In the previous section we noted that the salinity signal at the surface (Figure 3.8), unlike temperature, is well correlated with the one in the deeper ocean (on isopycnal 26.4). Because the deeper isopycnal is insulated from surface exchange processes, one would expect that the modulation of the deeper signal is primarily controlled by advection. Therefore the strong correlation between the surface and deep signals suggests that salinity variations throughout the water column are primarily controlled by advection. It is therefore instructive to analyze the behavior of a passive tracer, like spiciness

[Flament, 2002], on the deeper isopycnal 26.4 to show its relationship to advection in the recirculation region.

On deeper isopycnals, away from surface exchange processes, the offshore spread of spicy waters advected by the CU (Figure 3.5b) is a function of the cross-shore transport and the alongshore currents. The governing equation for spice (π) on the isopycnal can be written as:

$$\frac{\partial \pi}{\partial t} = -(\underset{\sim}{u} \cdot \nabla)\pi$$

where $\underset{\sim}{u} = (u, v)$ is the horizontal velocity. The contributions of cross isopycnal mixing and horizontal diffusion are assumed to be small and have been neglected.

Time-longitude plots of spiciness at several latitudinal cross-shore sections along the Southern California coast (Figure 3.14) reveal low frequency fluctuations of the spiciness signal in the cross-shore direction. During the 1950s and early to mid 1990's spicier waters are mostly confined to within 100 to 150 km of the coast. In contrast, the 1960s and late 1980s exhibit spicier signals extending further offshore. These fluctuations are generally coherent and in phase at all coastal locations. These deep spiciness fluctuations are correlated with the low-frequency salinity variations at depth ($r > 0.9$) and at the surface ($r > 0.6$).

The spiciness signal on this isopycnal 26.4 is summarized by the EOFs (Figure 3.15). The first spatial mode (Figure 3.15a) is uniformly positive with a cross-shore gradient (higher values at the coast). The time evolution of this mode (Figure 3.15b) shows strong interannual variability with clear ENSO signals but modest low frequency power. Physically we can think of this mode as the down-gradient spread of spice on the

isopycnal due to cross-shore advection or eddy mixing. The second mode, which captures the same interdecadal variations seen in salinity (Figure 3.15d), shows positive values in the very near coastal region and negative values offshore (Figure 3.15c). This mode is likely associated with the deep subsurface component of the SCE. When this cyclonic recirculation region intensifies more spice is advected to the inshore region from the south and more negative spice to the offshore region from the north.

3.7.2 Salinity variations in the PE model

Salinity variations in the PE model simulations can be explained by anomalous advection and a damping term:

$$\frac{\partial S'}{\partial t} = -u' \frac{\partial \overline{S}}{\partial x} - v' \frac{\partial \overline{S}}{\partial y} - \gamma S'$$

where $1/\gamma$ is the time scale over which the model open boundary nudging acts on the ocean interior. In the model, the cross-shore displacement of the CC core, u', is associated with cross-shore variations in the zero wind stress curl line. Since these cross-shore variations in wind stress curl are not properly resolved by the NCEP winds, we do not expect the PE model simulations to properly capture the observed low frequency variations of salinity. Moreover, the effects of boundary nudging will unrealistically reduce the low-frequency power of model salinity variations. However, we can still compare the structure of salinity variations in the model with observations, while ignoring the specific temporal variations.

The model surface salinity EOF 1 (experiment LF_TAU, Figure 3.12c) compares well with the observed salinity EOF 1 (Figure 3.7c). They both show a core of maximum

variance in the region between the shelf and further offshore. This maximum is associated with the tongue of fresh waters advected by the CC from the north. In the model, this region is smeared further offshore than observations. This is due to the lack of strong gradients in the NCEP wind stress that are needed to contain these oceanic structures closer to the shore [Di Lorenzo, 2003].

Contrary to CalCOFI, the model salinity EOF 1 explains a small fraction of the total salinity variance. In the model the salinity variations associated with the intense non-linear mesoscale eddy field are not smoothed by an objective analysis and therefore do not admit a clean separation of the modes of variability. In CalCOFI the smoothing procedure associated with the objective maps allows the EOF to retrieve a first mode explaining the majority of the variance. The temporal modulation of the model EOF 1 (Figure 3.12d), which is highly correlated with the timeseries of total model surface salinity (Figure 3.12d dashed line), does show the tendency for low frequency variations but the amplitude is small compared to the observed. These discrepancies are likely due to the boundary nudging of salinity, which is effectively a damping term in the model domain over decadal timescales.

A negative trend in salinity is also associated with the model EOF 1 as a response to the increased upwelling favorable winds. Such a trend is not as evident in the timeseries of model surface salinity, which is shown in Figure 3.12d (black dashed line) after being scaled to allow a direct comparison with the model EOF 1 temporal variations. In the CalCOFI surface salinity there is also a negative trend over the last 50 years (Figure 3.6b), however this trend is statistically insignificant and likely just an artifact of the aliasing of the decadal fluctuations.

3.8 Temperature warming trend

The spatial and temporal variability of CalCOFI upper ocean temperature is correlated with the PDO. This mode of large-scale SST variability is characterized by coherent and in phase changes of SST along the entire U.S. and Canadian west coasts. Although this indicates that temperature changes in the CCS are part of a large-scale response, it is still unclear if this response is driven locally by changes in large scale forcing functions such as surface winds and heat fluxes, or remotely by large-scale changes in ocean advection, which modulate the input of cold water masses from the north.

In the previous section we noted that changes in advection are important in the modulation of the salinity signal. The fact that temperature and salinity variability are uncorrelated suggests that changes in oceanic advection are not the dominant mechanism controlling decadal temperature changes. In addition we also noted that temperature changes in the upper ocean are decoupled from those on deeper isopycnal, unlike the salinity changes, which are coherent throughout the water column. This is evidence that the upper ocean temperature is heavily controlled by the surface forcing functions. These forcing functions are the winds and the heat fluxes. In this section we will discuss the potential role of each of these forcings.

3.8.1 Local response to wind stresses

We start by considering the PE model response to local changes in the NCEP surface winds (experiment LF_TAU). As noted before these winds contain a positive

trend in northwesterly winds, which tend to increase the upwelling of cold water masses. The model response to these winds (in isolation) is captured by EOF 1 of model SST (Figure 3.16a,b). This mode shows a clear cooling trend with colder waters inshore and warmer waters offshore. During summer and fall the surface poleward flow that develops at the coast carries warmer water from the south. This explains why in EOF 1 the core of cold waters is slightly detached from the coast. Model EOFs of SST during the upwelling season only show the core of maximum cold water right at the coast. The temporal amplitude of this mode (Figure 3.16b solid line) is well correlated with the timeseries of domain-averaged model SST (Figure 3.16b dashed line) so that we are confident that this mode is representative of the model response to the NCEP winds. This result strongly suggests that changes in the winds and coastal upwelling are in fact cooling the SCCS and cannot explain the warming trend. The magnitude of the cooling associated with this response is roughly 0.2 degrees Celsius over the last 40 years (Figure 3.17a).

3.8.2 Response to surface heat fluxes

We now consider the same model configuration but we include both the time dependent net surface heat fluxes and wind stress as forcing functions (experiment LF_Q). The model response for this experiment is again characterized by EOF 1 of SST. The temporal evolution of EOF 1 is very different from the previous case forced with winds alone (Figure 3.16d). We cannot identify a clear cooling trend associated with the winds, nor a warming trend. The temporal evolution of the mode is correlated with the decadal fluctuations of the surface net heat fluxes used to force the model (Figure 3.2b). These SST fluctuations show a period of warmer climate from the 1960s to the 1980s

followed by a sharp transition to a period of colder climate after the 1980s. This model response implies that changes in surface heating, rather than winds, exert a dominant control on SST. EOF 1 of the response has high variance in the offshore region (Figure 3.16c) where the heat fluxes used to force the model have higher amplitude. Because of the coarse resolution of the heat fluxes used to force the model it is difficult to attribute any significance to this pattern when compared to the CalCOFI observed pattern.

In this experiment the nudging to climatological values of SST at the open boundaries does not allow for propagation of any signal from outside the model domain. As noted previously for salinity, this type of open boundary condition causes model SST anomalies in the interior to be damped to zero. The timescale over which the relaxation is effective is estimated from the model to be roughly three years.

Because the surface heat fluxes are forcing the ocean SST coherently and in phase over a much larger domain than the model (Figure 3.2), this relaxation to climatological values at the open boundaries is inadequate for modeling decadal variations. The surface heat fluxes force ocean temperature anomalies outside the model domain that are then advected into the model domain by ocean currents. We therefore perform a model simulation in which we nudge the open ocean boundaries to track the observed changes in CalCOFI temperatures (experiment LF_REMOTE). The model response (Figure 3.16e an 16f) now shows the same warming trend as in the CalCOFI observations, which confirms the importance of ocean currents in transporting temperature anomalies.

In principal one could argue that the model only captures the signal because it is artificially prescribed by the relaxation at the open boundaries. On the other hand one could also argue that advection of temperatures anomalies from outside the CalCOFI

domain are fundamental to explaining the observed decadal fluctuations of temperature, which over the last decades yields a warming trend. To verify that this is the case we reinterpret the PE model results with a toy model of temperature forced by heat fluxes.

3.8.3 Toy model for temperature variations

Let us now reconsider experiment LF_Q in a simple dynamical framework

$$\frac{\partial \tilde{T}}{\partial t} = \frac{\tilde{Q}}{\rho CpH} - \gamma \tilde{T}$$

where the tilde indicates anomalies of the area average over the model domain, ρ the mean density, Cp the heat capacity, $1/\gamma$ the damping timescale associated with the relaxation at the open boundary, and *H* the average depth of the layer over which $\tilde{Q}$ is acting. For decadal variations in $\tilde{T}$ the depth of *H* is set to roughly 150 m, as estimated from the vertical extension of the warming in the CalCOFI temperature vertical EOF 1 (Figure 3.9a).

We can solve this simple model using the timeseries of surface heat flux forcing (Figure 3.2b). The characteristic timescale for $1/\gamma$ is set by $L/U \approx 0.8$ years, where $L \approx 800$ km is the narrowest extent of the box and $U \approx 3$ cm/s is the strongest mean current. The solution for $\tilde{T}$ obtained by this simple model is compared to the one obtained by the full physics PE model (experiment LF_Q) with open boundary nudging to climatology (Figure 3.17b). The solution predicted by the simple model agrees very well with that of the PE model. However these two solutions do not compare well with the observed CalCOFI temperatures (Figure 3.17b). This suggests that the simple model

in this form (which mimics the PE model with boundary nudging to climatology) is inadequate to explain the observed changes.

Since the nudging of temperature anomalies to zero at the open boundaries is clearly incorrect, we are motivated to parameterize the effects of heat fluxes forcing temperature anomalies over a domain much larger than that of the model. Therefore let us solve our simple model without the damping term:

$$\frac{\partial \tilde{T}}{\partial t} = \frac{\tilde{Q}}{\rho CpH}$$

The new solution for $\tilde{T}$ (Figure 3.17c thick solid line) now tracks the observed interdecadal temperature variations. It captures the proper amplitudes of the cooler period of the 1960s, the transition to warmer conditions during the 1970s and the commencement of a cooler climate in the late 1990s. This solution is also consistent with the PE model solution for experiment LF_REMOTE, which represents this mechanism through boundary nudging to observations (Figure 3.17c).

These results suggest that changes in ocean temperature along the coast of California occur as a result of spatially coherent changes in surface heat flux forcing acting over the entire eastern North Pacific Ocean. Therefore the observed warming trend between 1950 and 1998 can be explained by large amplitude decadal variations in Q alone. The recent observed cooling after 1998 is consistent with this idea. It is also clear that these temperature variations are only weakly controlled locally at the coast by changes in upwelling.

3.9 Changes in property of upwelled water masses

Although we have shown that changes in upwelling are not important in controlling the CalCOFI temperature variations, the deepening of the thermocline associated with the warming can affect significantly the properties of the upwelled water masses near the coast (50 - 80 km from the coast) and greatly impact the ecosystem.

To investigate how upwelling water masses are affected by changes in thermocline depth we consider two PE model experiments. In the first experiment (LF_TAU) we force the model only with the NCEP winds. In the second experiment (LF_REMOTE) we also include variations in thermocline depth by nudging to the observed temperature variability at the open boundaries. The salinity at the boundary for both experiment is nudged to its climatology. This enables us to use the model surface salinity in the coastal band as a proxy tracer for the amount of nutrients upwelled.

The time series of average surface salinity in the coastal band from experiment LF_TAU shows low frequency variations superimposed on a positive trend (Figure 3.18a). This positive trend is associated with the increase in upwelling favorable winds as discussed previously. If we now compare this timeseries with the one from experiment LF_REMOTE, which includes the deepening of isopycnals, we find that salinity exhibits the same low frequency fluctuations as in LF_TAU, but the trend is reversed (Figure 3.18b). The deepening of the isopycnal in experiment LF_REMOTE causes upwelling of shallower water masses and therefore an overall freshening. This response to the thermocline deepening will also affect the amount of nutrients mixed into the surface layer from below. It is interesting to note that both the negative trend and low frequency fluctuations of coastal salinity correspond well to the observed zooplankton time series

presented by Roemmich and McGowan [1995], which exhibits a prominent decline. This model result reinforces the suggestion and gives dynamical evidence that the deepening of the isopycnals associated with the long-term warming has impacted the amount of nutrients available at the ocean surface and therefore the abundance of zooplankton.

3.10 Changes in eddy variance

Eddies control the cross-shore transport in the SCCS as evidenced by observational studies [Lynn and Simpson, 1990; Simpson and Lynn, 1990]. The increase in the alongshore winds combined with the deepening trend of isopycnals may affect the stability properties, and consequently the eddy statistics of the recirculation region in the SCCS. Since these eddies are likely important for the offshore productivity of the ecosystem we will analyze if significant decadal changes occur in the model hindcast.

One measure of changes in eddy statistics on decadal timescales is an increase or decrease in velocity variance. We compare an average cross-shore section of cross-shore velocity (U) variance for the period E1 (1950s and 1960s) and E2 (1980s and 1990s) from the various PE model experiments. A significant change in variance is found in the offshore waters over the Southern California domain south of Point Conception in the case LF_REMOTE. This experiment includes both isopycnal deepening and increasing upwelling winds as forcing functions in the PE model (Figure 3.19). In experiment LF_TAU the changes, although still rather large, are not statistically significant. The alongshore velocity variance also shows a significant, but weaker, increase in variance in the offshore region for experiment LF_REMOTE. The significance was estimated using

the F test at the 95% level with 80 degrees of freedom. To compute the degrees of freedom we considered a temporal decorrelation timescale of 3 months. This timescale is a conservative estimate of the typical persistence time of the eddies (1-2 months) in the SCCS [Di Lorenzo et al., 2003].

The increase in variance is also evident in spatial maps of the differences in velocity variance for the period E2 minus E1 (Figure 3.20b,c). In case LF_REMOTE the changes are highly significant in the offshore region. In case LF_TAU the changes are not statistically significant but the spatial structure of the changes in variance is similar to case LF_REMOTE. This supports the idea that the intensification of the along-shore winds alone can produce a change in eddy variance. We also note that the higher variance is found in the offshore region where the eddies reach their mature stages (Figure 3.20a). At the model ocean boundaries the decrease in variance is associated with the nudging boundary condition, which damps the activity of the eddies.

These result motivate the need to further investigate the dynamical stability properties of the SCCS on long timescales and their effect on the distribution of nutrients and the ecosystem response.

3.11 Summary

The dynamics and thermodynamics controlling the long-term changes of temperature and salinity in the SCCS are reconstructed using a four dimensional space-time analysis of the CalCOFI 50 year-long hydrography and a sensitivity analysis of an eddy permitting primitive equation (PE) ocean model. The PE model experiments are

designed to interpret the observations by supplying insight on the physical processes that cannot be estimated directly from the observations.

A warming trend between 1950 and 1998 is evident in upper ocean temperature along the coast of California, together with strong interannual temperature variations. The observed warming trend extends over the top 200 m of the water column and is consistent with large scale studies of heat content change over the last 50 years [Stephens et al., 2001]. The temperature signal is coherent with indices of large-scale climate variability (e.g. PDO) and is uncorrelated with salinity on decadal timescales.

Simple and full physics model experiments reveal that these temperature changes are primarily controlled by net surface heat flux forcing, acting in phase over the entire Eastern North Pacific, combined with advection by the mean currents that redistributes the heat input to the ocean. These two mechanisms act together to cause a deepening trend in the isopycnals (thermocline depth).

It is apparent that the warming trend between 1950 and 1998 is driven in the model by decadal variations, rather than a trend, in Q. The recent cooling after 1998 is consistent with this interpretation. The lack of a trend in Q suggests that this forcing function does not reflect a response to greenhouse gas forcing.

Changes in upwelling dynamics are not a major contributor to the observed decadal changes of temperature. An SST cooling trend is evident in the PE model experiments in response to an increase in the upwelling favorable coastal winds over the last decades. This upwelling-forced trend is opposite to the observed warming trend. However the estimated magnitude of the cooling (0.2 degrees Celsius) is small compared to the warming trend (1 degree Celsius).

An intensification of the mean currents of the SCCS is also found in both observations and PE model simulations over the last decades. In the model this intensification occurs as a response to the increase in upwelling favorable winds. Mesoscale eddy variance is found to increase significantly in the last decades in the PE model experiments that include both the increased upwelling favorable winds and the isopycnal deepening. These changes in variance, which likely originate from changes in the dynamical stability property of the system, cannot be directly estimated from the observations.

Salinity is characterized by low frequency variations that do not correlate with indices of large-scale climate variability. These variations at the surface and at depth are strongly correlated on decadal timescales and are associated with anomalous advection by the currents.

Finally, the PE model simulations provide strong evidence that isopycnal deepening (associated with the warming trend) limits the amount of nutrients fluxed upward to the ocean surface near the coast (within 50-100 km). This counteracts the effects of the increased upwelling winds, which would otherwise give rise to a positive trend in upward nutrient flux. The model proxy nutrient (salinity in the coastal region) shows a negative trend with decadal fluctuations that are in agreement with observed zooplankton concentration. These physical changes suggest a concrete mechanism for explaining the observed decline in zooplankton. Further investigation of the impacts of these physical oceanographic changes on the ecosystem of the California Current System is in progress.

References

Bakun, A., Global Climate Change and Intensification of Coastal Ocean Upwelling, *Science*, 247 (4939), 198-201, 1990.

Bakun, A. and C. S. Nelson, The seasonal cycle of wind-stress curl in subtropical eastern boundary current regions, *Journal of Physical Oceanography*, 21 1815-1834, 1991.

Bretherton, F. P., R. E. Davis and C. B. Fandry, Technique for Objective Analysis and Design of Oceanographic Experiments Applied to Mode-73, *Deep-Sea Research*, 23 (7), 559-582, 1976.

Cayan, D. R., Latent and Sensible Heat-Flux Anomalies over the Northern Oceans - Driving the Sea-Surface Temperature, *Journal of Physical Oceanography*, 22 (8), 859-881, 1992.

Chereskin, T. K. and M. Trunnell, Correlation scales, objective mapping, and absolute geostrophic flow in the California Current, *Journal of Geophysical Research-Oceans*, 101 (C10), 22619-22629, 1996.

Di Lorenzo, E., Seasonal dynamics of the surface circulation in the Southern California Current System, *Deep-Sea Research II*, (in press), 2003.

Di Lorenzo, E., A. J. Miller, D. J. Neilson, B. D. Cornuelle and J. R. Moisan, Modeling observed California Current mesoscale eddies and the ecosystem response, *International Journal of Remote Sensing*, (in press), 2003.

Flament, P., A state variable for characterizing water masses and their diffusive stability: spiciness, *Progress in Oceanography*, 54 (1-4), 493-501, 2002.

Large, W. G., J. C. McWilliams and S. C. Doney, Oceanic Vertical Mixing - a Review and a Model with a Nonlocal Boundary-Layer Parameterization, *Reviews of Geophysics*, 32 (4), 363-403, 1994.

Levitus, S., R. Burgett and T. P. Boyer, World Ocean Atlas 1994, *NOAA Atlas NESDIS 4, U.S. Gov. Printing Office, Wash., D.C.*, 3-4 1994.

Lluch-Cota, D. B., W. S. Wooster and S. R. Hare, Sea surface temperature variability in coastal areas of the Northeastern Pacific related to the El Nino-Southern Oscillation and the Pacific Decadal Oscillation, *Geophysical Research Letters*, 28 (10), 2029-2032, 2001.

Lynn, R. J. and J. J. Simpson, The California Current System - the Seasonal Variability of Its Physical Characteristics, *Journal of Geophysical Research-Oceans*, 92 (C12), 12947-&, 1987.

Lynn, R. J. and J. J. Simpson, The Flow of the Undercurrent over the Continental Borderland Off Southern California, *Journal of Geophysical Research-Oceans*, 95 (C8), 12995-13008, 1990.

Mantua, N. J., S. R. Hare, Y. Zhang, J. M. Wallace and R. C. Francis, A Pacific interdecadal climate oscillation with impacts on salmon production, *Bulletin of the American Meteorological Society*, 78 (6), 1069-1079, 1997.

Marchesiello, P., J. C. McWilliams and A. Shchepetkin, Open boundary conditions for long-term integration of regional oceanic models, *Ocean Modelling*, 3 1-20, 2001.

Marchesiello, P., J. C. McWilliams and A. Shchepetkin, Equilibrium Structure and dynamics of the California Current System., *Journal of Physical Oceanography*, in press 2003.

McGowan, J., S. Bograd, R. J. Lynn and A. J. Miller, The biological response to the 1977 regime shift in the California Current, *Deep-Sea Research*, submitted 2003.

Miller, A. J., D. R. Cayan, T. P. Barnett, N. E. Graham and J. M. Oberhuber, Interdecadal Variability of the Pacific-Ocean - Model Response to Observed Heat-Flux and Wind Stress Anomalies, *Climate Dynamics*, 9 (6), 287-302, 1994.

NGDC, Digital relieve of the surface of the Earth, *NOAA, National Geophysics Data Center, Boulder, Colorado*, (Data announcement 88-MG-02), 1998.

Roemmich, D., Ocean Warming and Sea-Level Rise Along the Southwest United- States Coast, *Science*, 257 (5068), 373-375, 1992.

Roemmich, D. and J. McGowan, Climatic Warming and the Decline of Zooplankton in the California Current, *Science*, 267 (5202), 1324-1326, 1995.

Schneider, N., E. Di Lorenzo and P. Niiler, Decadal salinity changes in the California Current, manuscript in prep, 2003.

Schwing, F. B. and R. Mendelssohn, Increased coastal upwelling in the California Current System, *Journal of Geophysical Research-Oceans*, 102 (C2), 3421-3438, 1997.

Shchepetkin, A. and J. C. McWilliams, Quasi-monotone advection schemes based on explicit locally adaptive dissipation, *Monthly Weather Review*, (126), 1541-1580, 1998.

Shchepetkin, A. and J. C. McWilliams, A method for computing horizontal pressure-gradient force in an oceanic model with a non-aligned vertical coordinate, *Journal of Computational Fluid Dynamics*, in press 2003.

Simpson, J. J. and R. J. Lynn, A Mesoscale Eddy Dipole in the Offshore California Current, *Journal of Geophysical Research-Oceans*, 95 (C8), 13009-13022, 1990.

Song, Y. H. and D. Haidvogel, A Semiimplicit Ocean Circulation Model Using a Generalized Topography-Following Coordinate System, *Journal of Computational Physics*, 115 (1), 228-244, 1994.

Stephens, C., S. Levitus, J. Antonov and T. P. Boyer, On the Pacific Ocean regime shift, *Geophysical Research Letters*, 28 (19), 3721-3724, 2001.

Winant, C. D. and C. E. Dorman, Seasonal patterns of surface wind stress and heat flux over the Southern California Bight, *Journal of Geophysical Research-Oceans*, 102 (C3), 5641-5653, 1997.

Zhang, Y., J. M. Wallace and D. S. Battisti, ENSO-like interdecadal variability: 1900-93, *Journal of Climate*, 10 (5), 1004-1020, 1997.

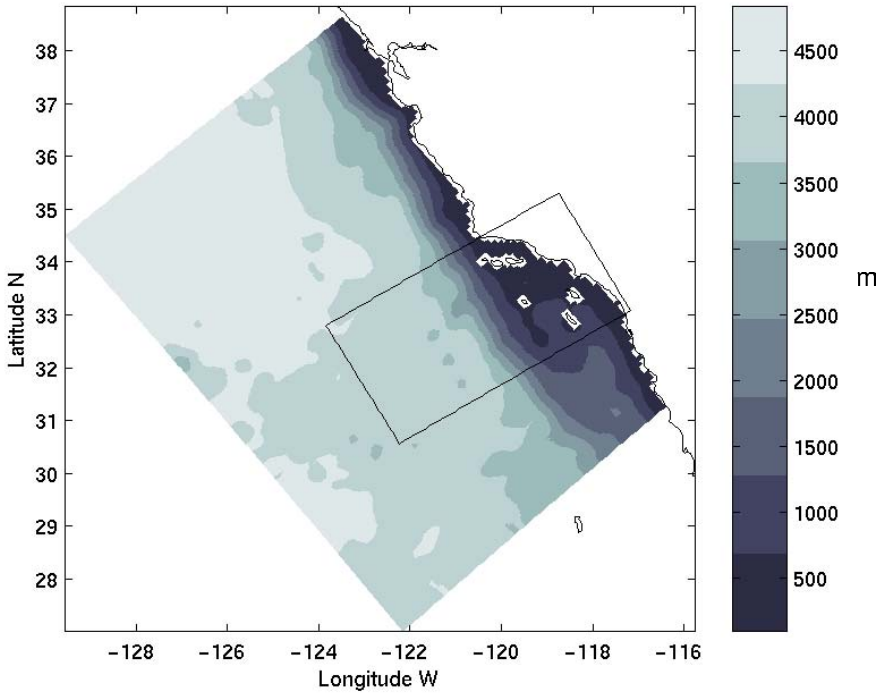

Figure 3.1. Model bathymetry for the Southern California Current System. Black rectangle identifies the domain of the CalCOFI data reanalysis.

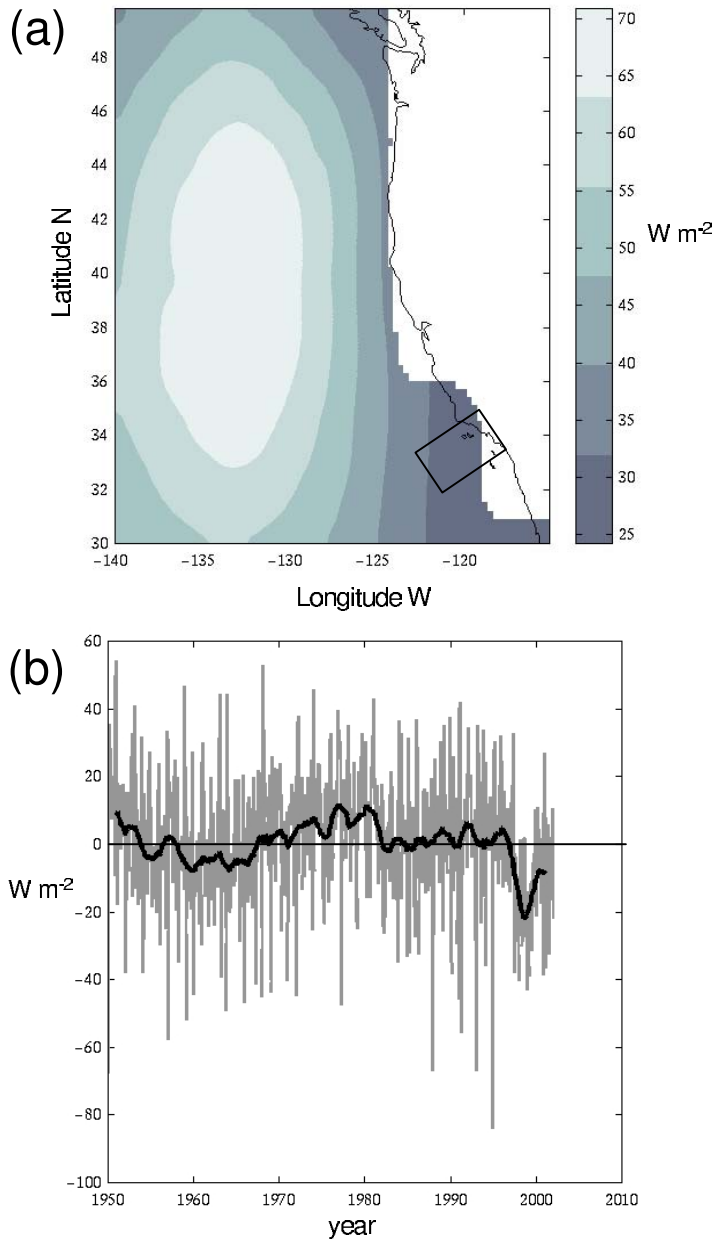

Figure 3.2. (a) EOF mode 1 for the net surface heat flux anomaly from Cayan (2003). The black box identifies the location of the CalCOFI data domain. (b) Average net heat flux over the CalCOFI model domain. Solid thick line is the 2 year running mean. This timeseries is correlated 0.9 with PC of EOF 1 (a), which is not shown.

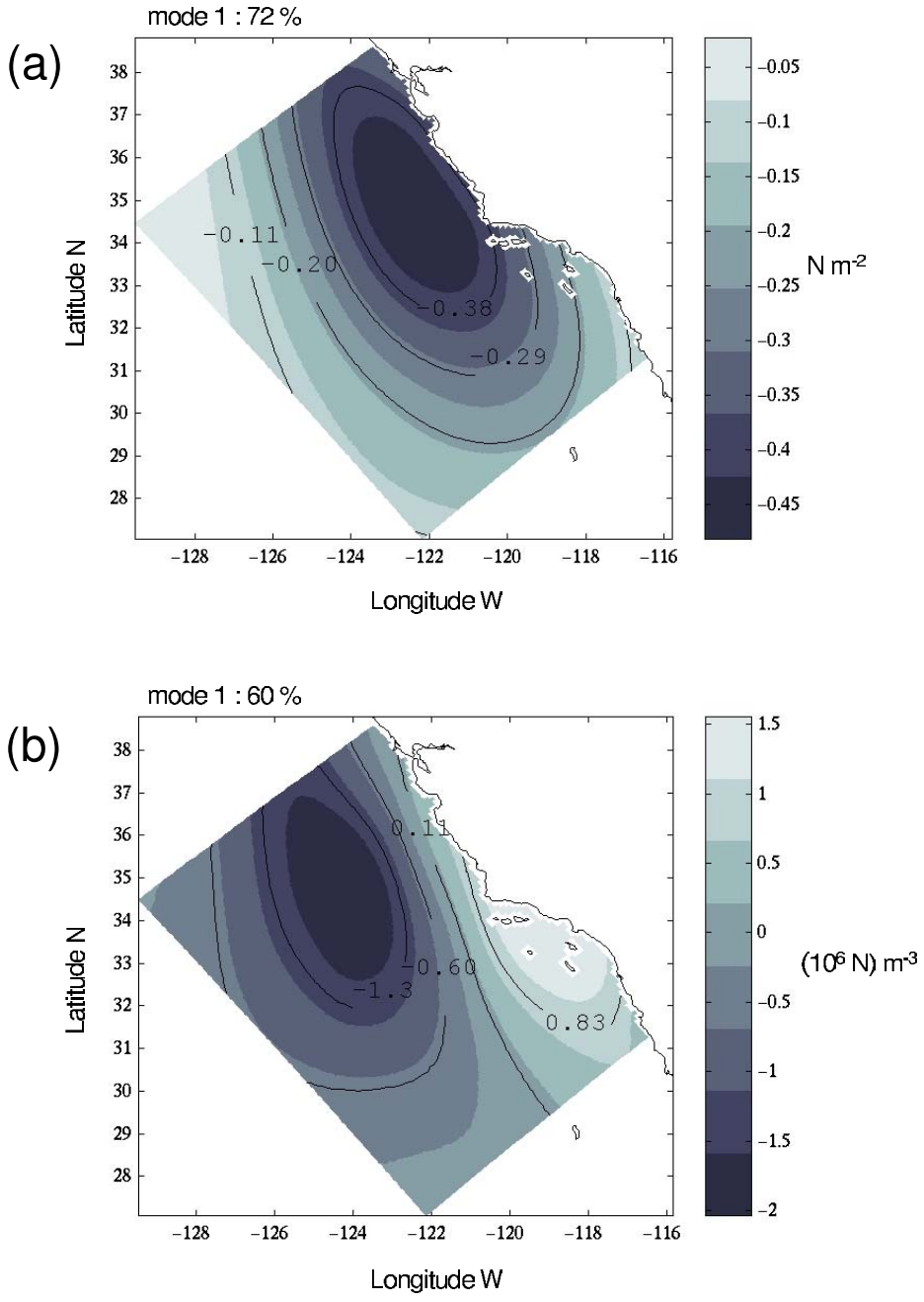

Figure 3.3. (a) EOF mode 1 of the January to April anomalies for alongshore wind stress (a) and wind stress curl (b) from NCEP over the PE model domain.

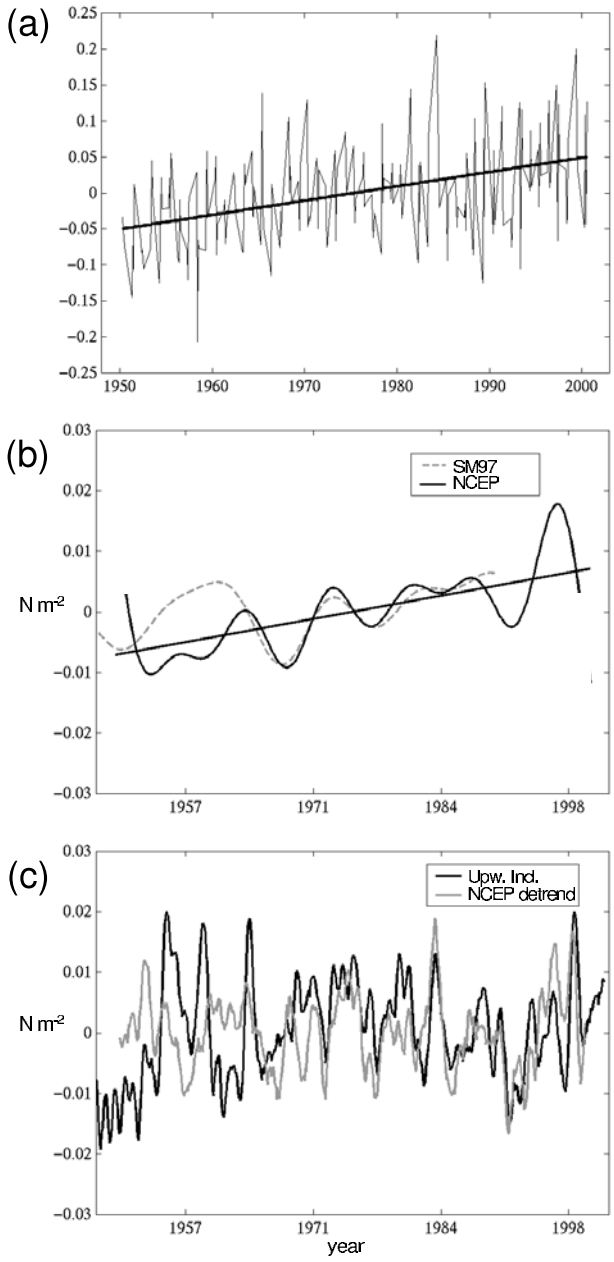

Figure 3.4. (a) PC 1 of EOF mode 1 for alongshore component of wind stress (Figure 3.3a). Solid thick line is 4 year running mean. (b) NCEP (black) and Schwing and Mendelssohn (1997) COADS analysis (gray) equatorward wind stress monthly anomalies (data is 8 year low passed). (c) Detrended NCEP equatorward winds (black) and average PFEL Upwelling Indices (gray) anomalies over the SCCS (1 year running mean is used).

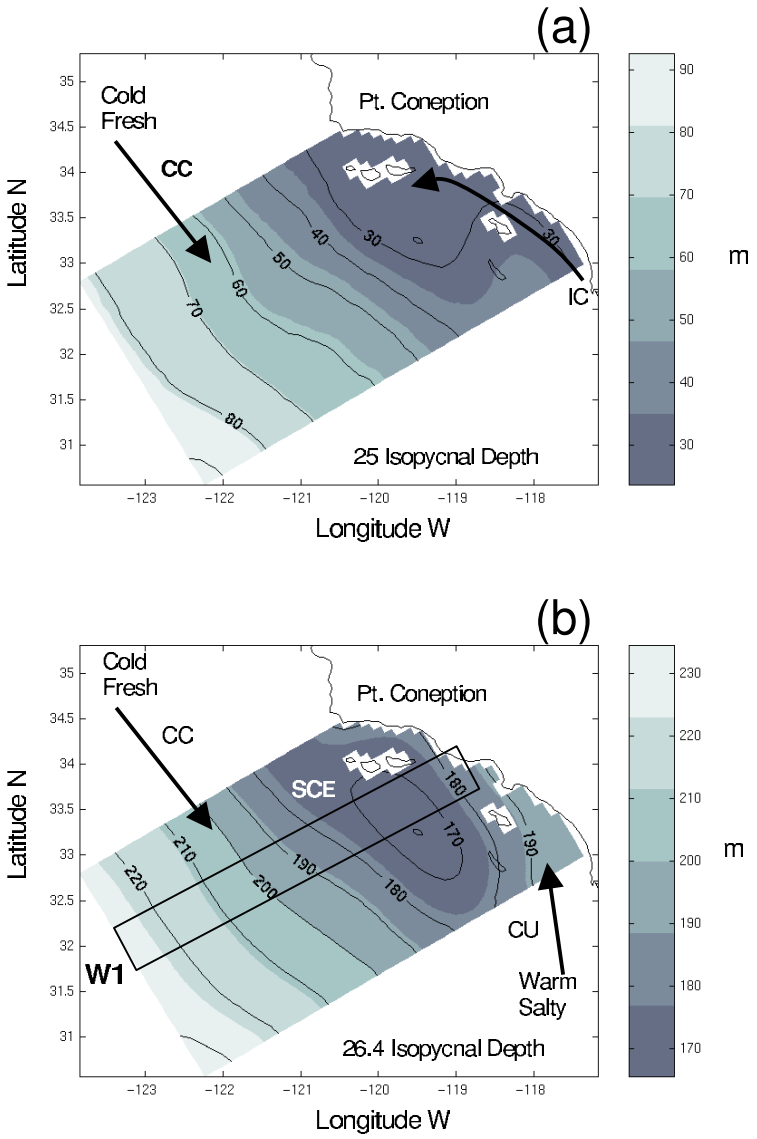

Figure 3.5. Average depths of isopycnal 25 (a) and 26.4 (b) for the period 1949 to 2000.

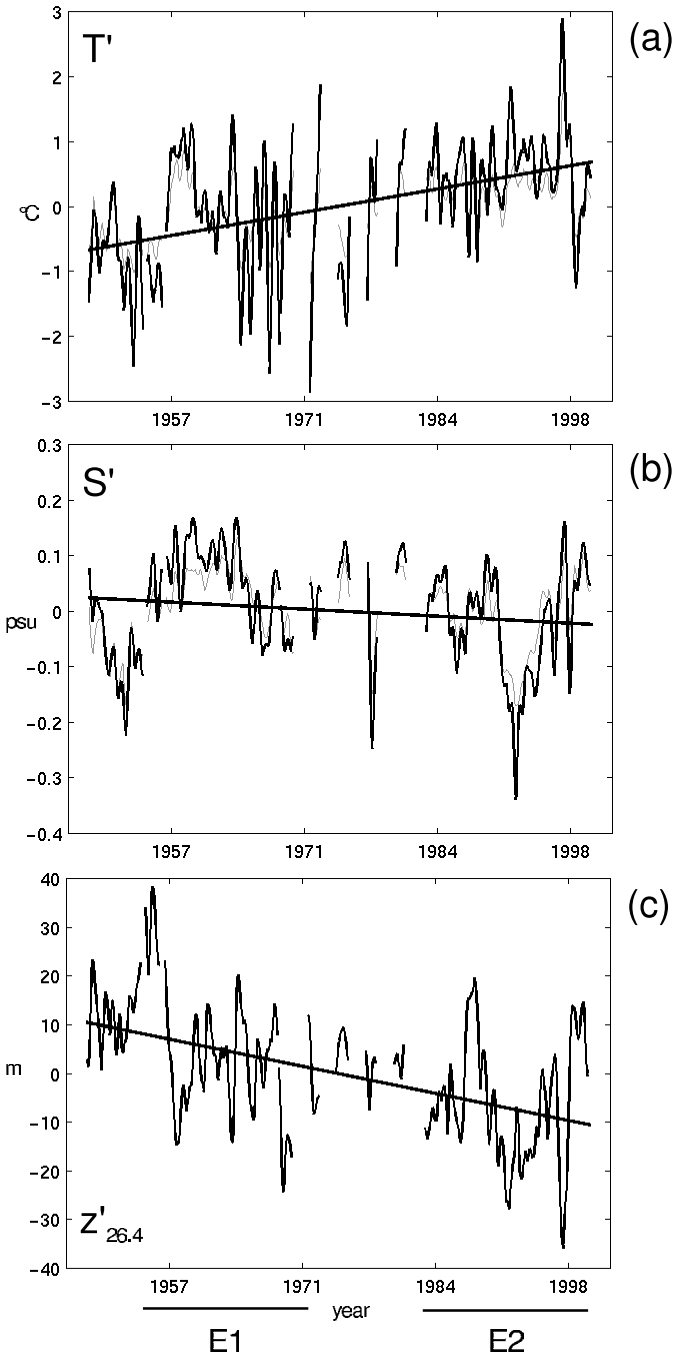

Figure 3.6. Timeseries of surface (black line) and isodepth-integrated (gray line) temperature (a) and salinity (b) anomalies averaged over the CalCOFI data domain. (c) Same average for the isopycnal 26.4 depth anomaly.

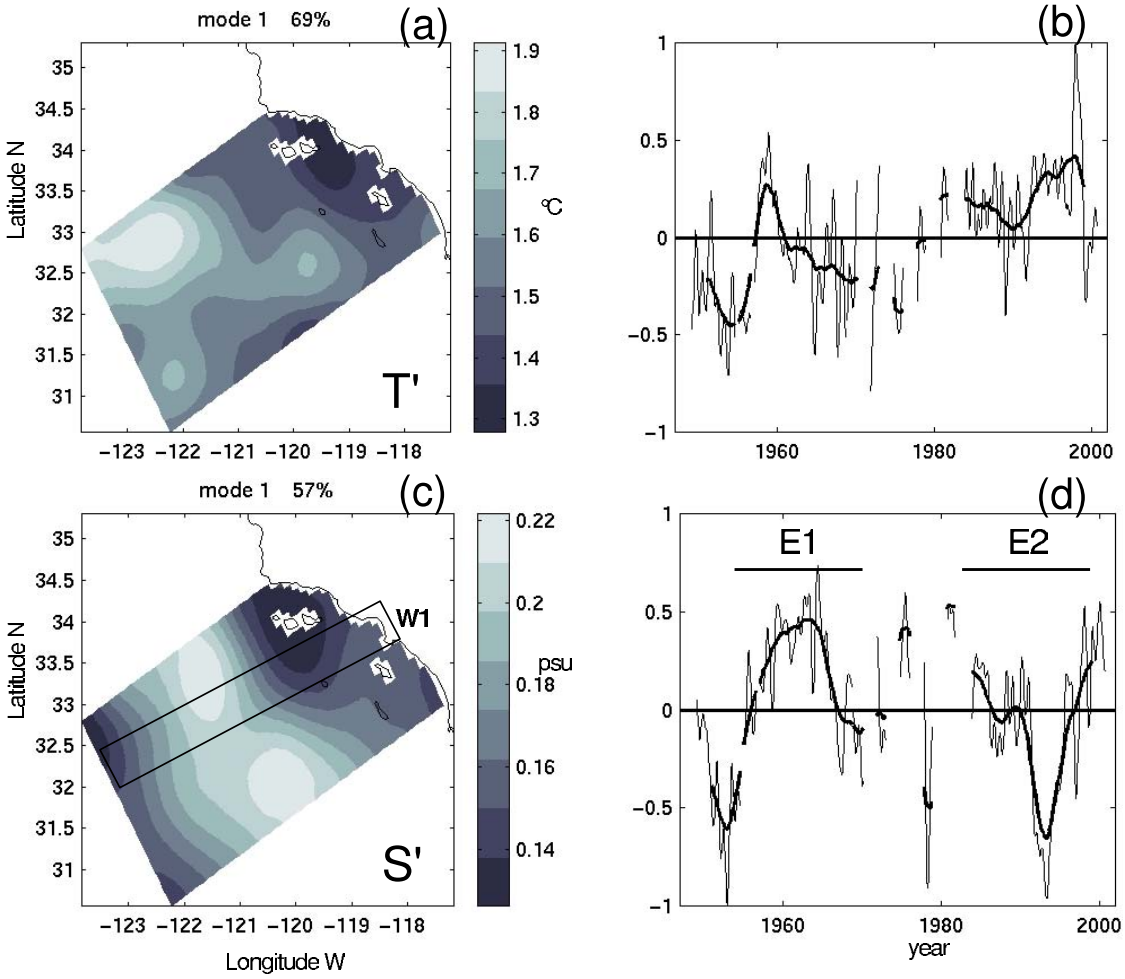

Figure 3.7. EOF mode 1 for depth integrated temperature (a) and salinity (c) anomalies from the CalCOFI data analysis and their respective (b,d) temporal amplitude.

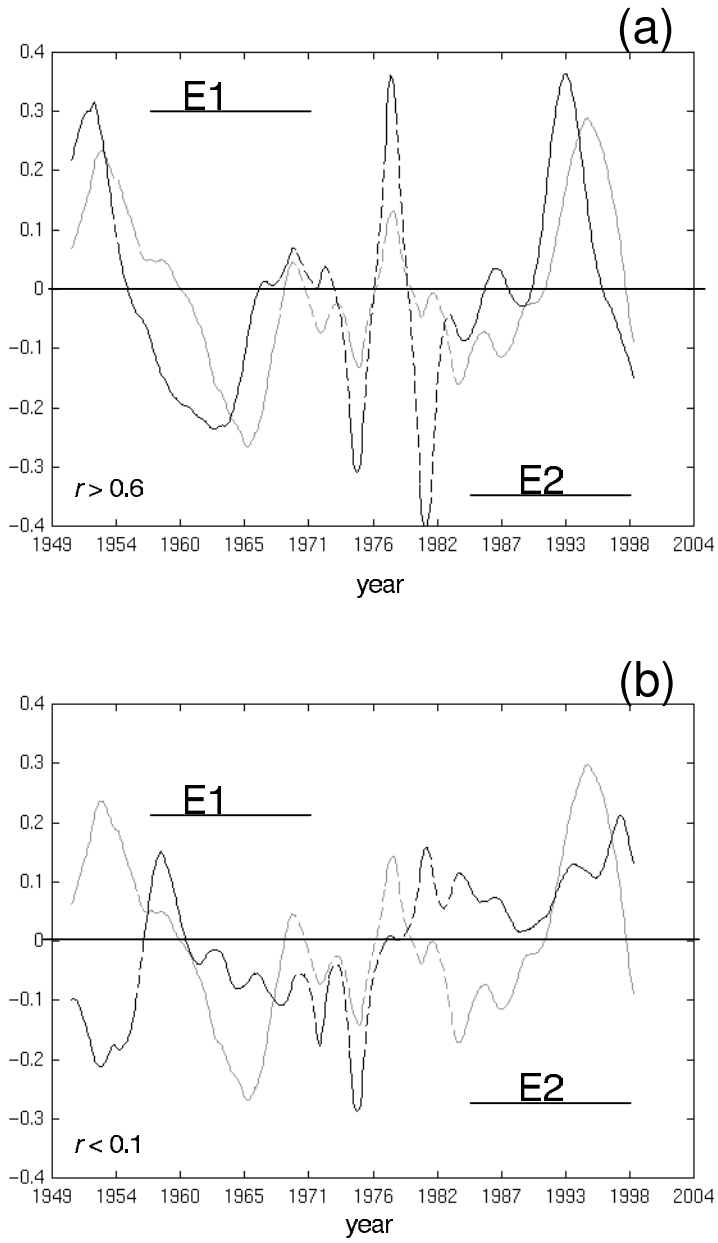

Figure 3.8. PC 1 for surface salinity (black line in a) and salinity on deep isopycnal 26.4 (gray line in a). PC 1 for SST (black line in b) and temperature on deep isopycnal 26.4 (gray line in b).The correlation coefficient between the surface and deep PC 1 (the black and gray lines in each panel) is denoted by r. An 8 year running mean is used. The dotted portions of the timeseries indicate gaps in the data.

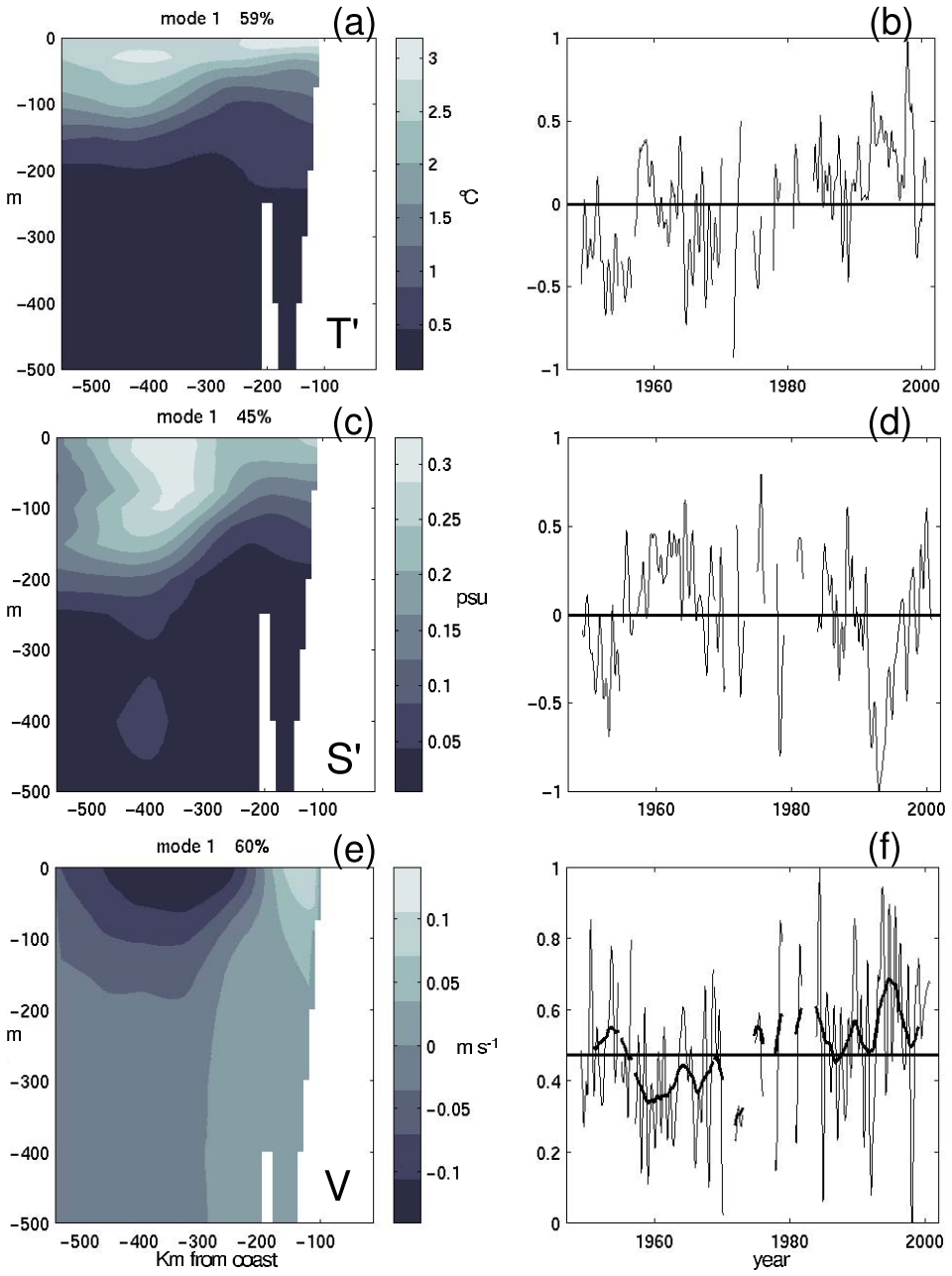

Figure 3.9. Vertical EOFs mode 1 for transect W1 in Figure 3.5. (a) Temperature and (c) salinity anomalies from the CalCOFI data analysis and are their respective (b,d) temporal amplitude. (e) Geostrophic alongshore currents relative to 500 m and its (f) temporal amplitude. This transect is representative for various cross-section in the CalCOFI domain.

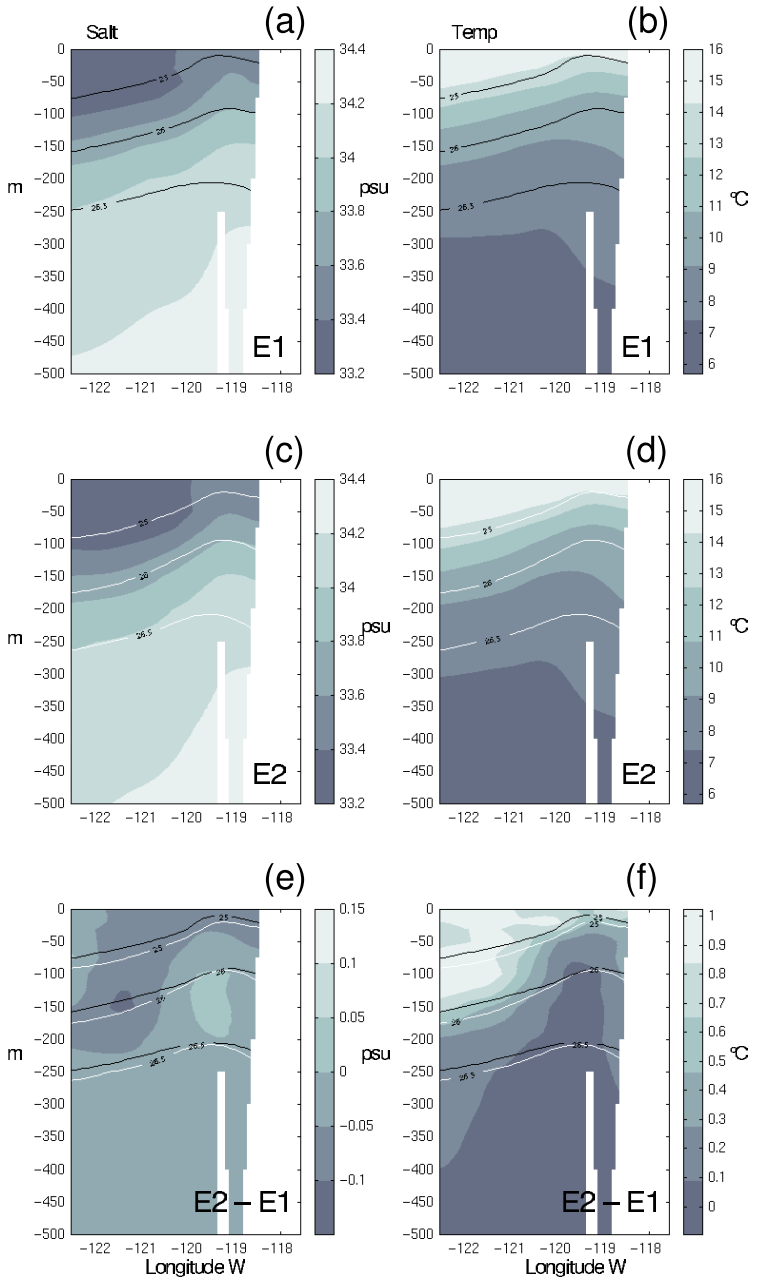

Figure 3.10. Vertical sections for salinity (a,c,d) and temperature (b,d,f) averaged along transect W1 in Figure 3.5. E1 denotes the mean from 1950-1970, E2 is the mean from 1980-2000 and E2-E1 their difference. This transect is representative for various cross-section in the CalCOFI domain.

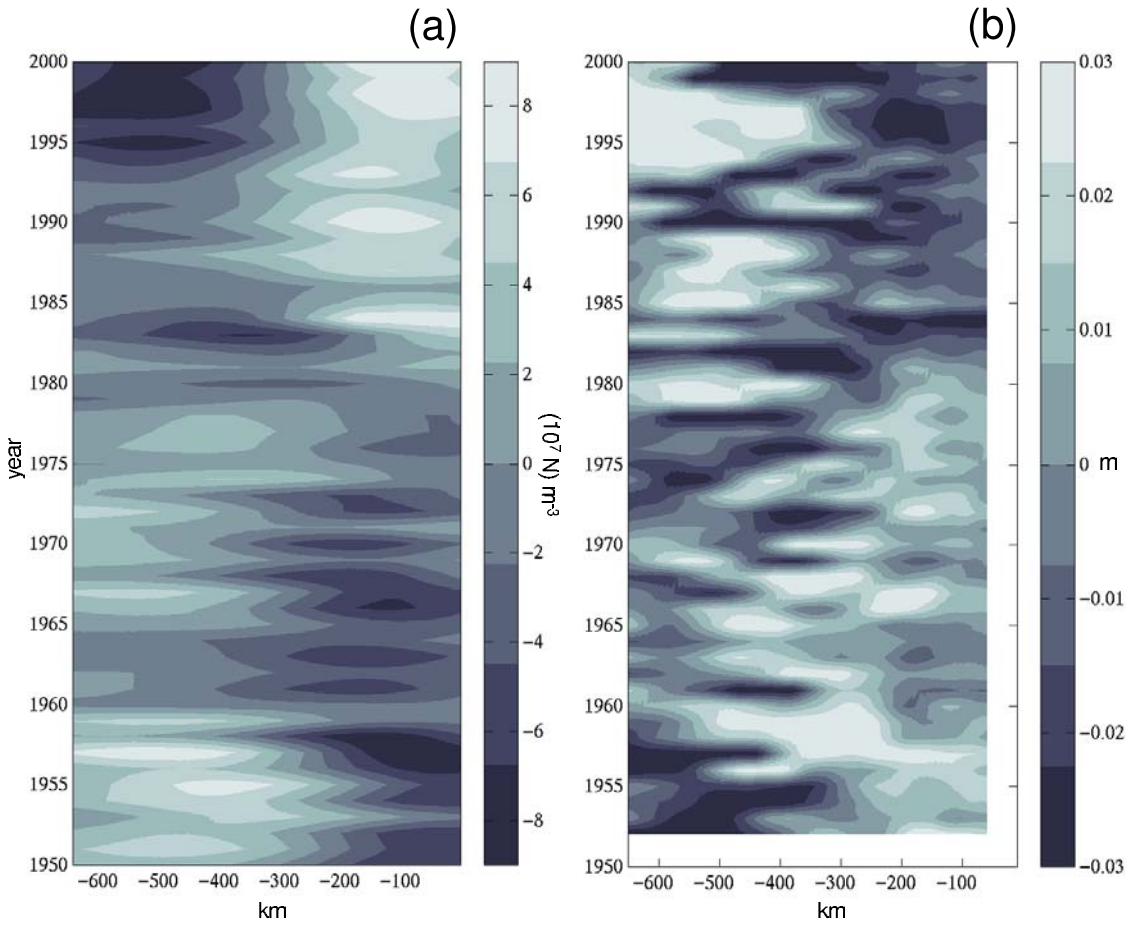

Figure 3.11. (a) Hofmuller for NCEP wind stress curl anomaly and (b) model SSH from experiment LF_TAU. This experiments isolates the PE model response to the winds alone. The x direction is cross-shore distance from the coast. This transect is representative for various cross-section in the CalCOFI domain.

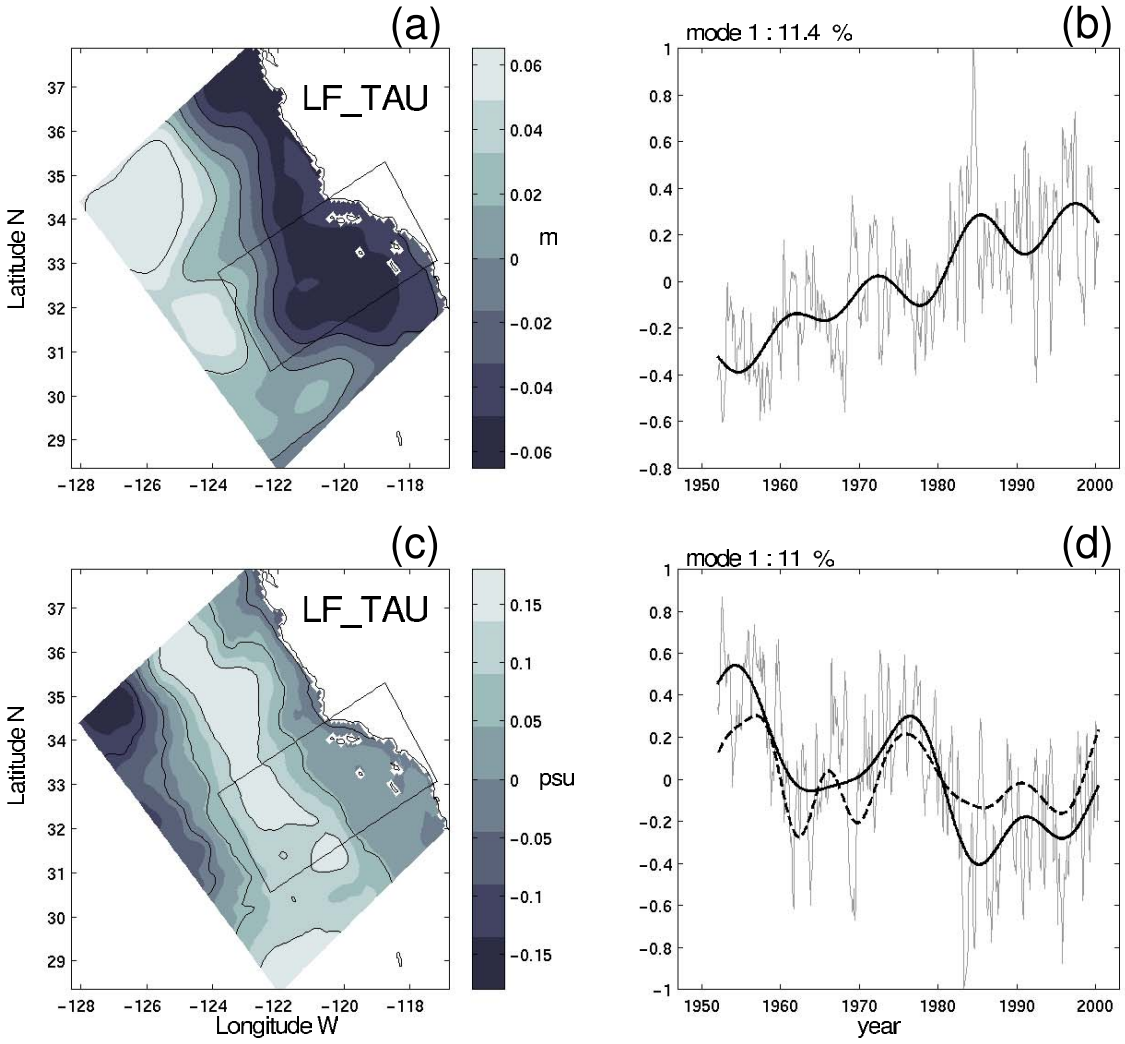

Figure 3.12. EOF 1 for model SSH (a) and surface salinity (c) and their respective PC 1 (b,c). These EOFs are computed from experiment LF_TAU. The black solid lines are the 10 year lowpass of the PCs. In panel (d) the black dashed line is the timeseries of model surface salinity anomaly (scaled by its maximum absolute value to compare with the PC 1).

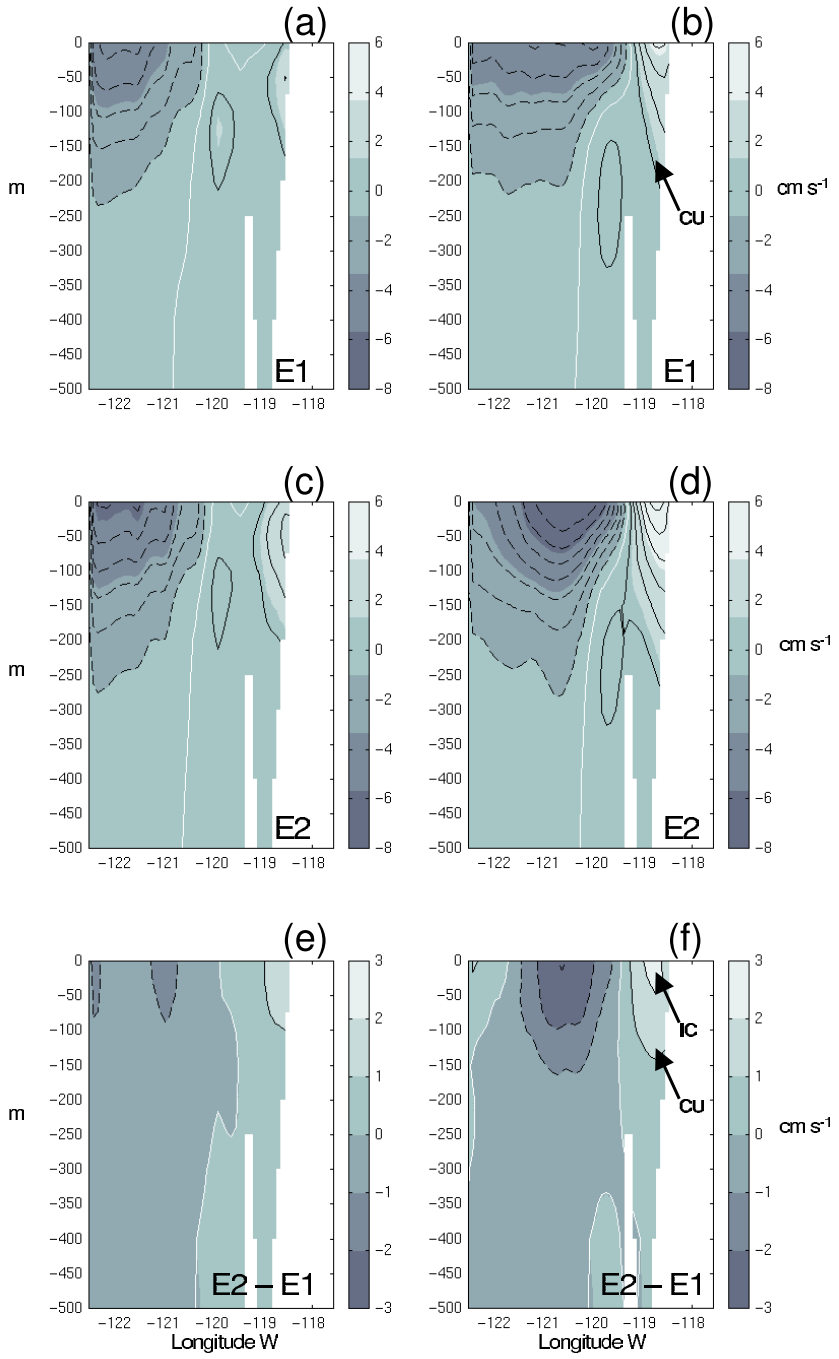

Figure 3.13. Vertical sections for alongshore model (a,c,d) and CalCOFI (b,d,f) geostrophic velocity averaged along transect W1 in Figure 3.1. E1 is the mean from 1950-1970, E2 is the mean from 1980-2000 and E2-E1 their difference. This transect is representative for various cross-section in the CalCOFI domain.

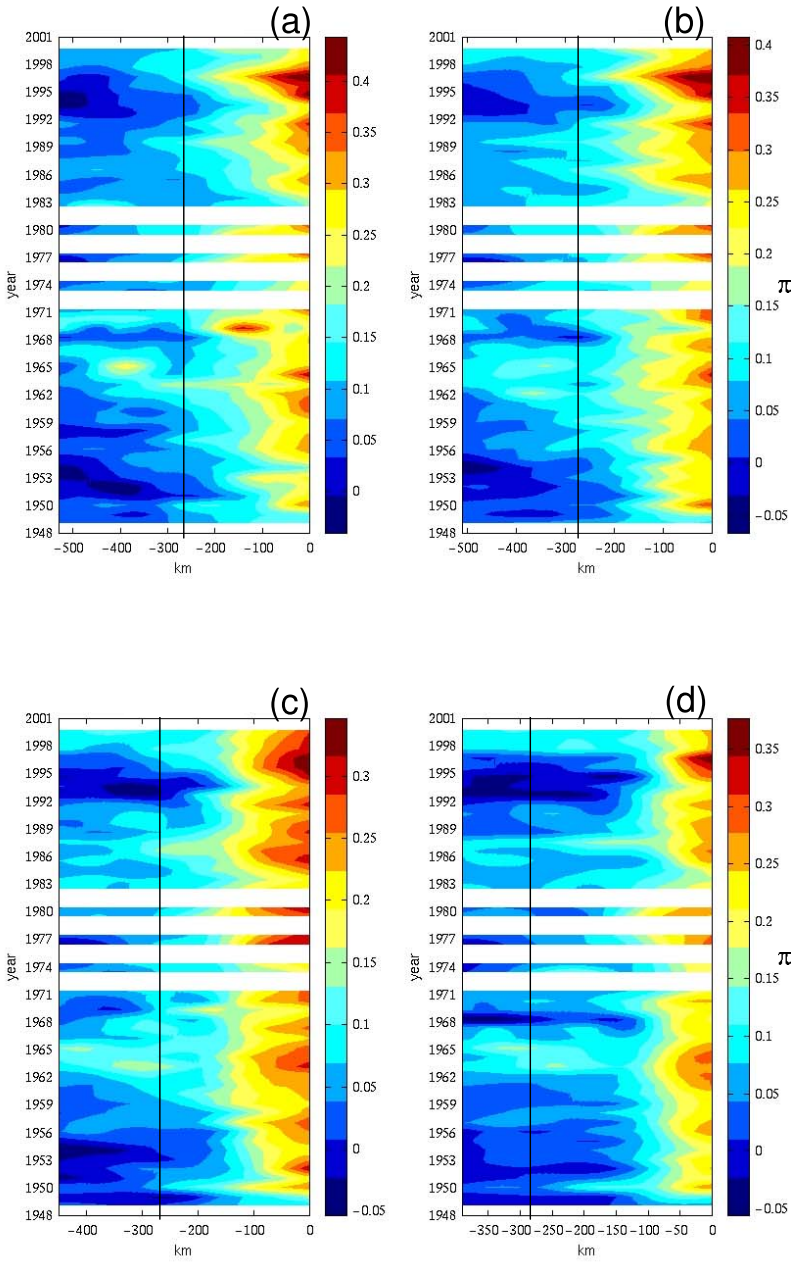

Figure 3.14. Hofmuller plot of spiciness on isopycnal 26.4 at various cross-sections in the CalCOFI data domain. (a) Southern bound, (b) 120 km north of (a), (c) 200 km north of (a) and (d) northern bound. The x is the distance in km from the coast. The black line is located approximately at 280 km from the coast.

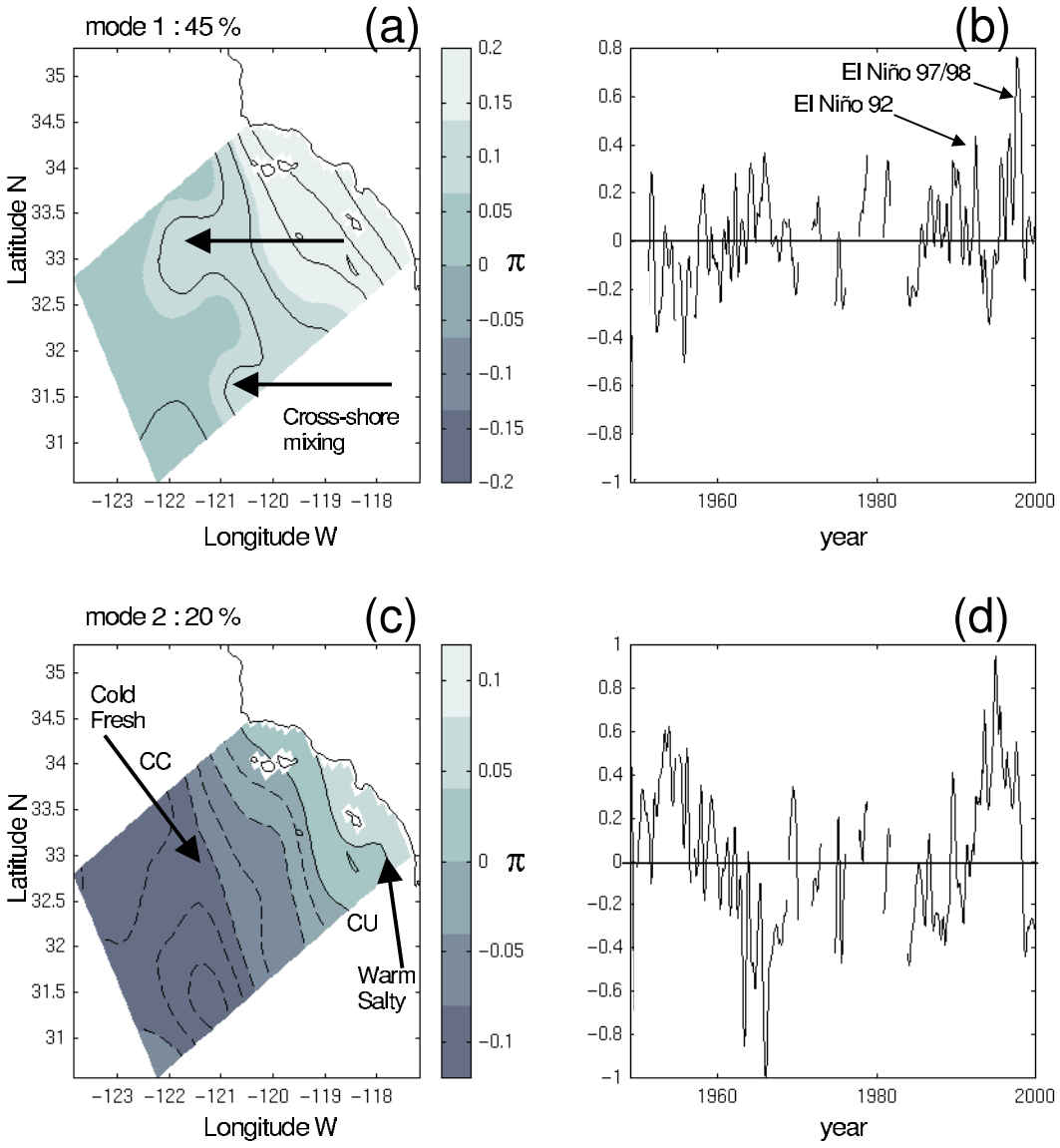

Figure 3.15. Horizontal EOF of spiciness on isopycnal 26.4 (a,c) and the temporal evolution of the mode (b,d).

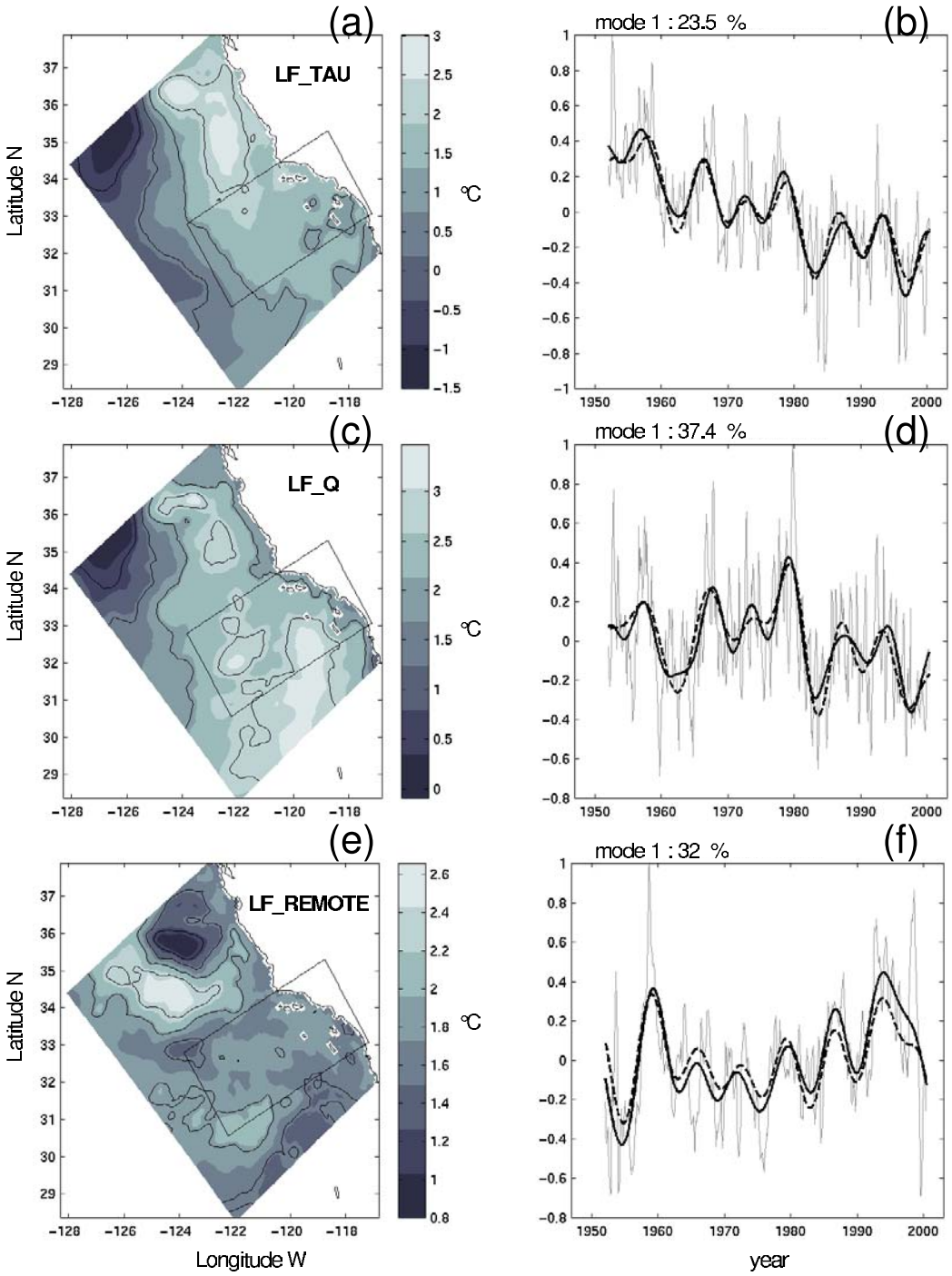

Figure 3.16. Horizontal EOFs of SST and their PCs. (a,b) Experiment LF_TAU. (c,d) Experiment LF_Q. (e,f) Experiment LF_REMOTE

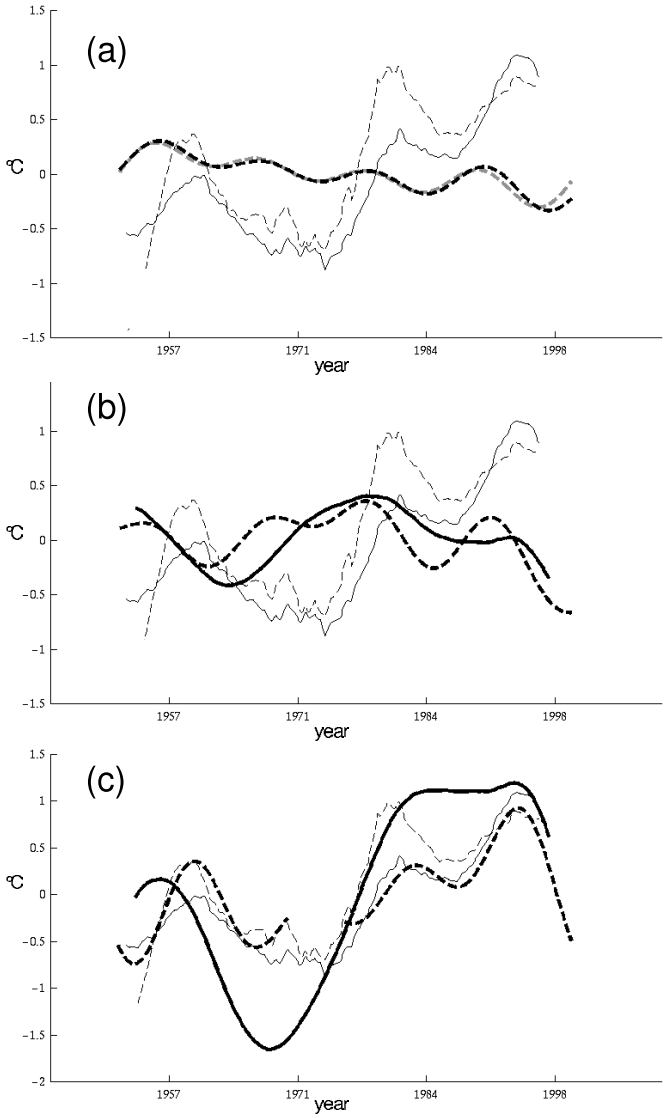

Figure 3.17. Time series of SSTa from CalCOFI averaged at inshore and offshore (respectively thin dashed and thin solid gray line in all panels). (a) Black thick dashed line is SSTa of experiment LF_MEAN-LF_TAU. Gray thick dashed line is SSTa of experiment LF_REMOTE2-LF_REMOTE. (b) SSTa predicted from simple models forced with heat fluxes and damping (black thick solid line) and SSTa from experiment LF_Q (black thick dashed line). (c) SSTa predicted from simple models forced with heat fluxes and no damping (black thick solid line) and SSTa from experiment LF_REMOTE (Black thick dashed line). An 8 year running mean is applied to all timeseries.

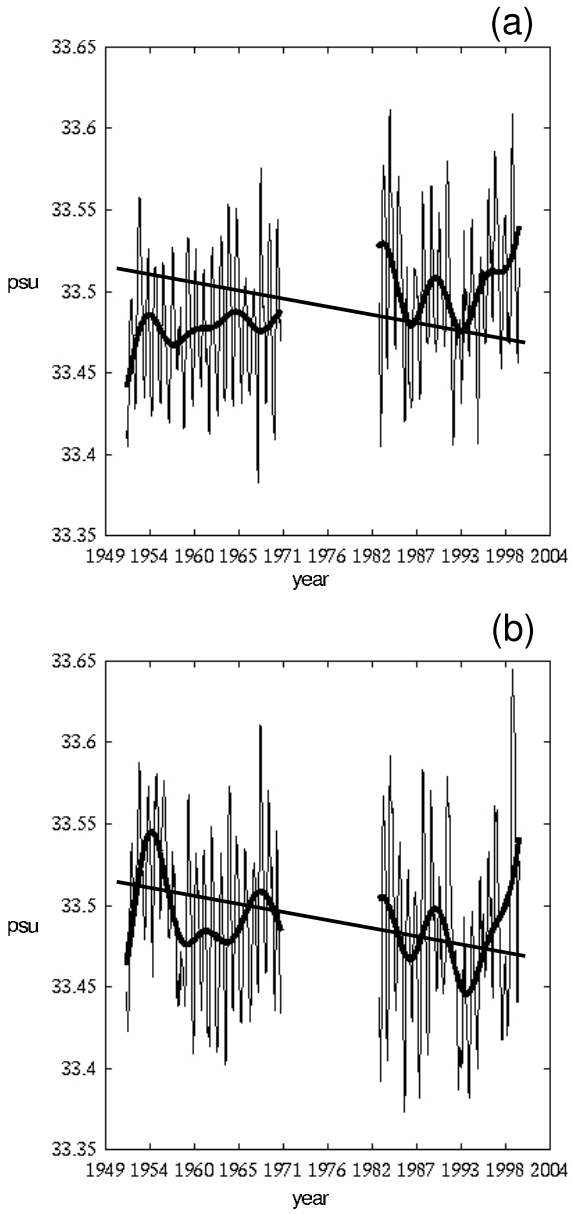

Figure 3.18. Timeseries of model surface salinity in the coastal band (within 60 km from the coast) average along the model coastline. This is used as a proxy for nutrients. (a) From experiment LF_TAU, which is forced with the increasing upwelling favorable winds. (b) From experiment LF_REMOTE, which is includes both the increasing upwelling favorable winds and the deepening of isopycnals. Black thick line is 8 year running average.

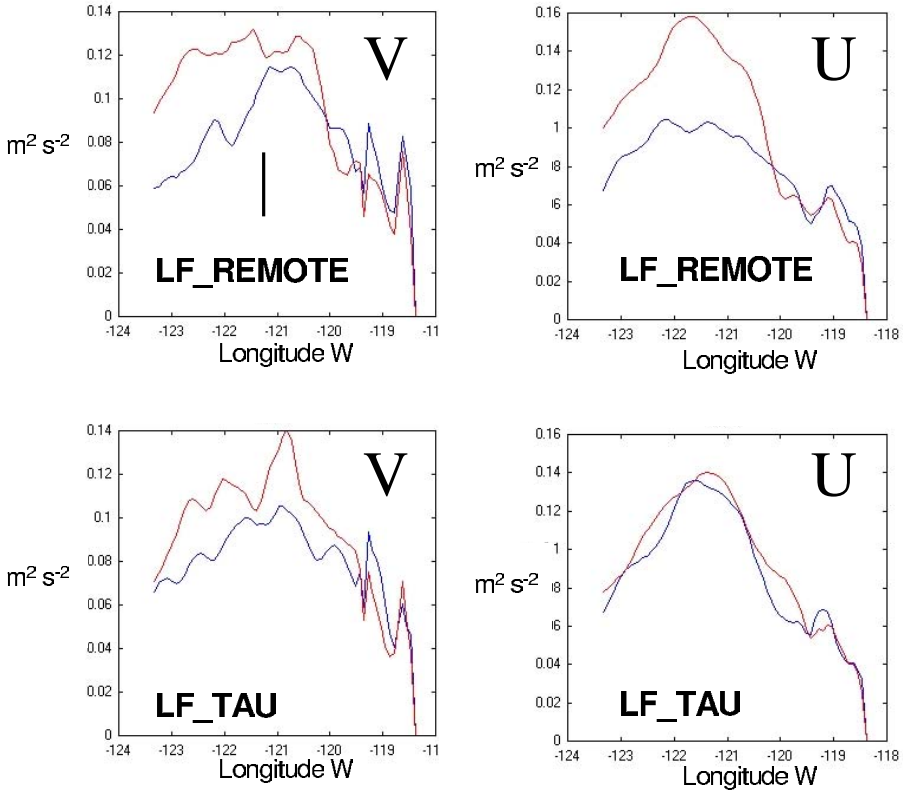

Figure 3.19.: Cross-shore transect W1 in Figure. 3.5 for model alongshore (V) and cross-shore (U) velocity variance for the periods 1957-1969 (blue line) and 1987-2000 (red line). The model experiment is labeled at the bottom. The vertical line indicates a significant change in variance at the 95% level based on an F test with 80 degrees of freedom.

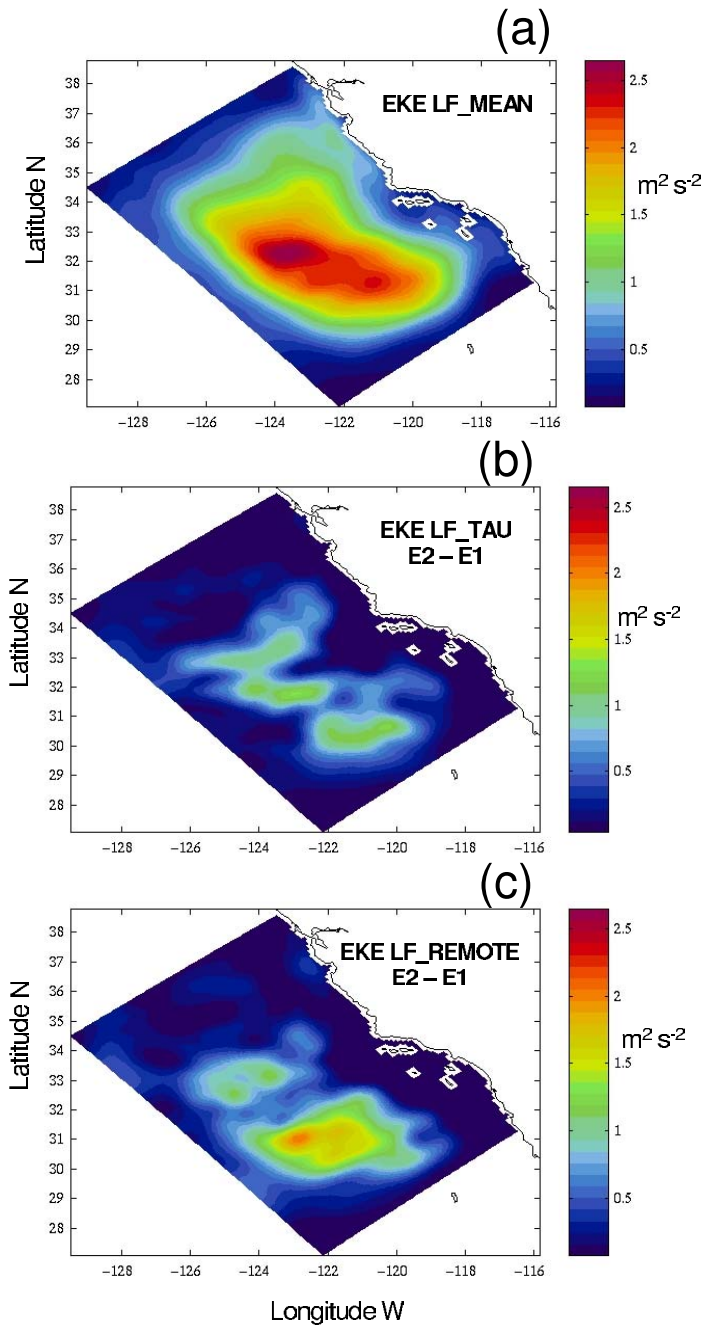

Figure 3.20. (a) Model eddy kinetic energy (EKE) for control run (experiment LF_MEAN). Difference in EKE for the periods E2 –E1 for different model experiments (b) LF_TAU and (c) LF_REMOTE. Period E1 is defined from 1950 to 1970 and period E2 from 1980 to 2000.